

**TOOL BREAKOUT INVESTIGATION IN DRILLING USING FEED AND  
CUTTING ENERGY**

by

Daniel Obiora Iruikwu

BEng in Mechanical Engineering and Production Technology, HAMK, Finland, 2010  
MSc in Electronics and Electrical Engineering, Aalto University, Finland, 2013

A Dissertation Submitted in Partial Fulfillment  
of the Requirements for the Degree of

**Doctor of Philosophy**

in the Graduate Academic Unit of Mechanical Engineering

Supervisor: Andy Simoneau, PhD, Mechanical Engineering

Examining Board: Tiger Jeans, PhD, Mechanical Engineering  
Gobinda Saha, PhD, Mechanical Engineering  
Clodualdo Aranas Jr., PhD, Mechanical Engineering  
Liuchen Chang, PhD, Electrical and Computer Engineering

External Examiner: Mohamed Elbestawi, PhD, Mechanical Engineering,  
McMaster University

This dissertation is accepted by the  
Dean of Graduate Studies

THE UNIVERSITY OF NEW BRUNSWICK

August, 2020

©Daniel Obiora Iruikwu, 2020

## **ABSTRACT**

Burr formation is a common problem in metal drilling processes leading to additional production costs in manufacturing. Since burrs cannot be prevented through process control and parameter optimization, obtaining a better understanding of the mechanism of the burr formation process and potentially paving the way for more appropriate development models that could mitigate the process is essential. Currently, the complex tool geometry and the dynamic nature of metal drilling pose challenges in the analysis of the drilling mechanics, and consequently, the burr formation process, thereby constraining researchers to approach the problems through the development of empirical models or alternative methods difficult to replicate. The objective of this work is to develop a new and novel method using energy analysis to identify unique points of process changes that characterize the breakout burr formation mechanism during the metal drilling process. The method developed identifies the onset of the burr breakout phenomenon, and also identifies critical points between the onset of the process and completion of the through-hole drilling process. Using a series of drilling experiments on Al 6061-T6 with standard twist drills, real-time thrust and cutting power data were collected and analyzed using a newly developed energy-difference approach (EDA). The resulting analysis was successfully mapped to the burr breakout phenomenon and validated using photomicrographs observation and microhardness testing at various points ahead of the drill point during burr breakout. Using an original approach through-hole drilling was separated into 3 primary sections identifiable using energy analysis. This work allowed for the third - critical zone, which is of primary interest in burr formation to be identified and isolated for analysis. Using the EDA process, 4 specific points of interest that characterize the actual burr

formation mechanism were identified and observed for the first time: burr breakout initiation, deformation zone depth ahead of the drill point, ploughing initiation, and ploughing dominance. By identifying and quantifying the positions and depths of these critical points in the breakout burr formation, future work will allow for proper modeling, prediction, and minimization of breakout burrs.

## **DEDICATION**

I dedicate this dissertation to my family and friends, especially to my loving parents Mr. and Mrs. Onosike Iruikwu, for the prayers, encouragement, and support through the course of this journey. You have been present in many ways difficult to describe even though physically far away, your every word of encouragement and prayers have been a boost that motivates me to carry on and for this am grateful. My siblings- Roseline, Ifeoma, Innocent, Kingsley, and Gloria have been sources of encouragement.

I dedicate this dissertation to my best friend, Betty. Thank you for your support, encouragement, and just been here. You inspire me to get better.

I also dedicate this dissertation to my supervisor and friend, Dr. Andy Simoneau. This project would not have been possible if you had not taken me in as a student under your mentorship and guidance.

## ACKNOWLEDGEMENTS

I want to express my sincere gratitude to everyone who has contributed to the success of this thesis.

First and foremost, I would like to thank my supervisor, Dr. Andy Simoneau, for the guidance and support throughout this journey. From my first day at UNB, you have been a mentor and father figure. I want to thank the members of the examining board- Dr. Clodualdo Aranas, Dr. Gobinda Saha, and Dr. Tiger Jeans, of the Mechanical Engineering Department at UNB, for the helpful suggestions and contributions. I also want to thank Dr. Liuchen Chang of the Department of Electrical and Computer Engineering, UNB, and Dr. Mo Elbestawi of the Department of Mechanical Engineering, McMaster University, for your feedback and helpful suggestions.

Next, I want to thank Brian Guidry, Allan Robinson, and the secretaries of the Department of Mechanical Engineering for the technical support and assistance. I also want to acknowledge my funding agencies- NBIF and NSERC.

Last but not least, my heartfelt gratitude goes to my family and friends for the prayers and support throughout this journey. And most of all, I want to thank God Almighty for the gift of life and salvation in Christ Jesus, and for the grace, wisdom, and strength in me to complete this research.

## Table of Contents

ABSTRACT.....	ii
DEDICATION.....	iv
ACKNOWLEDGEMENTS.....	v
Table of Contents.....	vi
List of Tables.....	xi
List of Figures.....	xii
Nomenclature.....	xviii
Chapter 1: Introduction.....	1
1.1 Overview.....	1
1.2 Background.....	3
1.3 Scope and Objective.....	5
1.4 Thesis Layout.....	7
Chapter 2: Literature Review.....	9
2.1 General Machining Operations.....	9
2.1.1 Machining and Chip Formation.....	11
2.2 Mechanics of Metal Cutting, Material Behavior and Chip Formation.....	15
2.2.1 Analysis of Thin-Zone Model.....	17
2.2.2 Analysis of Thick-Zone Model.....	20
2.2.3 Shear Angle Relationships in Metal Cutting.....	26
2.2.4 Mechanics of Oblique Cutting.....	28
2.2.5 Geometry of Single Cutting Edge.....	29
2.2.6 Shear Angle in Oblique Cutting.....	31

2.2.7 Oxley’s Parallel-Sided Shear Zone Theory .....	32
2.2.8 The Variable Flow Stress Theory .....	33
2.2.8.1 Shear Zone Stress.....	36
2.2.8.2 Tool-Chip Interfaces Stress.....	38
2.3 The Metal Drilling Process .....	40
2.3.1 Concept of Twist Drill Geometry and Design Features.....	41
2.3.1.1 Design Features and Nomenclature .....	41
2.3.1.2 Drill Point Design Model and Profile Optimization .....	45
2.3.2 Mechanics of Metal Drilling Process.....	46
2.3.3 Analysis of Drill Point Geometry .....	50
2.3.4 Torque and Thrust Force in Metal Drilling Processes .....	52
2.3.5 Problems Associated with Metal Drilling Processes .....	56
2.4 Burr Formation.....	57
2.4.1 Mechanism of Burr Formation in Metal Cutting Process .....	57
2.4.2 Mechanism of Burr Formation in Metal Drilling Process .....	60
2.4.3 Burr Minimization and Deburring Approach .....	67
2.4.4 Burr Minimization Scheme in Metal Drilling.....	68
2.4.5 Deburring Scheme .....	69
Chapter 3: Analysis of PCM and Fault Identification .....	71
3.1 Force Application in PCM and Analysis .....	71

3.2 Power Application in PCM and Analysis .....	72
3.3 PCM Summary.....	74
Chapter 4: Experimental Work .....	75
4.1 Hypothesized Deep-Hole Drilling Zone Classification .....	75
4.2 Workpiece Material .....	78
4.3 Experimental Setup – Data Acquisition.....	80
4.4 Experimental Drilling Tests .....	81
4.4.1 Preliminary Drilling Test Procedure .....	84
4.4.2 Experimental Drilling Test Procedure .....	84
4.4.3 Stepped Drilling and Photomicrograph Procedure .....	85
4.4.4 Hardness Test Procedure.....	88
4.5 Summary .....	89
Chapter 5: Experimental Results .....	90
5.1 Preliminary Drilling Test Results .....	90
5.2 Experiment Drilling Test Results.....	92
5.2.1 Thrust Force Results .....	92
5.2.2 Feed Power Results.....	95
5.2.3 Cutting Power Results.....	98
5.3 Deformation Zone Test Results .....	101
5.3.1 Photomicrographs of Breakout Burr .....	102

5.3.2 Hardness Test Results .....	103
Chapter 6: Discussion of Results .....	109
6.1 Discussion of Preliminary Test Results .....	109
6.2 Discussion of the Feed and Cutting Power Results .....	114
6.2.1 The Energy-difference Approach and Change-rate Curve .....	114
6.2.2 Analysis of the Feed Power .....	117
6.2.2.1 Breakout Burr Initiation and Deformation Zone Depth.....	125
6.2.2.2 Work-hardened Layer Thickness .....	128
6.2.3 Analysis of the Cutting Power .....	129
6.2.3.1 Point of Ploughing Initiation and Continuous Ploughing .....	138
6.2.4 Characteristics of the Breakout Burr Formation Mechanism .....	142
6.2.5 Summary of Feed and Cutting Power Data Analysis .....	143
6.3 Analysis of Material Changes in the Deformation Zone .....	144
6.3.1 Microstructure Analysis of the Deformation Zone .....	145
6.3.2 Material Hardness Property at the Deformation Zone.....	148
6.3.3 Summary of the Deformation Zone Material Behavior .....	152
Chapter 7: Conclusion.....	153
7.1 Summary of Work Done .....	153
7.2 Summary of Results and Findings .....	157
7.3 Contributions.....	159

7.4 Future Work .....	160
7.5 Summary .....	161
Bibliography .....	163
Appendix A. Drilling Energy Consumption .....	176
Appendix B. Okuma Machine Type ES-V4020 Power Requirements .....	178
Appendix C. Common Machining Center Power Calculations .....	179
Curriculum Vitae	

## List of Tables

Table 4.1: Chemical composition limits of the Al 6061-T6 alloys by wt. % [158].....	79
Table 4.2: Typical mechanical properties of Al 6061-T6 alloy.....	79
Table 4.3: Drill test parameter for workpiece material thickness, $t_w = 8.9$ mm. ....	85
Table 6.1: Work-hardened layer thickness, $t_H$ obtain at the breakout burr initiation P1. .....	129
Table 7.1: Energy consumed in drilling through-hole using type <i>A</i> twist drill on 8.9 mm thick Al 6061-T6 alloy.....	176

## List of Figures

Figure 2.1: CNC machine tool.....	10
Figure 2.2: Chip formation process. ....	11
Figure 2.3: Illustration of shearing strain $\epsilon$ , in orthogonal cutting process, $\epsilon = \Delta S / \Delta X$ [12]. .....	13
Figure 2.4: Suggested shape for plastic deformation zone in cutting: (a) thin shear plane (b) thick shear zone.....	16
Figure 2.5: Diagram of force components in orthogonal cutting.....	18
Figure 2.6: Shear stress and compressive stress relation. ....	20
Figure 2.7: Idealized plastic zone [29].....	21
Figure 2.8: Slip-line field constructed from observed flow field [22].....	23
Figure 2.9: Geometry for the approximate analysis.....	24
Figure 2.10: Suggested cutting process by Palmer and Oxley [29].....	25
Figure 2.11: Ideal plastic Solution for stress field at tool tip (a) Lee and Shaffer slip-line field (b) Mohr circle diagram for the stress zone <b>ABC</b> . ....	28
Figure 2.12: Plan view of oblique cutting.....	29
Figure 2.13: Rake angle and velocity in oblique cutting. ....	30
Figure 2.14: Illustration of shear plane in chip formation process [24].....	33
Figure 2.15: Model of shear zone during chip formation [24]. ....	34
Figure 2.16: Shear zone element [24]. ....	35
Figure 2.17: Illustration of contact between chip and tool: (a) Elastic (b) Plastic [22]....	39
Figure 2.18: Cutting with restricted tool-chip contact [35]. ....	40
Figure 2.19: Standard twist drill nomenclature [36].....	43

Figure 2.20: Drilling process [11].....	47
Figure 2.21: Photomicrographs of different cutting sections across the cutting lips and chisel edge of a twist drill [61]. .....	49
Figure 2.22: Illustration of a typical drill point [58].....	51
Figure 2.23: Schematic illustration at transient cutting state [97]. .....	58
Figure 2.24: SEM photomicrograph of annealed copper sample due to (a) fracture casing chip separation and (b) development of burr formation [99]. .....	59
Figure 2.25: Burr types formed in dry drilling of Ti-6Al-4V alloy (a) Type I (b) Type II (c) Type III (d) Type IV [7]. .....	60
Figure 2.26: Burr formation with drill cap [7].....	61
Figure 2.27: Classification of drilling burr formation and location of the crack at breakout [103].....	62
Figure 2.28: Illustration of (a) Case I, geometry and loading (b) Case II, burr formation sequence [109]. .....	64
Figure 2.29: Von Mises stress contour in (a) burr initiation, (b) burr development (c) at pivoting stage (d) burr formation [111]. .....	65
Figure 4.1: Classification of the zones in a through-hole drilling processes. ....	76
Figure 4.2: Micrograph of undeformed Al6061-T6 alloy [159]. .....	80
Figure 4.3: Experimental setup for the drilling process.....	81
Figure 4.4: Flow chart of experimental procedure.....	83
Figure 4.5: Through-hole for 15 different hole-depths.....	86
Figure 4.6: Cross-section of the drilled samples at depths 1,2,3,5,6,8,9,14 &15 at spindle speed of 2037 rpm at feeds (a) 0.05 mm/rev, (b) 0.20 mm/rev. ....	87

Figure 4.7: Illustration of Vickers hardness test indentation on workpiece sample. ....	89
Figure 5.1: Drilling a 25.4 mm thick Al6061-T6 workpiece using 7.5 mm black-oxide HSS standard twist drill at 3860 rpm and feeds: (i) 0.05mm/rev (ii) 0.10 mm/rev (iii) 0.15 mm/rev (iv) 0.20 mm/rev (v) 0.25 mm/rev.....	91
Figure 5.2: Thrust forces in the drilling of Al6061-T6 workpiece of thickness 8.9 mm using standard twist drill type <b>A</b> at 2037 rpm, (a) 0.05 mm/rev (b) 0.20 mm/rev. .....	93
Figure 5.3: Thrust forces in the drilling of Al6061-T6 workpiece of thickness 8.9 mm using standard twist drill type <b>B</b> at 2037 rpm, (a) 0.05 mm/rev (b) 0.20 mm/rev. .....	94
Figure 5.4: Thrust force data during the drilling of 8.9 mm Al6061-T6 stock thickness using standard twist drill (a) type <b>A</b> , (b) type <b>B</b> .....	95
Figure 5.5: Feed power in the drilling of Al6061-T6 workpiece of thickness 8.9 mm using standard twist drill type <b>A</b> at 2037 rpm, (a) 0.05 mm/rev (b) 0.20 mm/rev. .	96
Figure 5.6: Feed power in the drilling of Al6061-T6 workpiece of thickness 8.9 mm using 3/8-inch un coated HSS standard twist drill type <b>B</b> at 2037 rpm, (a) 0.05 mm/rev (b) 0.20 mm/rev.....	97
Figure 5.7: Cutting power in the drilling of Al6061-T6 workpiece of thickness 8.9 mm using standard twist drill type <b>A</b> at 2037 rpm, (a) 0.05 mm/rev (b) 0.20 mm/rev. .....	98
Figure 5.8: Cutting power in the drilling of Al6061-T6 workpiece of thickness 8.9 mm using standard twist drill type <b>B</b> at 2037 rpm, (a) 0.05 mm/rev (b) 0.20 mm/rev. .....	99

Figure 5.9: Cutting power data during the drilling of 8.9 mm Al6061-T6 stock thickness using standard twist drill (a) type <b>A</b> , (b) type <b>B</b> . .....	100
Figure 5.10: Micrograph of samples drilled to depths (I) 8.328 mm, (II) 8.614 mm, (III) 8.90 mm & (IV) 10.616 mm, at rotation speeds of 2037 rpm (A) feed of 0.05 mm/rev & (B) feed of 0.20 mm/rev.....	103
Figure 5.11: Illustration of data representation for hardness test values. ....	105
Figure 5.12: Vickers hardness values of Al6061-T6 at breakout depth, $t_{Br1}$ of 1.5 mm to exit surface, using drill type <b>B</b> at feed 0.15 mm/rev and speed 2037rpm. ..	106
Figure 5.13: Vickers hardness values of Al6061-T6 at breakout depth, $t_{Br2}$ of 0.8 mm to exit surface, using drill type <b>B</b> at feed 0.15 mm/rev and speed 2037rpm. ..	107
Figure 5.14: Vickers hardness values of Al6061-T6 at breakout depth, $t_{Br3}$ 0.5 mm to exit surface, using drill type <b>B</b> at feed 0.15 mm/rev and speed 2037rpm. ....	108
Figure 6.1: Schematic illustration of deep-hole drilling Power data. ....	110
Figure 6.2: Illustration of successive incremental hole-depth in drilling. ....	115
Figure 6.3: FED curve in the drilling of Al6061-T6, workpiece thickness 8.9 mm using standard twist drill type <b>A</b> , at (a) 2037 rpm (b) 2547 rpm.....	118
Figure 6.4: FED curve in the drilling of Al6061-T6, workpiece thickness 8.9 mm using drill type <b>B</b> , at (a) 2037 rpm (b) 2547 rpm (c) 3056 rpm. ....	119
Figure 6.5: Points of interest on the change-rate curve for FED data.....	120
Figure 6.6: Change-rate curve for FED using drill type <b>A</b> at 2037 rpm and feed (a) 0.05 mm/rev (b) 0.10 mm/rev (c) 0.15 mm/rev (d) 0.20 mm/rev.....	122
Figure 6.7: Change-rate curve for FED using drill type <b>A</b> at 2547 rpm and feed (a) 0.05 mm/rev (b) 0.10 mm/rev (c) 0.15 mm/rev (d) 0.20 mm/rev.....	123

Figure 6.8: Change-rate curve for FED using drill type <b>B</b> at 2037 rpm and feed (a) 0.05 mm/rev (b) 0.10 mm/rev (c) 0.15 mm/rev (d) 0.20 mm/rev.....	123
Figure 6.9: Change-rate curve for FED using drill type <b>B</b> at 2547 rpm and feed (a) 0.05 mm/rev (b) 0.10 mm/rev (c) 0.15 mm/rev (d) 0.20 mm/rev.....	124
Figure 6.10: Change-rate curve for FED using drill type <b>B</b> at 3056 rpm and feed (a) 0.05 mm/rev (b) 0.10 mm/rev (c) 0.15 mm/rev (d) 0.20 mm/rev.....	124
Figure 6.11: Chisel edge positions at breakout (a) breakout burr initiation, P1 (b) deformation zone depth, P2, during the drilling of 8.9 mm thick Al6061-T6 workpiece using twist drill type <b>A</b> .....	125
Figure 6.12: Chisel edge position at breakout (a) breakout burr initiation, P1 (b) deformation zone depth, P2, during the drilling of 8.9 mm thick Al6061-T6 workpiece using twist drill type <b>B</b> .....	126
Figure 6.13: CED curve in the drilling of Al6061-T6, workpiece thickness 8.9 mm using standard twist drill type <b>A</b> , at (a) 2037 rpm (b) 2547 rpm.....	131
Figure 6.14: CED curve in the drilling of Al6061-T6, workpiece thickness 8.9 mm using standard twist drill type <b>B</b> , at (a) 2037 rpm (b) 2547 rpm (c) 3056 rpm.....	133
Figure 6.15: Points of interest on the change-rate curve for a CED data.....	134
Figure 6.16: Change-rate curve for CED using drill type <b>A</b> at 2037 rpm and feed (a) 0.05 mm/rev (b) 0.10 mm/rev (c) 0.15 mm/rev (d) 0.20 mm/rev.....	135
Figure 6.17: Change-rate curve for CED using drill type <b>A</b> at 2547 rpm and feed (a) 0.05 mm/rev (b) 0.10 mm/rev (c) 0.15 mm/rev (d) 0.20 mm/rev.....	135
Figure 6.18: Change-rate curve for CED using drill type <b>B</b> at 2037 rpm and feed (a) 0.05 mm/rev (b) 0.10 mm/rev (c) 0.15 mm/rev (d) 0.20 mm/rev.....	136

Figure 6.19: Change-rate curve for CED using drill type <b>B</b> at 2547 rpm and feed (a) 0.05 mm/rev (b) 0.10 mm/rev (c) 0.15 mm/rev (d) 0.20 mm/rev.....	136
Figure 6.20: Change-rate curve for CED using drill type <b>B</b> at 3056 rpm and feed (a) 0.05 mm/rev (b) 0.10 mm/rev (c) 0.15 mm/rev (d) 0.20 mm/rev.....	137
Figure 6.21: Critical points at breakout (a) ploughing initiation, P3 (b) continuous ploughing, P4, during the drilling of 8.9 mm thick Al6061-T6 workpiece using twist drill type <b>A</b> . .....	139
Figure 6.22: Critical points at breakout (a) ploughing initiation, P3 (b) continuous ploughing, P4, during the drilling of 8.9 mm thick Al6061-T6 workpiece using twist drill type <b>B</b> . .....	140
Figure 6.23: Mechanisms of breakout burr formation and Drilling Zones.....	142
Figure 6.24: 15 steps drilling of Al 6061-T6 alloy at tool breakout using type <b>A</b> twist drill at spindle speed of 2037 rpm and feed of 0.05 mm/rev.....	147
Figure 6.25: The average Vickers hardness values of Al6061-T6 at breakout depth, $t_{Br1}$ of 1.5 mm to exit surface, using drill type <b>B</b> at feed 0.15 mm/rev and speed 2037rpm.....	149
Figure 6.26: The average Vickers hardness values of Al6061-T6 at breakout depth, $t_{Br2}$ of 0.8 mm to exit surface, using drill type <b>B</b> at feed 0.15 mm/rev and speed 2037rpm.....	150
Figure 6.27: The average Vickers hardness values of Al6061-T6 at breakout depth, $t_{Br3}$ of 0.5 mm to exit surface, using drill type <b>B</b> at feed 0.15 mm/rev and speed 2037rpm.....	151

## Nomenclature

ASTM	American Society for Testing and Materials	
CNC	Computer Numerical Control	
CED	Cutting energy-difference	
DAQ	Data Acquisition	
EDA	Energy-difference Approach	
FED	Feed energy-difference	
HSS	High Speed Steel	
NC	Numerical Control	
PCM	Process Condition Monitoring	
$b$	Depth of cut	[ <i>mm</i> ]
$C, C_1, C_2$	Constants of approximation	
$E_A$	Energy expended in drilling to point A	[ <i>joules</i> ]
$E_B$	Energy expended in drilling to point B	[ <i>joules</i> ]
$E_{AB}$	Energy expended in drilling from point A to B	[ <i>joules</i> ]
$E_{diff}$	Energy difference	[ <i>joules</i> ]
$E_k$	Energy measured at arbitrary hole depth	[ <i>joules</i> ]
$E_n$	Energy at an incremental drilled depth	[ <i>joules</i> ]
$d$	Tool diameter or twist drill diameter	[ <i>mm</i> ]
$d_{inc}$	Drill point depth increment	[ <i>mm</i> ]
$D$	Constants of approximation	

$F$	Friction force in orthogonal cutting	[N]
$F_N$	Normal force	[N]
$F_C$	Cutting force in orthogonal cutting	[N]
$F_t$	Thrust force in orthogonal cutting	[N]
$f_r$	feedrate	[m/min]
$F_S$	Shear force on the shear plane	[N]
$F_{th}$	Thrust force in metal drilling	[N]
$HV$	Vickers hardness	[N/mm <sup>2</sup> ]
$i$	Angle of inclination or angle of obliquity	[degrees]
$k, k_1, k_2$	Shear stress on slip-line and shear flow stress	[N/mm <sup>2</sup> ]
$K$	Constant of material	[degrees]
$L$	Lead of the flute helix of the twist drill	[mm]
$M$	Moment of forces along the slip-line	[Nm]
$N$	Normal to friction force in orthogonal cutting	[N]
$N_S$	Normal to shearing force in orthogonal cutting	[N]
$p, p_B, p_r$	Normal stress/hydrostatic stress on the slip-line	[N/mm <sup>2</sup> ]
P1	Point of breakout burr initiation	[mm]
P2	Deformation zone depth	[mm]
P3	Point of ploughing initiation	[mm]
P4	Point of ploughing dominance	[mm]
$r$	Radius at any point of twist drill cutting edge	[mm]
$r, r_A, r_B$	Distance long the slip-line in orthogonal cutting	[mm]

$r_b$	Chip depth ratio	
$r_t$	Chip thickness ratio	
$R$	Resistance force	[N]
$S_1, S_2$	Distances along slip-line	[mm]
$t$	Depth of cut in orthogonal cutting	[mm]
$t_c$	Chip thickness	[mm]
$t_H$	Work-hardened layer thickness	[mm]
$t_{Br}, t_{Br_1}, t_{Br_2}, t_{Br_3}$	Breakout distance or breakout depth	[mm]
$t_W$	Workpiece thickness	[mm]
$t_{Wc}$	Critical depth	[mm]
$u$	Drilling power/total power expended in drilling	[Nm/s]
$u_{cl}$	Power due to chip clogging effect	[Nm/s]
$u_{cut}$	Specific cutting power due to shearing	[Nm/s]
$u_f$	Power due to chip flow resistance	[Nm/s]
$u_{th}$	Feed power/power expended due to thrust force	[Nm/s]
$V$	Cutting speed	[m/min]
$V_c$	Chip velocity	[m/min]
$w$	Web thickness	[mm]
$\alpha$	Rake angle	[degrees]
$\alpha_e$	Effective rake angle	[degrees]
$\alpha_f$	Face rake angle	[degrees]
$\alpha_n$	Normal rake angle	[degrees]

$\alpha_v$	Velocity rake angle	[degrees]
$\beta$	Friction coefficient angle	[degrees]
$\delta$	Helix angle of a twist drill	[degrees]
$\eta$	True chip-flow angle	[degrees]
$\eta_c$	Chip-flow angle	[degrees]
$\eta_p$	Projected chip-flow angle	[degrees]
$\xi$	Web angle	[degrees]
$2\rho$	Drill point angle	[degrees]
$\sigma_n$	Normal stress/compressive stress on shear plane	[N/mm <sup>2</sup> ]
$\tau, \tau_s$	Shear stress on shear plane	[N/mm <sup>2</sup> ]
$\tau_o$	Constant of material	[N/mm <sup>2</sup> ]
$\phi$	Shear angle	[degrees]
$\phi_e$	Effective shear angle	[degrees]
$\phi_n$	Normal shear angle	[degrees]
$\Phi$	Elevation angle	[degrees]
$\psi$	Inclination of the slip-line to some datum direction	[degrees]

## **Chapter 1: Introduction**

An investigation of the burr formation mechanism at the exit surface of a workpiece during the metal drilling process is the subject matter of this research. The approach put forth in this study has implemented and developed new knowledge in energy-aware machining, material deformation mechanics during metal cutting (specifically drilling), and basic material analysis to focus on exploring the tool breakout phenomenon which leads to the formation of an exit burr in metal drilling. Central to the research, a novel approach that uses energy analysis to investigate the drilling mechanics and process changes in metal drilling processes have been developed. The following section begins with an overview of the research work performed to investigate exit burr (breakout burr) formation in metal drilling processes. This is followed by a brief explanation of the background and the scope and objectives of the research. The section concludes with a presentation of the thesis layout.

### **1.1 Overview**

Metal cutting is a chip formation process that removes unwanted material from a workpiece material to form some predefined shape and geometry. The material removal process occurs through severe plastic deformation or shearing, which is characterized by large plastic strains, high strain rates, and elevated temperatures. The process involves a considerable amount of energy. The tool-workpiece interaction in cutting is based on the relative movement between a cutting tool, which is a harder material with a relatively sharp

edge or wedge-shape, and some stock workpiece material that results in the formation of chips and a newly machined surface. Common machining processes are drilling, milling and turning operations, which are carried out on machine tools. Each material removal process comes with its own challenges and all of them generate newly machined surfaces, produce chips and machining burrs.

Drilling is one of the most common machining operations, used to create round holes in workpiece materials using cutting tools known as drill bits. The operation involves rotating a cutting tool and feeding the tool into the workpiece in a direction parallel to its axis of rotation. An essential feature is a variation in cutting speed along the cutting edges with the maximum speed at the periphery that generates the cylindrical machined surface. The complex nature of the tool geometry and subsequent mechanics have posed significant challenges to researchers in studying and modeling the process. Practical challenges in metal drilling processes range from designing the right tool for the operation to creating a hole with the required geometrical accuracy, surface integrity, and a minimal burr form.

Burr formation in drilling is a major concern in manufacturing. Burrs are projections of plastically deformed material left at the edge of a round hole or machined edge. They are a dangerous by-product of machining as the sharp burr can result in cuts to operators and present challenges in the assembly of machined components. Deburring operations are costly and always required, thus raising the cost of machined components. It has been found from both theoretical and experimental observations that burrs cannot be prevented by changes in feed, speed, and tool geometry alone. However, the size of the burrs produced can be minimized by appropriate machining parameters [1].

The need for an efficient and cost-effective system has led researchers to undertake several studies in the areas of process planning, energy-aware studies, and the design of tools and machine tools used in production processes. Machining time and process parameter optimization are generally key features for producing products at a reduced cost, but metal drilling processes are also faced with the difficulty of drilling holes at accurate eccentricity, good surface roughness, and controlled burr formation.

The current research puts forth an innovative approach that combines thrust force and cutting power data to identify the onset of burr formation during the metal drilling process. In addition, energy analysis is used to identify critical process changes in the mechanics of drilling and identify material deformation information during the drilling and subsequent burr formation process.

## **1.2 Background**

Metal drilling involves the removal of unwanted chip material from metals and alloys to form a round hole. The process occurs through rotating a drilling tool and feeding it into a work material in a direction parallel to the axis of rotation of the tool. The drilling tools are end-cutting tools and are designed with one to four flutes or grooves for chip disposal, and as a passage for the application of cutting fluid. The chip formation process occurs through shearing of the workpiece material as the cutting edges or lips interact with the workpiece material, and new surfaces are formed. Metal drilling is a highly dynamic machining process, which is mainly due to the complex nature of the drill point geometry and the operation. This poses difficulties in the development of a simplistic model that makes possible the analysis of the process. The tool geometry design plays a significant role in

the performance of the chip formation process, the surface integrity of the hole and burr formation in relation to work material and process parameters.

Like other machining operations, metal drilling processes are faced with the problem of burr formation on the exterior of the machined surfaces. This occurs at both the entrance and the exit surface of a drilled through-hole. Entrance burrs are a result of plastic flow as the tool drills into the workpiece material, and the exit burr is a projection of plastically deformed material at the exit of the hole. These burrs impact the quality and efficiency of the process, and the overall cost of the manufactured product, as deburring operations are required and costly. Most burr related problems are associated with exit burrs since the burrs formed at the exit of a hole are much larger than those at the entrance.

A great deal of research has focused on the deburring of machined parts and components [2-5], while very little has focused on understanding the mechanism of exit burr formation in metal drilling [6-10]. Since breakout burrs cannot be prevented, they must be reduced through controlled strategic planning based on an understanding of exit burr formation mechanisms, thereby reducing deburring costs. Most of the research work has been done through methods that are difficult to replicate and near impossible to implement on a practical level. There is a need to develop a method used to investigate the breakout mechanism and burr formation process that considers a technique that takes into account the mechanics of the drilling process in relation to work material and the process parameters. Understanding the burr formation phenomenon and mechanism could aid in developing a method or machining approach that minimizes the drilling breakout burrs.

### **1.3 Scope and Objective**

To better understand the burr formation process and reduce burrs that form during drilling, an understanding of the mechanism of the chip formation process and the changes in the mechanics of the process as the drill point approaches the exit surface of the work material is required. The behavior of the work material prior to tool breakout is an essential parameter in the study of burr formation. However, the complex geometry and highly dynamic nature of the metal drilling process make developing a simplistic model for the analysis of the mechanics of the process a challenging task. However, several researchers have embarked on the analysis of the process through the development of empirical models and some laborious models difficult to replicate.

As a result, the research work presented in this thesis focuses on developing an approach that uses experimental data to investigate the exit burr formation process. The research has the following objectives:

1. To develop a novel method that uses energy analysis to identify unique points that correspond to process mechanics changes during the drilling process.
2. To develop a novel method for identifying the initial onset of the burr formation mechanism.
3. To develop a method for discretizing and identifying changes that occur during the actual burr formation process so that the process can be better understood.
4. To combine experimental thrust force and cutting power data from drilling experiments to create an energy analysis approach for drilling research.

5. To use photomicrographs observation and microhardness testing of experimental samples to analyze the different stages of the burr formation process and validate the results obtained from the energy analysis.

To achieve these objectives, a series of drilling experiments were performed with the aim of using thrust force and cutting power signals to identify critical points of burr formation and burr formation initiation during drilling. Using real-time power data, the research attempts to identify the transition from steady-state cutting to ploughing of the cutting tool, and the deformation zone that forms at the start of the burr formation process. This novel work will combine thrust force and cutting power signals with knowledge of the microstructure and hardness characteristics of the workpiece material below the drill point of the twist drill to identify the transition in the cutting process and deformation mechanics that lead to burr formation.

Combining experimental thrust force and cutting power measurements to investigate the burr formation mechanism will allow for the identification of changes in the cutting process during cutting tool breakout. This will then be used to analyze the exit burr formation mechanism in the metal drilling processes. The findings could aid in the development of predictive models for breakout burr formation during metal drilling. Furthermore, an understanding of the exit burr formation mechanism could aid in the development of process planning strategically designed to mitigate the exit burrs formed during drilling processes. It is important to note that this innovative approach to investigating the breakout burr formation will open a whole new world to the study of breakout burrs in drilling operations. It will also introduce the use of energy analysis in

identifying process changes and change in the mechanics of drilling and machining processes in relation to the process and material.

## **1.4 Thesis Layout**

The content of this dissertation has been organized into seven distinct chapters, which begins with an introduction and a brief background of the proposed research and an outline of the scope and objective of the research work, in Chapter 1. Chapter 2 presents the literature review- which includes a review of the chip formation process and the mechanisms of plastic deformation during chip formation in metal cutting, an overview of the metal drilling processes with a look into the tool design concept and features as well as some of the early research conducted on the mechanics of drilling processes, the concept of drill point geometry and analysis of thrust force and torque in metal drilling, problems associated with metal drilling processes, burr formation and the mechanisms of the process in metal cutting processes and specifically drilling. Since burr formation cannot be prevented, some of the work on the burr minimization schemes and deburring approaches are also reviewed.

Chapter 3 reviews the application and implementation of force and power signals in process condition monitoring. The experimental work of this research is detailed in Chapter 4. The chapter begins with a brief overview followed by an introduction of a new concept of classifying through-hole in drilling by zones, a discussion of the workpiece material used in the experiment, the experimental setup, and the procedure used in this research. Chapter 5 is a presentation of the experimental results for all of the work performed, followed by a comprehensive discussion of the results in Chapter 6. Finally,

Chapter 7 presents the conclusion, with a summary of the research work done, results and findings, the contributions made, and potential future work.

## **Chapter 2: Literature Review**

In metal cutting, workpiece material is removed through a shearing process that results during the interaction between a harder material (cutting tool) and the workpiece from which the required part or component is produced. There are several metal cutting operations performed in industries, and each operation uses a defined cutting tool for the process. These cutting tools have very good hardness and toughness characteristics and have relatively sharp edges for the cutting of workpiece materials. In this section, an extensive review of literatures in the area of the general machining operations in relation to chip formation, the mechanics of metal cutting and material behavior, the metal drilling process, and the burr formation process with focus placed on metal drilling, will be reviewed.

### **2.1 General Machining Operations**

The process of shaping an object or component through the removal of excess material to form the desired shape is a very old practice. Unwanted materials are removed using a harder material with a distinct cutting edge. These cutting tools could be a single point as in turning, or multiple points as in drilling, milling, etc., and these processes are performed on a machining system known as machine tools.

Machine tools can be grouped into three principal types: conventional machine tools, production machine tools, and CNC (computer-numerically-controlled) machine tools. Keeping in line with this research, we will only focus on CNC machine tools, which are used in the machining of complex parts with a high degree of accuracy and

repeatability. They are used for low and high-volume production as long as the materials and cutting parameters are adequate and available. An example of a CNC machine is the Okuma OSP-U100M three-axis CNC machine tool shown in Figure 2.1.



**Figure 2.1: CNC machine tool.**

Poor design of a cutting tool may lead to reduced productivity through tool wear or failure that would result in increased production costs. A cutting tool material should be strong enough to withstand high stress, tough enough to withstand impact without fracture, and should have a good heat resistance property. The commonly available cutting tool materials are high-speed steel (HSS), carbides, ceramics, diamond, and some cobalt-based alloys. A 50% increase in tool life reduces the total cost per component by 1 to 2%, and a 20% increase in the material removal rate could reduce the total cost per component by 15% [11]. Depending on tool design and the type of cutting operation, the cutting edge of the tool interacts with the workpiece material at relative motion removing unwanted workpiece material through a shearing process.

### 2.1.1 Machining and Chip Formation

Machining is a chip formation process in which a volume of plastically deformed material is removed from the workpiece to form the chip. In this process, there is relative motion between the cutting edge and workpiece material. This requires large amounts of energy as the chip formed is moved across the cutting tool face. A new surface of the desired shape is formed by the removal of the unwanted materials from the parent workpiece material. The material removed is plastically deformed and subjected to a concentration of shear along a shear plane, as illustrated in Figure 2.2. The shear plane is extended from the tip of the cutting tool to the free surface of the workpiece material at an angle  $\phi$  known as the shear angle. The type of chip formed is greatly influenced by the cutting process and the physical properties of the work material. The chip types formed in machining processes could be continuous, discontinuous, or continuous with a build-up-edge.

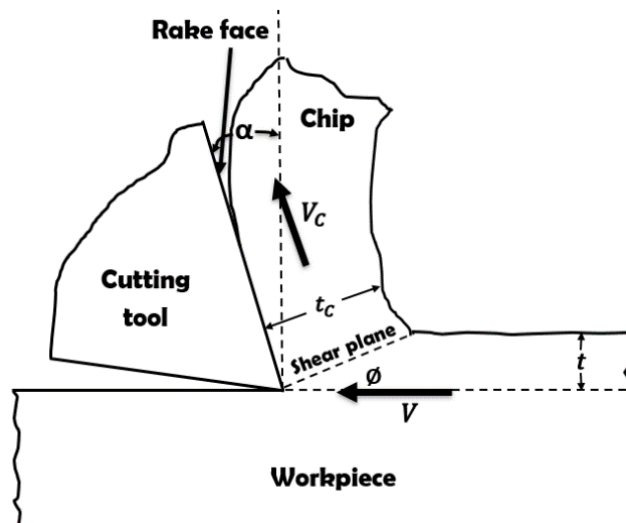


Figure 2.2: Chip formation process.

One of the earliest findings that give a quantitative understanding of the mechanism of metal cutting was set forth by Merchant [12]. His research developed simplified equations that made it possible to analyze metal cutting analytically. This analysis has been limited to the formation of continuous chips in an orthogonal cutting process (i.e. tool has a plane face and a single straight cutting edge, with the cutting-edge perpendicular to the direction of relative motion of the tool and workpiece). This is illustrated in Figure 2.2, with the cutting tool traveling from left to right. The cutting parameters of the cutting process are the cutting speed,  $V$ , the feed per revolution,  $t$ , and the depth of cut,  $b$ . The angle  $\alpha$  is the rake angle of the cutting tool edge. As the cutting tool moves relative to the workpiece at the cutting speed,  $V$ , the material is deformed and shears across the shear plane to form chips. The chip formed, with chip thickness  $t_c$ , moves across the rake face of the tool at a chip velocity,  $V_c$ , leading to further plastic flow of the chip as it rubs on the tool surface. This region is known as the secondary shear zone. A force relationship that permits the computation of the significant force components, the stresses, the coefficient of friction between the chip and cutting tool, and the work done in shearing the metal and in overcoming friction on the tool face has been obtained [12].

During steady-state cutting, as the friction between the tool rake-face and chip interface is increased, the plastic strain in the chip increases, and the shear angle decreases, leading to an increase in the chip thickness. The resulting increase in the length of the shear plane leads to an increase in the area of the shear plane. Therefore, the force required to shear the workpiece material along the shear plane also increases, assuming the shear stress on the shear plane remains constant. The reverse occurs with a decrease in friction at the tool-chip interface. There is a significant rise in temperature due to the energy expended

during the plastic deformation of the workpiece, especially when cutting at high speed. The steady-state cut referred to here is the cutting process leading to the formation of continuous chips.

Chip formation has been treated as a shearing process through a single plane extending from the cutting edge to the work surface ahead of the tool known as the shear plane. The shearing that occurs on the shear plane during the process has been illustrated by the successive displacement of cards, as shown in Figure 2.3. Each successive card is displaced forward a small amount with respect to its neighbor as the cutting tool progresses.

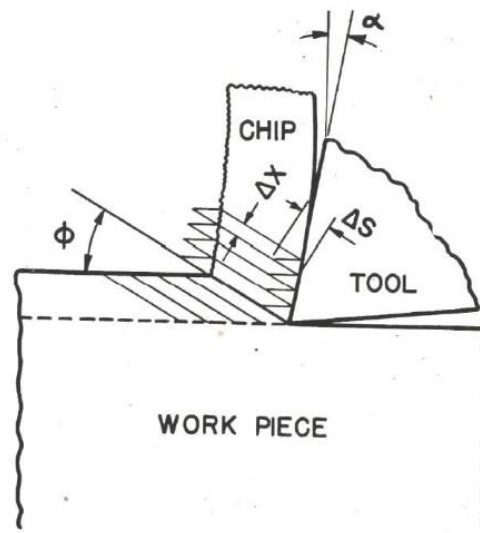


**Figure 2.3: Illustration of shearing strain  $\epsilon$ , in orthogonal cutting process,  $\epsilon = \Delta s / \Delta x$  [12].**

According to the principle of minimum energy, the shear angle  $\phi$  will assume a value so as to make the work done in cutting a minimum. Using the principle of minimum energy and assuming that the shear strength of the material is constant and is the only quantity controlling its plastic behavior, a simple plasticity condition was obtained for the

shear angle. However, it was found by experiment to give a poor approximation in the cutting of polycrystalline metal. The shear strength of metals is known to be influenced by temperature, rate of shear, shear strain, and the compression stress acting normal to the shear plane during cutting. By taking the compressive stress on the shear plane into account as a function of shear strength, a plasticity condition that establishes a relationship between the force system and the geometry of chip formation to a good approximation was obtained [13].

Many reports have taken a more general assumption in the analysis of the mechanics of the metal cutting process. Lee and Shaffer [14] proposed a model based on slip-line field theory using a simplified plasticity analysis for orthogonal metal cutting problems. In the analysis, it was assumed that the material is a rigid plastic, and the behavior is independent of the rate of deformation. The effects of temperature rise during deformation and inertia effects resulting from the acceleration of material during deformation were considered negligible. The deformation occurs on a plane that is inclined at an angle  $\phi$  with respect to the plane of cutting and the material is stressed to the yield point. Most research has work to compare predicted relationships between the shear angle,  $\phi$ , friction coefficient angle,  $\beta$ , and the rake angle,  $\alpha$ , with results from experiments [15-19]. These models are somehow limited in correlating with general experimental results. The analysis of orthogonal cutting that takes into account the material work-hardened effects have been reported by Oxley [20-24]. The model also varies the normal stress along the shear plane, giving a good agreement to the experimental results.

## **2.2 Mechanics of Metal Cutting, Material Behavior and Chip Formation**

Metal cutting is a chip formation process that involves the removal of unwanted materials from stock material to form a pre-defined shape or geometry. The material separation is essentially a plastic-flow process and occurs at exceptionally large strain and strain rate. The deformation is localized to an extremely small plastic zone and requires a large amount of energy. In an attempt to model the chip formation process, a photomicrograph technique was applied to observe the plastic-flow region that occurs during the process [12, 21, 25, 26]. However, there have been doubts as to the actual shape and size of the plastic zone for any machining operation. There are two prominent views in the study of plastic flow during metal cutting processes. One point of view claimed that the chip formation occurs by a simple shear plane that extends from the tool point to a point on a free surface, and no plastic flow occurs at either side of the shear plane [12, 27]. Based on this, a model was proposed, as shown in Figure 2.4(a). The other view suggested a plastic flow zone is extended from the tool point to the free surface, as shown in Figure 2.4(b), with Oxley as a major contributor [20-23].

Cautious investigation of photomicrographs and motion picture films indicate that the plastic deformation process during chip formation approximates to one of the suggested models under different conditions. Nonetheless, the mechanism of the cutting process can be analyzed by a single cutting edge. The simplest case of which has the cutting-edge perpendicular to the relative cutting velocity between the cutting tool and the work material, as illustrated in Figure 2.2, known as orthogonal cutting. This has been discussed briefly in Section 2.1.1. A case of a single tool cutting edge inclined to the relative cutting

velocity is known as oblique cutting. In this section, a detailed analysis of the mechanisms of plastic deformation during chip formation in metal cutting processes and the material behavior characteristics shall be reviewed.

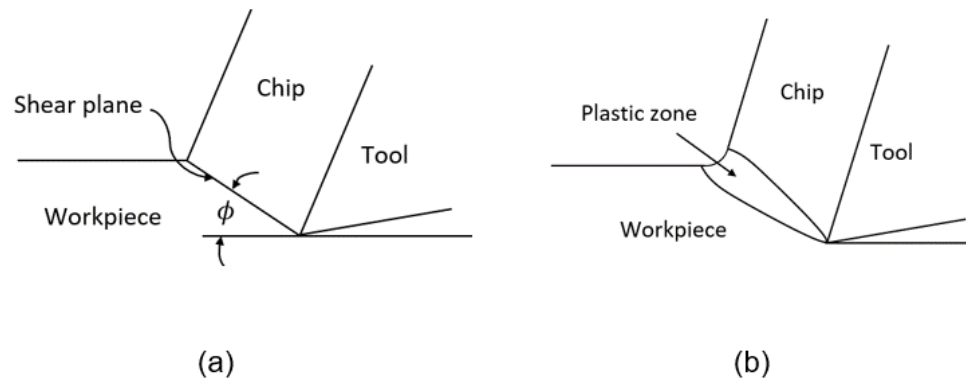


**Figure 2.4: Suggested shape for plastic deformation zone in cutting: (a) thin shear plane (b) thick shear zone.**

In the past century, various attempts have been made to develop a realistic model that would aid the understanding of the mechanism of chip formation in metal cutting without the need for empirical testing. These attempts have led to the understanding that the chip formation process occurs through the shearing of the workpiece material. However, there has been conflicting evidence about the nature of the deformation zone, as shown in Figure 2.4. Most experimental evidence indicates that the thick-zone model may describe the cutting process at very low speeds, whereas at higher speeds, most evidence indicates that a thin shear plane is reached [28]. The thin shear plane model also leads to a simpler mathematical model making it most likely used for analysis involving practical cutting conditions. In this section, some of the analysis of the chip formation in orthogonal cutting that uses these two models will be discussed.

### 2.2.1 Analysis of Thin-Zone Model

Merchant [12], research work on the analysis of the mechanics of orthogonal cutting with type 2 chip was put forth to develop an analytical model that makes possible the prediction of basic physical quantities during metal cutting processes. And by presenting a set of assumptions required for the orthogonal cutting process, a force diagram was constructed, as shown in Figure 2.5, for the analysis of the force system and geometrical quantities due to the shearing of the work material and chip flow during the chip formation process. This illustrates that the chip is formed through a shearing process which is approximately confined to a single plane extending from the cutting edge to a free surface on the workpiece ahead of the cutting tool. This plane of deformation was observed from the photomicrograph and is known as the shear plane. An illustration of the cutting process is shown in Figure 2.2.

In this analysis, the chip was considered as a body held in stable equilibrium by the action of two forces exerted at the chip-tool interface and across the shear plane. The resultant of the forces,  $R$ , keeps the chip in equilibrium. By resolving  $R$  into components, the cutting force,  $F_C$ , which is responsible for the work done in cutting has been obtained in the direction of motion of the tool relative to work, and the thrust force,  $F_t$ , which is perpendicular to  $F_C$ . Along the shear plane is the shearing force,  $F_S$ , responsible for the work expended in the shearing of the workpiece material, and a normal component,  $N_S$ , which exerts compressive stress on the shear plane. Along the chip-tool interface is the friction force,  $F$ , responsible for the work expended in friction as a result of the chip sliding over the rake face of the cutting tool, while the normal force,  $N$  is perpendicular to  $F$ .

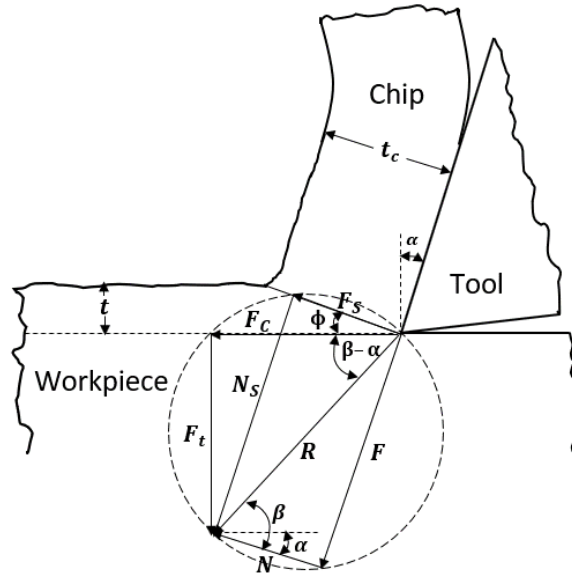


**Figure 2.5: Diagram of force components in orthogonal cutting.**

By resolving the resultant force into force components, as shown in Figure 2.5, the cutting force and the thrust force are obtained as

$$F_c = \frac{tb\tau \cos(\beta - \alpha)}{\sin \phi \cos(\phi + \beta - \alpha)} \quad (2.1)$$

$$F_t = \frac{tb\tau \sin(\beta - \alpha)}{\sin \phi \cos(\phi + \beta - \alpha)} \quad (2.2)$$

where  $\beta$  is the friction angle between chip and tool rake face,  $\tau$  is the shear stress on the shear plane of the material been cut and is assumed to have the value of the yield shear strength of the work material and is constant over the plane irrespective of the shear angle  $\phi$ , and  $b$  is the width of cut.

It is evident that the physical properties governing the plastic behavior of work material determine what value the shear angle,  $\phi$  will take up for a given value of the angle  $(\beta - \alpha)$ , as shown in Figure 2.5. The plasticity condition for the cutting condition was applied, by using the principle of minimum energy, that  $\phi$  will assume a value to make the

total work done in cutting a minimum. This was achieved by differentiation of equation (2.1) and equating to zero, which gives

$$\frac{dF_C}{d\phi} = \frac{tb\tau \cos(\beta - \alpha) \cos(\phi + \beta - \alpha)}{\sin^2 \phi \cos^2(\phi + \beta - \alpha)} = 0$$

Thus, the shear angle

$$\phi = \frac{\pi}{4} + \frac{\alpha}{2} - \frac{\beta}{2} \quad (2.3)$$

Merchant [13], found that the shear angle,  $\phi$ , obtained by applying equation (2.3) gives a poor approximation with experimental results in the case of polycrystalline metal. This is because the shear strength of the polycrystalline metal is not constant along the shear plane but is influenced by different quantities, like the shearing strain, strain rate, temperature and the compressive stress acting normal to the shear plane. By reconsidering the assumption used in the theory and accounting for the effect of the compressive stress, a new relationship was obtained for the shear stress as

$$\tau_s = \tau_o + K\sigma_n \quad (2.4)$$

where  $\tau_o$  and  $K$  are constants of the material. This indicates that the shear strength  $\tau_s$  across the shear plane increases linearly with increasing normal stress  $\sigma_n$ , as shown in Figure 2.6. At zero compressive stress,  $\tau_s$  is equal to  $\tau_o$ . By putting the new expression for shear strength into equation (2.1) and applying the principle of minimum energy. The plasticity condition for the shear stress is rewritten as

$$2\phi + \beta - \alpha = \cot^{-1} K \quad (2.5)$$

This expression for the shear angle is also an approximation, since it takes no account of the effect of the plastic strain, shear rate, and the temperature rise that occurs

during the chip formation process. However, it has been found to offer a good degree of approximation accurately enough for many metal cutting processes.

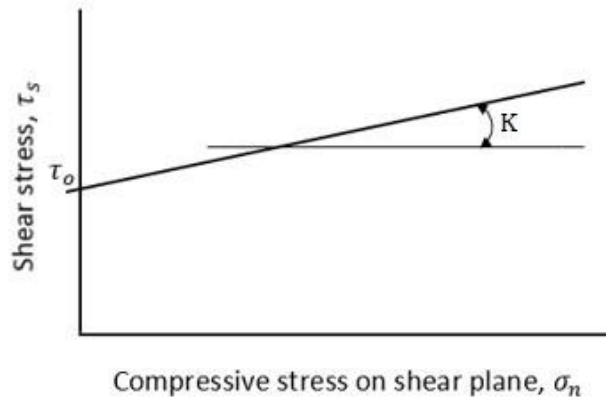


**Figure 2.6: Shear stress and compressive stress relation.**

### **2.2.2 Analysis of Thick-Zone Model**

Palmer and Oxley in 1958, made a laborious effort to investigate plastic flow that occurs during the metal cutting process, using a single point tool [29]. An experimental technique that uses film shots and photomicrographs was developed to observe individual grain paths during the metal cutting process at extremely slow speeds, and consequently, low temperatures. The technique was applied to a case of machining with the work material moving across a stationary cutting tool. Based on the observation capture by the film shots, two theoretical considerations were made in an attempt to analyze the cutting process. The first was based upon the ideal theory of plasticity, which poses challenges as it was impractical to find a consistent slip-line field that conforms with the observed results. On a second attempt, the theory of plasticity was expanded on by assuming the work-hardening

alone contributes to the variation of the material flow stress. Finally, an approximate analysis that incorporates the theory of plasticity and work-hardening effect was used to examine the experimental results.

At first attempt, the general shape of the plastic zone was idealized, as shown in Figure 2.7, which gives the possibility of constructing a slip-line field consistent with the idealized theory. Whereas, in fulfillment of the free-surface condition for a slip-line the boundaries, ADFB and BEC bend to meet the uncut surface at  $45^\circ$ . A major inconsistency in the use of the idealized theory of plasticity concerns the direction and position of the resultant force of the cutting tool. It was noted that the concepts of velocity discontinuities and stress singularities do not hold for a material of variable flow stress.

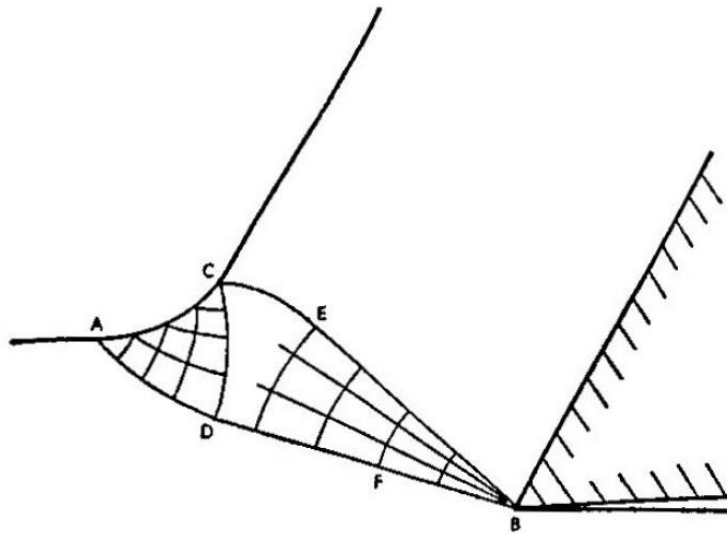


**Figure 2.7: Idealized plastic zone [29].**

Next, the analysis was done by assuming that work-hardening alone contributes to the variation in flow stress. The value of the flow stress at each point, relating equilibrium to the slip lines, was found by a modified form of the Hencky equations.

$$\left. \begin{aligned} p + 2k\psi + \int \frac{\delta k}{\delta S_2} \delta S_1 &= \text{constant along I slip-line} \\ p - 2k\psi + \int \frac{\delta k}{\delta S_1} \delta S_2 &= \text{constant along II slip-line} \end{aligned} \right\} \quad (2.6)$$

where  $S_1$  and  $S_2$  are distances along slip-lines of each family,  $p$  is the normal stress on the slip-line (hydrostatic stress),  $k$  is the shear stress on slip-line (shear flow stress), and  $\psi$  is the inclination of the slip-line to some datum direction. It was assumed that the curves represent slip-lines, and the boundary condition set by the velocity of the work entering the plastic zone. It was also suggested that the tool point does not make contact with the work material and that tool-chip contact occurs somewhere up the face of the tool. The slip-line field near the tool point was not determined using Hencky relations eliminating the possibility of a stress singularity or discontinuity at the tool point.

The introduction of the work-hardening effect to the theory produced a stress distribution that conformed with observed results, for the position and direction of the tool force. However, the tasking nature of the analysis prompted the development of some more approximate approach for the analysis. The boundary  $AB$  between the work and plastic zone was assumed to be a straight slip-line inclined at an angle  $\phi$  to the direction of cutting. This slip-line bends at the free surface to make an angle  $45^\circ$  with the surface at an insignificant distance. The straight slip-line field  $AB$  was illustrated as part of a centered fan with its center at  $O$ , as depicted in Figure 2.9. From equation (2.6), the hydrostatic stress on the boundary at  $A$  is given by

$$p = -k_1 \left[ 1 + 2 \left( \frac{\pi}{4} - \phi \right) \right] = -Ck_1 \quad (2.7)$$

where  $k_1$  is the flow shear stress constant along  $AB$ . The negative sign indicates compressive stress at  $A$ . By considering the adjacent slip-line  $OE$  inclined at an angle  $\delta\phi$

to the first, the strain and flow shear stress along  $AB$  must be constant. Applying the modified Hencky equation, the rate of change of  $k$ , a distance  $r$  from  $O$  is expressed as

$$\frac{\delta k}{\delta S_1} = \frac{k_2 - k_1}{r \delta \phi} = D \cdot \frac{k_1}{r} \quad (2.8)$$

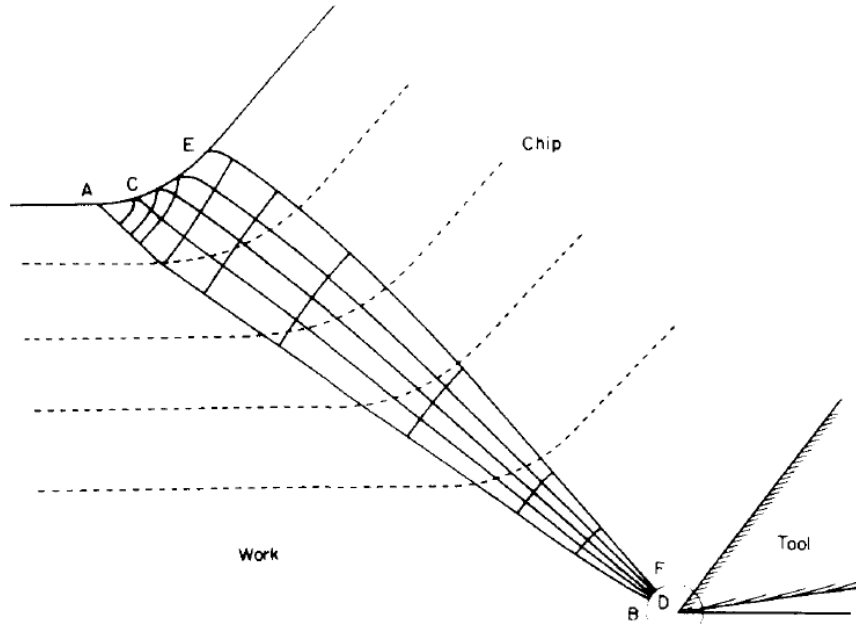


**Figure 2.8: Slip-line field constructed from observed flow field [22].**

The normal or hydrostatic stress on  $AB$  at a distance  $r$  from  $O$  is given by

$$p_r = -Ck_1 + \int_r^{r_A} \frac{\delta k}{\delta S_1} \delta S_2 \quad (2.9)$$

and is integrated to

$$p_r = -Ck_1 + Dk_1 \ln\left(\frac{r_A}{r}\right) \quad (2.10)$$

Similarly, the hydrostatic stress at the tool point  $B$  is given by

$$p_B = -Ck_1 + Dk_1 \ln\left(\frac{r_A}{r_B}\right) \quad (2.11)$$

The normal force across the line  $AB$  is given by

$$F_N = -k_1 b \left\{ C k_1 (r_A - r_B) - D k_1 \left[ (r_A - r_B) - r_B \ln \left( \frac{r_A}{r_B} \right) \right] \right\} \quad (2.12)$$

and the shear force along  $AB$  is given by

$$F_S = -k_1 b (r_A - r_B) \quad (2.13)$$

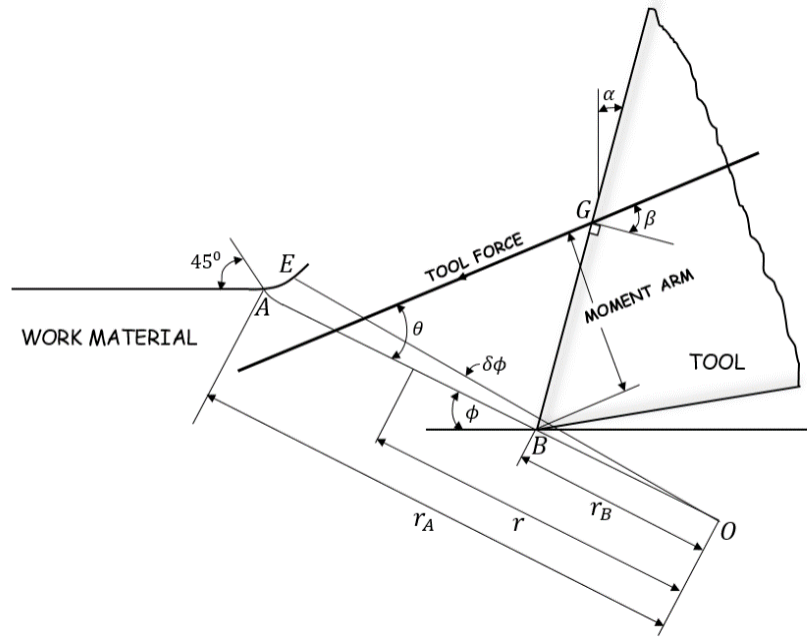


**Figure 2.9: Geometry for the approximate analysis.**

Therefore, the angle  $\theta$  measured counterclockwise from  $AB$  is expressed as

$$\tan \theta = \frac{F_N}{F_S} = C - D + \frac{C + \frac{p_B}{k_1}}{e^{\frac{1}{D}(C + \frac{p_B}{k_1})} - 1} \quad (2.14)$$

while the moment of the forces acting on  $AB$  about the fan center  $O$  is expressed as

$$M = -b \frac{k_1}{2} \left[ (r_A^2 - r_B^2) \left( C - \frac{D}{2} \right) + D r_B^2 \ln \left( \frac{r_A}{r_B} \right) \right] \quad (2.15)$$

The magnitude, direction, and position of the resultant cutting force for given friction angle,  $\beta$ , rake angle,  $\alpha$ , and depth of cut,  $b$ , can be determined as long as suitable values of  $p_B$  and  $D$  could be determined. From equilibrium of the forces on the tool and chip,

$$\theta = \phi + \beta - \alpha \quad (2.16)$$

An approximate relation between  $D$ ,  $\phi$ , and  $\theta$  on the condition that  $AB$  and the adjacent slip-line must transmit the total cutting force. Thus, for small  $\delta\phi$  it is reduced to

$$D \cong \cot \phi - \tan \theta \quad (2.17)$$

On account of this analysis, Palmer and Oxley suggested a chip formation geometry once the steady-state condition of cutting is attained, as depicted in Figure 2.10. This shows that the tool cutting edge takes no part in the cutting and that the line of action of the tool cutting force is conveyed at a distance above the cutting edge. Stress within the plastic zone varied from compression near the outer free surface to large tension near the tool point.

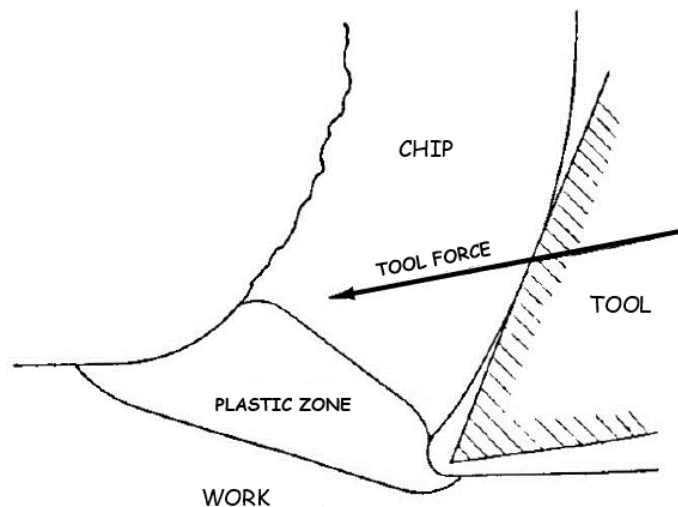


**Figure 2.10: Suggested cutting process by Palmer and Oxley [29].**

A notable feature of the analysis is that the effect of work-hardening incorporated in the theory of plasticity can be used in the study of the chip formation process when cutting at very low speed. Nonetheless, the letdown in this investigation is that the deformation and cutting forces cannot be predicted analytically. Also, there have been concerns regarding the line of action of the cutting force and the feature of no contact at the tool point of the cutting tool.

### 2.2.3 Shear Angle Relationships in Metal Cutting

The analysis of the metal cutting process has shown that the shear angle is an essential quantity for the prediction of cutting forces and is a very important feature in the estimation of plastic flow and deformation during metal cutting. Over the years, a significant amount of effort has been put into the study of the shear angle relationship. A thorough review of these relationships shows that most could be reduced to the form

$$\phi = C_1 - C_2(\beta - \alpha) \quad (2.18)$$

where  $C_1$  and  $C_2$  are constants [28].

One of the earliest and possibly the best approximate model is known as the Merchant's shear angle [12]. The chip formation process assumes a shear angle,  $\phi$ , such that the work-done and cutting force is minimum. The shear angle relationship was obtained as

$$\phi = \frac{\pi}{4} - \frac{1}{2}(\beta - \alpha) \quad (2.19)$$

where  $\alpha$  is the rake angle, and  $\beta$  is the angle of friction at the tool-chip interface during the chip formation process. Based on experimental observation, it was found that values

obtained from this expression were in poor agreement with experimental results. In an attempt to improve the results, Merchant [13] assumed that the shear strength of the work material is dependent on the normal compressive stress acting on the shear plane, and from this, a modified equation was obtained for the shear stress along the shear plane. This is given as

$$2\phi = \cos^{-1} K - (\beta - \alpha) \quad (2.20)$$

where the slope of the curve of the shear strength against the normal stress is given by  $K$ .

Detailed analysis of the work done by Merchant has been presented in Section 2.2.1.

The shear angle model by Lee and Shaffer [14], was obtained by applying the theory of plasticity to the problem of orthogonal cutting. The model has assumed that all deformation occurs along the thin shear plane and that there must be a stress field within the chip to transmit the cutting forces from the shear plane to the tool face. This was represented by a slip-line field in which no deformation occurs due to the transmission of force, although the material was stressed to the yield stress in the region  $ABC$ , as shown in Figure 2.11a). It has assumed that the full cutting force transmits over the base of the plastic zone in contact with the tool.

The model has based on the assumption that the state of stress in the plastic zone is constant and the normal compressive stress on the shear plane is equal to the shear stress  $\tau$ . The uniform stress state in the rigid region  $ABC$ , has made possible the application of Mohr's circle for the stresses at the boundaries of the stress zone as depicted in Figure 2.11b).

From the geometry on the stressed zone shown in Figure 2.11(a),

$$\phi = \alpha + \eta$$

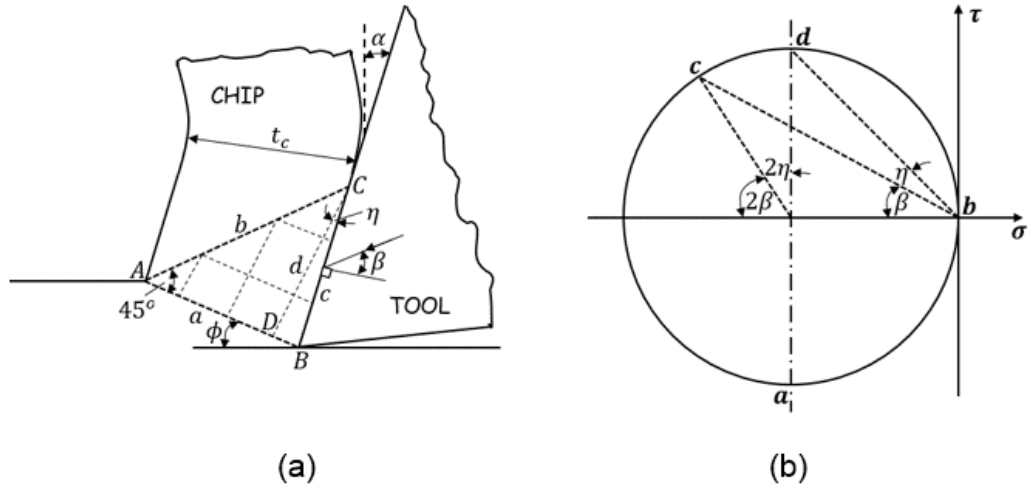


**Figure 2.11: Ideal plastic Solution for stress field at tool tip (a) Lee and Shaffer slip-line field (b) Mohr circle diagram for the stress zone *ABC*.**

From the Mohr's circle in Figure 2.11(b),

$$\eta = \frac{\pi}{4} - \beta$$

Thus, the shear angle relationship was obtained, given as

$$\phi = \frac{\pi}{4} - (\beta - \alpha) \quad (2.21)$$

## 2.2.4 Mechanics of Oblique Cutting

In oblique cutting unlike in orthogonal cutting, the motion of the cutting tool relative to the work material is not perpendicular to the cutting edge of the tool, but is inclined at an angle with it. Almost all cutting processes are oblique in practice, with the cutting edge of the tool inclined at an angle to the relative velocity between the tool and work material, as shown in Figure 2.12. Although some processes may approximate to an orthogonal cutting

case, it is essential to understand the mechanics of oblique cutting as its application extends to most machining processes with complex tool geometry. This could be cases of cutting tools with single or multiple cutting edges.

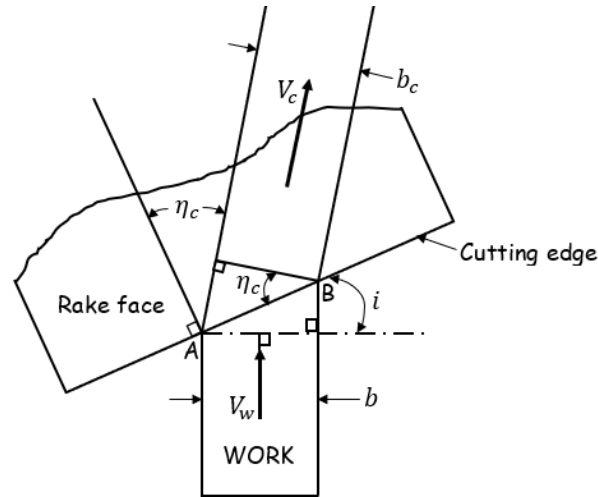


**Figure 2.12: Plan view of oblique cutting.**

### 2.2.5 Geometry of Single Cutting Edge

The tool rake angle is an important fundamental variable that determines the shear angle and cutting force. Due to the complexities introduced by the geometry of oblique cutting, Armarego and Brown [28, 30], put forth a solution that extends and alters the mechanics of orthogonal cutting to describe the oblique cutting condition. In an attempt to solve the problem of rake angle selection in oblique cutting corresponding to the rake angle in orthogonal cutting, three planes which have been considered to be important in the study of orthogonal cutting were selected for analysis, as shown in Figure 2.13. These include:

(i) a plane normal to the cutting edge used by Merchant [31], in which the rake angle is

now generally referred to as normal rake,  $\alpha_n$ . (ii) a plane parallel to the cutting velocity vector and normal to the machined surface used by Kronenberg [32], with the rake angle termed the velocity rake angle,  $\alpha_v$ , and (ii) a plane containing the cutting velocity vector and the chip flow vector used by Stabler [33], with the rake angle known as the effective rake angle,  $\alpha_e$ .

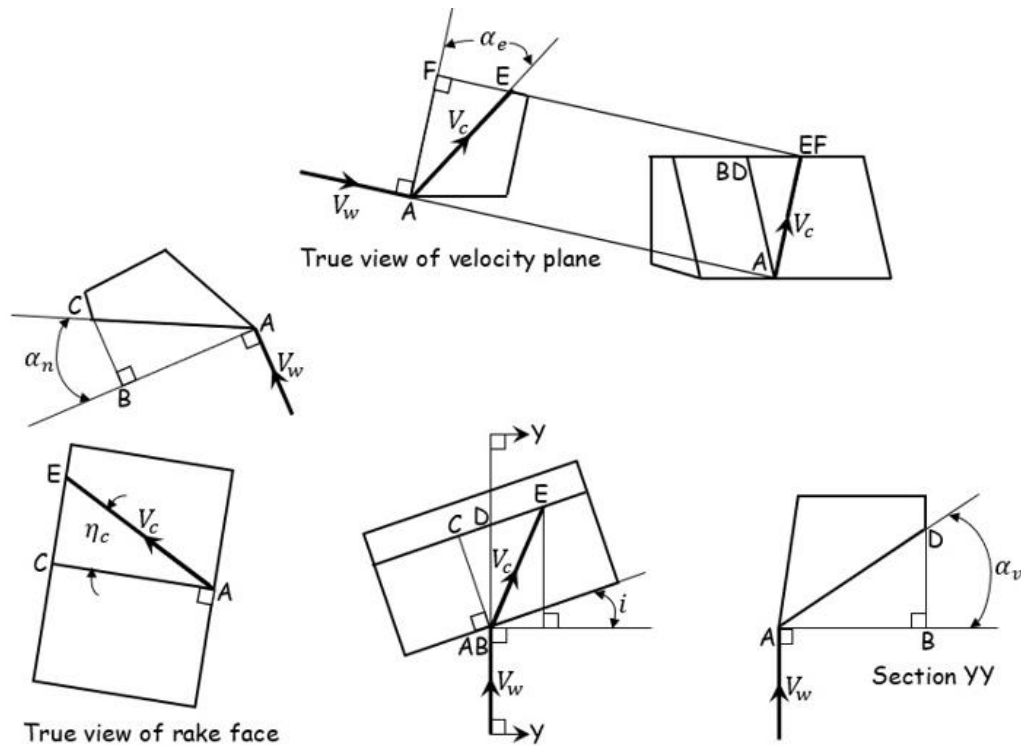


**Figure 2.13: Rake angle and velocity in oblique cutting.**

Based on the rake angle relationships, it was found that

$$\tan \alpha_v = \frac{DB}{AB} = \frac{CB}{AB} \cdot \frac{DB}{CB}$$

this gives

$$\tan \alpha_v = \frac{\tan \alpha_n}{\cos i} \quad (2.22)$$

Using the relationship,

$$\sin \alpha_e = \frac{FE}{EA} = \frac{DB + DE \sin i}{EA}$$

this is expressed as

$$\sin \alpha_e = \sin i \sin \eta_c + \cos i \cos \eta_c \sin \alpha_n \quad (2.23)$$

where  $i$  is the angle of inclination or angle of obliquity, and in the plane of the rake face the angle between the chip-flow velocity and the normal to the cutting edge is called the chip-flow angle,  $\eta_c$ .

### 2.2.6 Shear Angle in Oblique Cutting

On account of various alternative possible definitions for the shear angle as with the rake angle, one clear definition is the angle measured from the shear plane to the plane containing the newly machined surface known as the normal shear angle  $\phi_n$ . An alternative is an angle that corresponds with the effective rake angle, measured in the velocity plane  $V_w, V_c$ , from the shear plane to the approach velocity  $V_w$ . This is known as the effective shear angle  $\phi_e$ .

Using the approach of Merchant derivation of the normal shear angle based on chip thickness ratio [12], the normal shear angle can be expressed as

$$\tan \phi_n = \frac{t/t_c \cos \alpha_n}{1 - t/t_c \sin \alpha_n} = \frac{r_t \cos \alpha_n}{1 - r_t \sin \alpha_n} \quad (2.24)$$

and the effective shear angle

$$\tan \phi_e = \frac{V_c/V_w \cos \alpha_e}{1 - V_c/V_w \sin \alpha_e} = \frac{r_t r_b \cos \alpha_e}{1 - r_t r_b \sin \alpha_e} \quad (2.25)$$

where from volume continuity and incompressibility,

$$r_t r_b = \frac{t}{t_c} \cdot \frac{b}{b_c} = \frac{V_c}{V_w}$$

It should be noted that  $i = 0$ ,  $\alpha_e = \alpha_n$  and  $r_b = 1$ , so that  $\phi_e = \phi_n = \phi$ .

### 2.2.7 Oxley's Parallel-Sided Shear Zone Theory

Over the years, several models have been developed which analyzes chip formation processes in metal cutting, and because of the complexity of the geometrical representation of the cutting process the mechanics of metal cutting problems have been limited to a simple two-dimensional case, known as orthogonal cutting (in which the cutting edge is parallel to the work surface and perpendicular to the direction of cutting), as shown in Figure 2.14. This is essentially a plain strain problem since the depth of cut,  $t$ , is small compared to the width of cut,  $b$ .

Some of the earlier models that investigated the mechanics of metal cutting have been reviewed, with a majority of the models assuming that the shear stress is constant along the shear plane  $AB$  and makes an angle  $\phi$  with the direction of cutting. They characterized the chip formation processes into either discontinuous, which is made up of segments as a result of fracture, continuous, which is formed by continuous plastic flow, or continuous but with built-up edge which forms in a cyclic fashion. To investigate the mechanics of metal cutting, attention was laid on the steady motion problem, which is the continuous chip formation under plane strain conditions. The expression for the shear

angles obtained by Marchant (equation (2.19)), and Lee and Shaffer (equation (2.21)) show an increase in shear angle  $\phi$  with rake angle  $\alpha$  as friction angle  $\beta$  decreases. It has been observed that the shear angle varies for different materials and cutting speed.

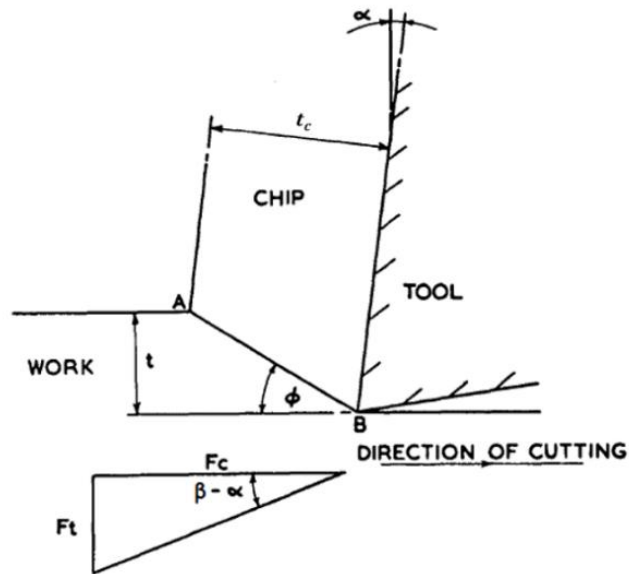


**Figure 2.14: Illustration of shear plane in chip formation process [24].**

Several years later, Oxley developed a shear zone and tool interface model that uses the slip-line field theory. They investigated the plastic deformation along the shear zone and the tool-chip interface, and how the tool rake angle and friction angle relate the shear angle at the tool-chip interface, with focus laid on the parallel-sided shear zone theory. This subject shall be discussed in the proceeding section.

## 2.2.8 The Variable Flow Stress Theory

Some of the early investigations by Oxley [23, 24, 34], has assumed the normal stress distribution to be linear along  $AB$  in the shear zone, and that the stress distribution along

the tool-chip interface was constant. This was shown to be only true for material whose flow stress does not change during cutting. It was also assumed that the removed chip is formed by plastic deformation in a parallel-sided shear zone  $CDEF$ . A more realistic stress distribution in an orthogonal cutting process was introduced as shown in Figure 2.15, with the straight parallel slip-lines  $AB$ ,  $CD$  and  $EF$  representing the directions of maximum shear stress and maximum shear strain rate.

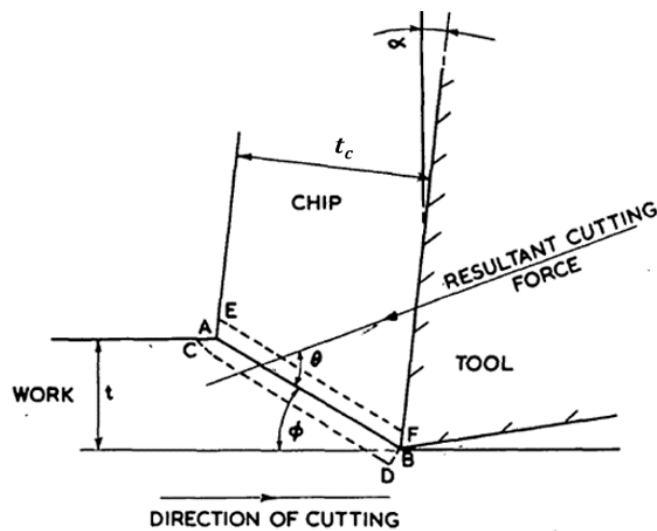


**Figure 2.15: Model of shear zone during chip formation [24].**

The effect of work-hardening, thermal softening, etc., on the change of flow stress as the work material passes through this zone was considered in the chip formation analysis. Knowledge of the shear angle is a necessary part of the complete geometry for the analysis with the rake angle and depth of cut known. The method used to find the shear angle has been summarized [23]. In view of the shear zone element as shown in Figure 2.16, and by considering the shear flow stress along  $CD$  with zero plastic strain (initial shear flow stress) and at  $EF$  the total change in shear flow stress is given by  $\Delta k$  and the

expression which gives the variation of the normal (hydrostatic) stress along  $AB$  is simplified as

$$\Delta p = \frac{\Delta k}{\Delta s_1} \Delta s_2 \quad (2.26)$$

where  $\Delta p$  is the change in hydrostatic stress along the element,  $\Delta s_1$  is the width of the shear zone, and  $\Delta s_2$  is measured along  $AB$ . Taking the free surface just ahead of  $A$ , the normal stress acting along  $AB$  in Figure 2.15 is given as

$$p_A = k \left\{ 1 + 2 \left( \frac{\pi}{4} - \phi \right) \right\} \quad (2.27)$$

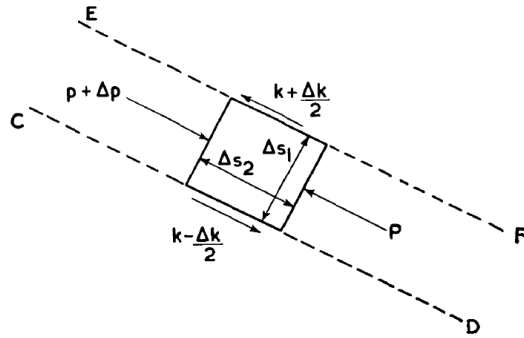


**Figure 2.16: Shear zone element [24].**

and the stresses between the chip and tool at  $B$  is

$$p_B = k \left\{ \frac{\cos 2(\phi - \alpha)}{\tan \beta} - \sin 2(\phi - \alpha) \right\} \quad (2.28)$$

where  $k$  is the shear flow stress along  $AB$ ,  $\tan \beta$  is the ratio of the shear stress to the normal stress at the tool-chip interface and  $p_A$  and  $p_B$  are compressive normal (hydrostatic) stress, at  $A$  and  $B$  respectively. The equations for the hydrostatic stress have also been obtained for estimating the normal shear stress when cutting at higher speeds [22]. If the normal

stress distribution is linear and it is assumed that no force acts on the clearance face of the tool, then the angle of inclination  $\theta$  of the resultant cutting force with  $AB$  is given by the equation

$$\tan \theta = \frac{p_A + p_B}{2k} \quad (2.29)$$

The angle  $\theta$  is expressed in terms of the friction angle, rake angle, and the shear angle as

$$\theta = \phi + \beta - \alpha \quad (2.30)$$

The shear angle  $\phi$  has been defined uniquely and can be determined for given values of  $\alpha$  and  $\beta$ .

### 2.2.8.1 Shear Zone Stress

The normal (hydrostatic) stress distribution in the shear zone was considered as linear [20, 22, 23], and to show the variation of the normal stress along the shear zone, a small element of the parallel-sided shear zone  $CDEF$  was considered, as shown in Figure 2.16. The values  $k - \frac{\Delta k}{2}$  and  $k + \frac{\Delta k}{2}$  are the shear flow stresses along  $CD$  and  $EF$  respectively.  $p + \Delta p$  and  $p$  are the normal compressive stresses at sections distance  $\Delta s_2$  apart, and  $\Delta s_1$  is the width of the shear zone. The normal stress acting along  $AB$  a distance  $x$  from  $A$  was obtain as

$$p_x = p_A - \frac{\Delta k}{\Delta s_1} x \quad (2.31)$$

$\Delta k$  is the change in the flow stress on passing from  $CD$  to  $EF$  and it is positive under normal cutting condition,  $\frac{\Delta k}{\Delta s_1}$  is constant along  $AB$  for the parallel-sided zone  $CDEF$ , which shows that the distribution of the normal stress along  $AB$  is linear.

In an experimental investigation of the shear zone when cutting at slow-speeds, the shear zone was photographed through a microscope during the actual cutting process [22]. It was shown that the shear zone is not parallel-sided but roughly triangular in shape as depicted in Figure 2.8. The triangular shear zone is thinner near the cutting edge than near the chip-free surface, as a result it was suggested that the variation in  $p_x$  will not be linear, that is, the decrease in  $\Delta s_1$  as the cutting edge is approached would cause an increase in the rate of change of  $p_x$ . Although, the actual distribution of  $p_x$  was not predicted at this stage, the increase in its rate of change was accounted for. A new expression was obtained for  $\theta$  as

$$\tan \theta = \frac{F_N}{F_S} = \frac{p_A + p_B}{2k} \quad (2.32)$$

By applying the slip-line theory for the material of variable flow stress, with the assumption that the slip-lines are lines of maximum shear stress and maximum shear strain rate [22, 24]. Equations for the variation of the normal stress along the slip-lines were then obtained as given in equation (2.6).

When cutting was directly examined at slow speed, and the variable  $k$  was assumed to vary as a result of strain-hardening only. A striking feature observed in the analysis was a variation in the normal stress along  $AB$ , as compressive at  $A$  and tension at  $B$ . This was attributed to a direct result of allowing for variable flow stress [20, 21]. The strain-hardening gives a tensile increment in  $p$  as it passes from  $A$  to  $B$  while the change in  $\psi$  gives a compressive increment. This shows a good agreement between the stresses along  $AB$  and the observed cutting force.

### 2.2.8.2 Tool-Chip Interfaces Stress

The contact between the chip and tool was first thought of as essentially elastic in character and analogous to that between a disc and a plane. It was shown by calculations on the lines that the chip and tool would make no contact at the cutting edge, causing a free surface of plastic adjacent to the cutting edge, as shown in Figure 2.17(a). After a direct observation of the cutting zone at slow speed, it was suggested that the contact at the tool-chip interface was essentially plastic and that the cutting force acted closer to the cutting edge than was initially thought. This is shown in Figure 2.17(b).

The analysis of the shear zone presented earlier has revealed that Oxley analysis would require the measurement of the friction angle before the shear angle can be calculated. In order to avoid this problem, the analysis was performed based on an idealized cutting model with a restricted contact tool-chip interface. This was done by reducing  $h$  below its natural value (i.e., to the value it would have when cutting with a normal cutting tool) as shown in Figure 2.18. Considering the shear plane stresses and computing the total normal force acting on the tool face, we have

$$F_n = \frac{\tau t \cos \beta}{\sin \phi \cos(\phi + \beta - \alpha)} \quad (2.33)$$

where  $t$  is the depth of cut, and  $\tau$  is the yield stress along the shear plane. The chip-tool contact length was determined by dividing the normal force by normal stress, thus

$$\frac{h}{t} = \frac{\sin \beta}{\sin \phi \cos(\phi + \beta - \alpha) \cos(\phi - \alpha)} \quad (2.34)$$

for a given cutting tool, as shown in Figure 2.18. With a known  $\frac{h}{t}$  ratio and for a given rake angle  $\alpha$ , the shear angle  $\phi$  and friction angle  $\beta$  can be calculated from equations (2.27)-(2.30) and equation (2.34).

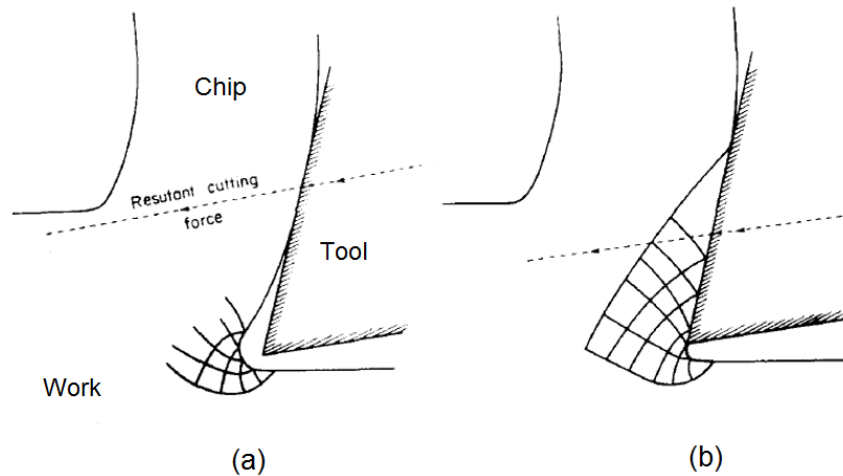


**Figure 2.17: Illustration of contact between chip and tool: (a) Elastic (b) Plastic [22].**

It has been shown theoretically that for a decrease in contact length, the shear angle increases [35]. However, it was assumed that the material has the same value of yield shear stress at the tool-chip interface as along the shear plane. Also observed was that at relatively low speeds, it might be expected that work-hardening will cause higher yield strength on the material along the interface, while at higher cutting speed the yield strength at the interface can be expected to be lower than that along the shear plane. The disappointing feature of Oxley analysis is that deformation cannot be predicted analytically, this brings about the problem of not being able to predetermine the cutting force. The analysis was mostly based on suggestions that the theory of plasticity and work-hardening may be used to study the mechanics of metal cutting at least at low speed.

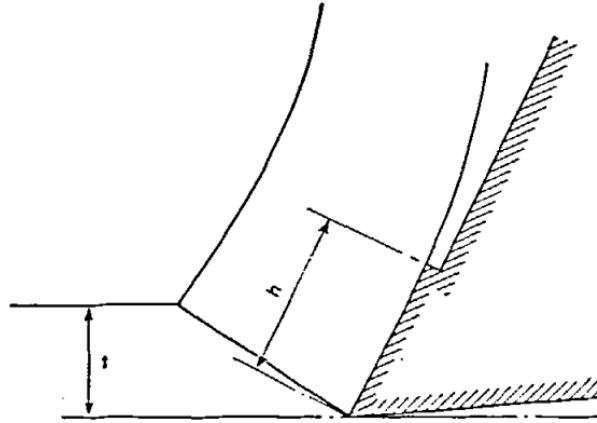


**Figure 2.18: Cutting with restricted tool-chip contact [35].**

### **2.3 The Metal Drilling Process**

Metal drilling is a machining process used to create round holes in metal and core materials using cutting tools known as drill bits and is one of the most common machining operations used in the manufacturing industries. The operation involves rotating a cutting tool and feeding the tool into the workpiece in a direction parallel to its axis of rotation. An essential feature is a variation in cutting speed along the cutting edge with the maximum speed at the periphery that generates the cylindrical surface. The cutting tools of metal drilling operations are an end-cutting tool having one or multiple cutting edges. These usually have one or more straight or helical flutes or grooves and could have a hollow build for the passage of cutting fluid or chips during the drilling of a hole. This section covers a review of the design concept and features of drill geometry, analysis of the mechanics of the process, the drill point geometry, and the analysis of drilling torque and forces. It concludes with a review of the problems associated with metal drilling processes.

### **2.3.1 Concept of Twist Drill Geometry and Design Features**

Drills are designed to be best used for specific applications and the type of drill employed depends on the work materials to be drilled, the structural characteristics of the drill, and other factors like the type of hole (whether through or blind holes, deep or shallow hole), the entrance and exit features of the work material, the cutting condition and even the machine tool and fixtures. These factors play an essential part in the performance of the cutting tool and the drilling process. There are several types of drilling tool designs, and they vary widely in form, dimension, and tolerance. However, for this literature, the focus is specifically on two-flute twist drills.

#### **2.3.1.1 Design Features and Nomenclature**

The types of drills used in hole-making operations are essentially identified by their geometric characteristics. Twist drills are classified based on the kind of shank, the numbers of flutes, and the hand of cut [36]. The shank type at the butt end of the drill determines the holding system of the twist drill, whether a holder or a spindle. These are of two types: the straight shank and the taper shank drill. The straight shank drill has a cylindrical shank with the same or a different diameter than the body of the drill. The shank may be with or without driving flats, grooves or threads, and is usually mounted in an end mill holder, collet, chuck or special clamping hydraulic or mechanical system. The taper shank is a conical shank suited for direct mounting into a tapered hole in machine spindles, driving sleeves, or sockets. A tag, often found in a tapered shank, is used with a drift bar to eject the drill from its mating socket.

The number of flutes influences the finish and hole quality. The most extensively used twist drills in drilling operations are the standard twist drill with two flutes. Three-flute and four-flute drills are core drills essentially used for enlarging and finishing drilled, cast, or punched holes [11, 36]. The hand of cut is the direction of the drill rotation when viewed from the cutting point, and it may be either the right-hand cut (counterclockwise rotation) drill or a left-hand cut (clockwise rotation) drill. The flutes or helical grooves permit the evacuation of a formed chip and allow cutting fluids to reach the cutting edges. The flute also forms part of the rake face of the cutting edge and connects at the leading edge of the land to form an angle with the axis of the drill known as the helix angle,  $\delta$ .

An essential feature of the standard twist drill is the cutting lips or cutting edges extending from the chisel edge to the periphery, which shear the workpiece material during the chip formation process. The central portion of the body that joins the lands is the web, which forms the chisel edge at the cutting end of a standard twist drill. Viewed from the end of the drill between the chisel edge and the cutting lips is the chisel edge angle. At the cutting end of the drill is the drill point with a form like a cone, which is made up of the cutting edges, the chisel edge, the web, and the ends of the land. The projection of the cutting edges along the plane parallel to the drill axis forms an angle between the cutting edges known as the point angle,  $2\rho$ . Figure 2.19 shows the nomenclature of a standard twist drill with the drill point clearly presented. Other features are the margin, the neck and the lip relief angle.

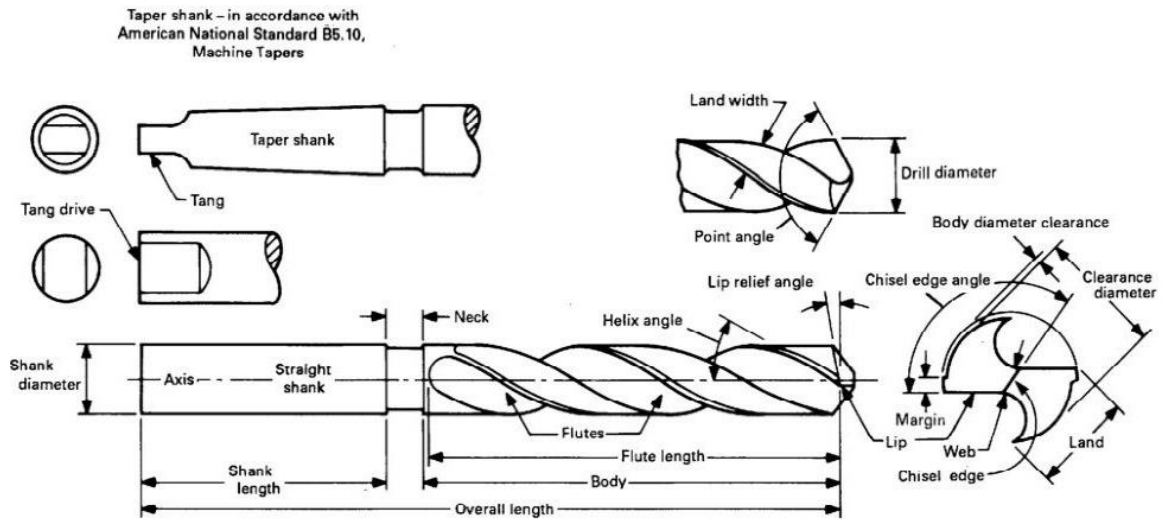


**Figure 2.19: Standard twist drill nomenclature [36].**

A proper design structure is essential to the performance of the cutting tool. From a structural point of view, various features are significant for the twist drill performance, these include the helix angle, the web and flute geometry, the shank type and the twist drill material. Standard helix drills have a helix angle,  $\delta$  of approximately  $30^\circ$  for drilling malleable material, cast iron, carbon steel, stainless steel, hard aluminum alloys, brass, bronze, hard rubber and plexiglass [11]. Twist drills of a typical helix angle of about  $12^\circ$  are known as low helix drills or slow-spiral drills. These have increased strength at the cutting edges and are used for drilling high-temperature alloys and hard to machine materials. They also provide quick chip removal at a high penetration rate when used on aluminum alloys and similar materials when machining shallow holes. This minimizes the chip rubbing effect on the hole wall that raises the cutting force during deep hole drilling operations. High helix drills or fast-spiral drills have a typical helix angle of about  $40^\circ$  and

have narrow lands and wide flute. These are used for drilling low strength non-ferrous metals and low carbon steels.

In an investigation of the dynamic distortion of twist drill by Webb [37] in which the helix angle and the torsional rigidity were two parameters used in the dynamic model, has found that the value of the helix angle governs the magnitude of the longitudinal extension with the circumferential displacement of the twist. The helix angle has a direct effect on the torsional rigidity of the twist drill. Notwithstanding, for a helix angle larger than  $30^\circ$ , further increases in the helix angle result in an increase in the axial displacement [38]. The influence of the helix angle on the torsional stiffness of a drill has been suggested as the probable basis for the traditional popularity of a  $28^\circ$  to  $30^\circ$  helix angle for drills [39]. It was shown that the torsional stiffness increases parabolically with the helix angle and has a maximum at  $28^\circ$ . The radial and angular deflection at the cutting point of twist drill decrease with an increase in helix angle, with the optimum helix angle at  $39.776^\circ$  for large drill diameter of 25 mm, and  $43.403^\circ$  and  $43.921^\circ$  for small drill diameter sizes of 10 mm and 8 mm respectively [40]. The radial deformation of the twist drill has been found to be minimum for helix angles between  $33^\circ$  and  $36.5^\circ$ , which may correspond to improved radial stability and better drilling accuracy [41]. These findings conform with Lorenz's prediction that the optimum helix angle is in the vicinity of  $40^\circ$  in an experimental study for drill tool life improvement [42].

The web thickness is the primary factor affecting the torsional rigidity of a twist drill. The ratio of the web thickness to the drill diameter has a direct effect on the torsional rigidity and the strength of the drill. The ratio of the web thickness to the drill diameter in the range 0.25-0.35 was suggested, provided the chisel edge of the thick web is thin in

order to reduce the thrust force [38]. However, increasing the flute size of the twist drill has an adverse effect on the torsional rigidity and the quality of the drilled hole. Enough flute area is needed for efficient chip removal and high drill rigidity to reduce drill deflection and increase the dynamic stability. The right tool material is also important to permit high throughput when drilling different materials. Some of the most common twist drills are made from high-speed steel (HSS), tungsten carbide (WC), carbide, ceramic, and cermet. Carbide drills are well suited for high throughput precision hole drilling. This permits increased production capacity by a factor of 2 to 10 and increases hole quality when compared to HSS drills [11].

### **2.3.1.2 Drill Point Design Model and Profile Optimization**

The complexity of the twist drill geometry has made accurate measurement of the tool geometry for tool design purpose a difficult task. The drill point geometry has a significant effect on the performance of a twist drill, and any variation in the features may affect the torque and forces as well as the hole quality. These challenges fostered the development of mathematical models that facilitate the determination of wheel profiles for various drill point design [43-47]. This includes the web thickness, chisel edge angle, rake angle, and clearance angle. The cutting angles along the cutting edges of a twist drill were determined by the combination of its flute and flank surfaces. Mathematical models were developed for flute and flank wheel profile for twist drill design [48-52]. A tool that is based upon accurate and convenient implementation and analysis of mathematical models of drill point and flute geometry by computer has been presented by Tsai and Wu. [53]. The approach

has enabled the calculation of the shape of cutting edges and chisel edges and their relationship with the grinding parameters.

An approach that allows the regrinding of standard twist drill into a drill point of the desired profile has been suggested by Paul et al. [54], with the flank grinding profile parameters optimized in order to reduce the drilling thrust and torque. Results indicate an increase in the rake angle and a reduction in the thrust and torque of the twist drill profiles studied. A reduction in the thrust force by an average of 23.8% and the torque by an average of 13.2% as compared to conventional twist drill under similar cutting condition, has been obtained in the drilling of ASSAB 4340 high-tensile steel using TiN coated HSS drill with a modified plane rake face [55]. The modified drill point yields a positive normal rake angle on the entire cutting lips, which brings about a reduction in the cutting forces and power in this region, as well as point relieving in the vicinity of the chisel edge to reduce the thrust force.

### **2.3.2 Mechanics of Metal Drilling Process**

Metal drilling is a complex three-dimensional cutting and a highly dynamic process. The complex geometry of the cutting tool has made developing a realistic model for estimating the mechanics of the entire process a challenging task. The cutting action of the twist drill is centered around the drill point. The two cutting lips of a standard twist drill are out of phase by  $180^\circ$  and joined across the drill web by the chisel edge, as shown in Figure 2.20. The geometry across the cutting lips of the drill point is a function of the helix angle,  $\delta$ , the drill point angle,  $2\rho$ , and the web thickness,  $w$ . Relationships have been presented for

the various angles on the cutting lips and chisel edge of a twist drill, and the effect of radius and feed on the parameters over the cutting lips and chisel edge [56].

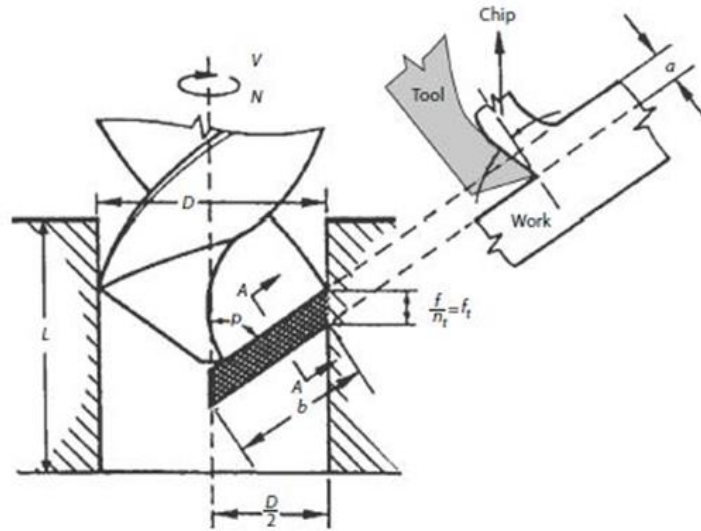


**Figure 2.20: Drilling process [11].**

An important feature that poses difficulties in the modeling of the metal drilling process results from the variation of the rotational velocity from the center to the outside of the tool corner, with the maximum at the tool periphery. There is also a variation in the normal rake angle from positive at the periphery to negative at the chisel edge [57]. The variation in the cutting velocity and effective rake angles across the cutting edges of the twist drill attributes to the highly dynamic nature of metal drilling processes, which makes developing a simplistic model for the analysis of the process a difficult task.

Unlike conventional turning processes that use a single-point cutting tool, the complex geometry of the drill point of a twist drill makes modeling the process challenging. The cutting edges of a twist drill are inclined and result in oblique cutting. However, the

metal under the chisel edge is likened to an extrusion process under a high compressive load. Knowledge of the mechanics of the process at the tool-chip-workpiece interface during chip formation is essential for proper tool design and efficient control of the cutting tool, workpiece material, and process parameters. The mechanics of the drilling process would necessitate the analysis of elements that makes possible the prediction of the cutting forces, torque, and power during the creation of holes.

One of the early analysis of the drill point of a twist drill has shown variation in the normal rake angle, effective rake angle and the inclination angle across the radius of the drill point [58]. The helix angle, web thickness, and point angle are quantities of high importance in determining the performance of a twist drill. The helix angle is controlled by the manufacturer while the web thickness and the drill point can be altered by the condition or extent of use by the user. An analysis performed to investigate the influence of changes in the helix angle, web thickness, and the drill point has shown a large increase in the normal and effective rake angle at the circumference of the drill, as the helix angle increases. This also means a smaller increase in these quantities near the center. Photomicrographs of the tip-geometry of the twist drill are depicted in Figure 2.21, which demonstrate the variation in the rake angle across the cutting edge and the chisel edge of a twist drill during drilling. An increase in the web thickness indicates a strengthening of the cutting edge near the center and has negligible influence at the periphery of the drill. The point angle has a direct effect on the normal rake angle, while the effective rake angle is increased similarly near the drill center.

The torque, thrust, and tool life are significant criteria for determining drilling tool performance. An investigation of the effect of the point geometry on the cutting

performance of twist drills with straight lips was assessed using variance analysis [59]. The analyses performed on the web thickness, helix angle, margin length, point angle, and relief angle show that the torque increases significantly with web thickness and margin length but decreases with the helix angle. The torque is minimized at an optimal point angle and is unaffected by the relief angle. The thrust increases significantly with the web thickness and the relief angle and decreases with the point angle and the helix angle, while the margin length does not affect the thrust. Similar results have been shown by Shaw and Oxford Jr. [60], that the web thickness has a significant influence on the thrust and torque, while the torque and thrust only show a slight decrease with increasing helix angle.

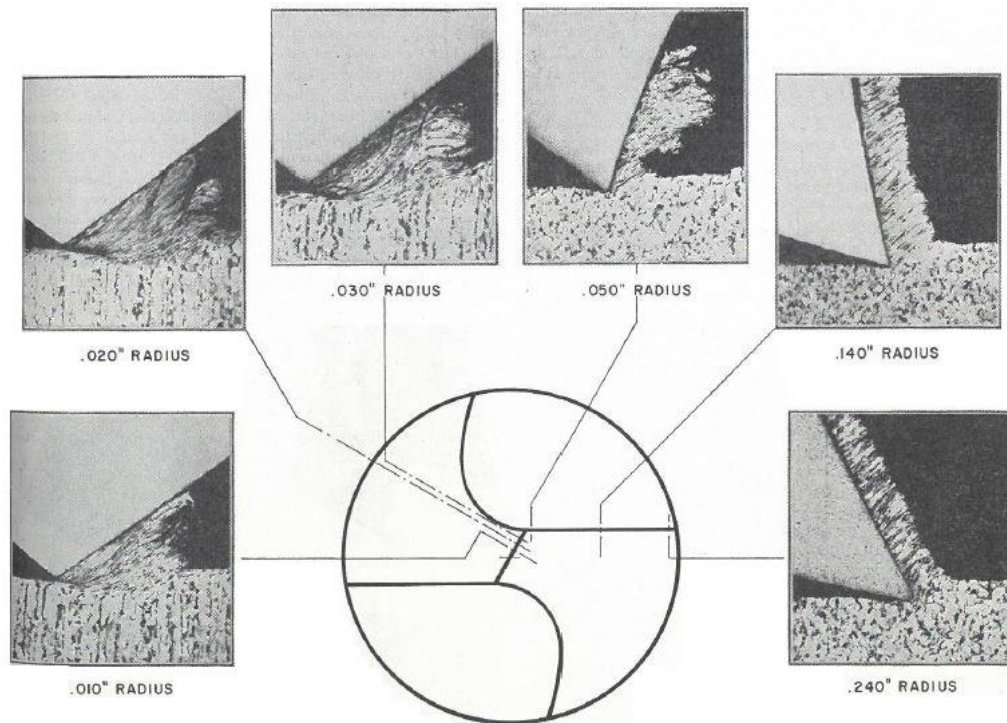


**Figure 2.21: Photomicrographs of different cutting sections across the cutting lips and chisel edge of a twist drill [61].**

Attempts have been made to develop theoretical methods for computing the torque and thrust force in metal drilling processes. Pal et al. [62], has investigated a theoretical approach for calculating the drilling torque in ductile materials. The investigation was limited to a case with pilot holes to avoid the extrusion process at the chisel edge. The total torque accounts for the torque on the spindle due to cutting and the torque due to friction force along the flank, which was accounted for as uniformly distributed along the cutting edge and assumed to be concentrated at the mean radius of the drill. The theoretical and experimental results show close agreement. However, the influence of the chisel edge and the uncut area on the shear angle relationship requires further studies.

### 2.3.3 Analysis of Drill Point Geometry

In an attempt to investigate the direction of chip flow during chip formation in a set of experiments, Oxford Jr. [58] derived a set of equations in relation to the point geometries for the analysis of metal drilling processes. He found that the chip flow angle varies across the cutting edge of the twist drill. From the analysis, the relationship between the projected chip-flow angle  $\eta_p$  and the true chip-flow angle  $\eta$  obtained is

$$\tan \eta = \tan \eta_p \cos \alpha_f \quad (2.35)$$

where  $\alpha_f$  is the face rake angle defined as the angle measured in a plane normal to the cutting edge between the cutting face (plane) and the plane parallel to both the cutting edge and the axis of the drill, as shown in Figure 2.22. This is expressed as

$$\tan \alpha_f = \frac{\tan \delta \cos \xi}{\sin \rho - \frac{\pi W}{L} \cos \rho} \quad (2.36)$$

where  $\delta$  is the helix angle,  $\rho$  is half the point angle,  $\xi$  is the web angle,  $w$  is the web thickness, and  $L$  is the lead of the flute helix of the twist drill. The helix angle and the web angle are obtained in relation to the radius  $r$  at any point of the cutting edge of the twist drill by the expressions:  $\delta = \arctan \frac{2\pi r}{L}$  and  $\xi = \arcsin \frac{w}{2r}$ .

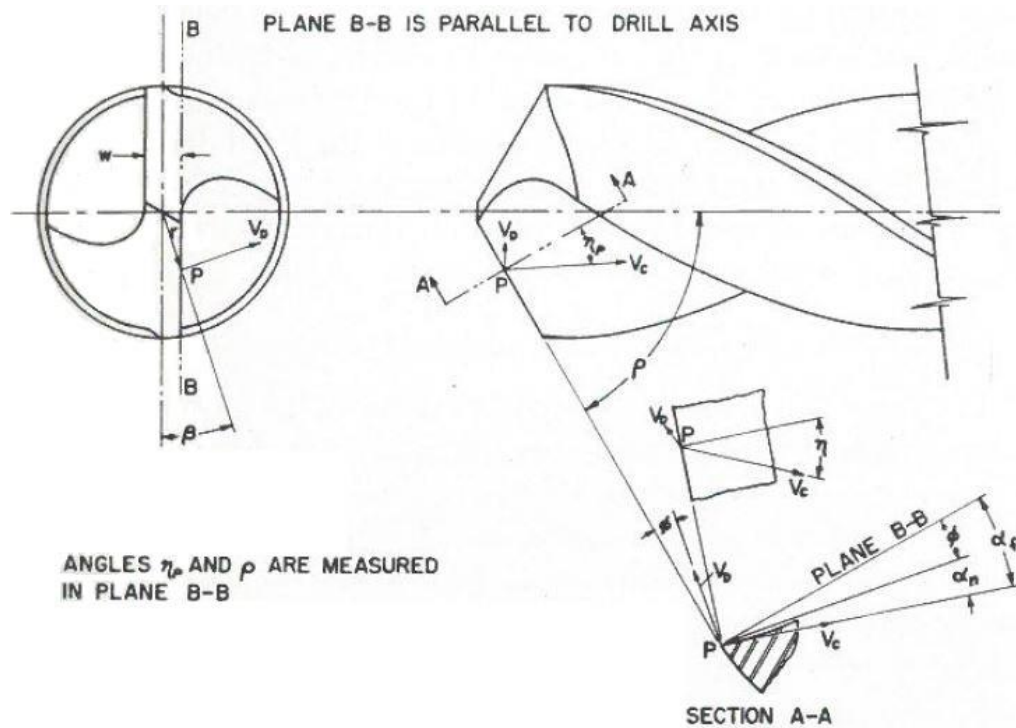


**Figure 2.22: Illustration of a typical drill point [58].**

By reducing the cutting edges of the twist drill to a simple inclined cutting tool, an expression for the inclination angle  $i$  was obtained as

$$\sin i = \sin \xi \sin \rho \quad (2.37)$$

The inclination angle is defined as the angle between the tool velocity vector and a normal to the cutting edge lying in a plane containing the cutting edge and the tool velocity vector.

According to Stabler's law [33], the chip-flow angle  $\eta$  equals the inclination angle  $i$ . The

relationship between the effective rake angle  $\alpha_e$ , chip-flow angle  $\eta$ , inclination angle  $i$ , and normal rake angle  $\alpha_n$  is

$$\sin \alpha_e = \sin \eta \sin i + \cos \eta \cos i \sin \alpha_n \quad (2.38)$$

The normal rake angle  $\alpha_n$  is the angle measured in a plane normal to the cutting edge between the cutting face and a normal to the plane containing both the cutting edge and the drill velocity vector. The effective angle is the angle between the drill velocity vector  $V_D$  and the chip-flow velocity vector  $V_C$ , less than  $90^\circ$ . The normal rake angle is given by

$$\alpha_n = \alpha_f - \Phi \quad (2.39)$$

where  $\alpha_f$  is the face rake angle, and  $\Phi$  is the elevation angle given as

$$\tan \Phi = \tan \xi \cos \rho \quad (2.40)$$

### 2.3.4 Torque and Thrust Force in Metal Drilling Processes

One of the prerequisites for the study of the mechanics of metal cutting processes is the access to realistic models that make possible the analysis and prediction of the basic physical quantities such as the forces, temperature, energy distribution, etc. The torque and thrust are commonly used to quantify metal drilling performance. There has not been a realistic model generally accepted for the analysis or prediction of the mechanics of the process. The system is highly dynamic, and the complex geometry poses difficulties in developing a simplistic and realistic model for the process. Over the years, attempts have been made to model the torque and thrust force during drilling processes. An early work that gave useful empirical equations for computing the torque and thrust was developed by Boston and Oxford Sr. [63]. The torque and thrust were obtained in relation to the feed and

drill diameter. Other attempts to model the process have led to several assumptions; Most researchers have likened the whole of the chisel edge as a wedge indenter [64-68], while some has eliminated the effect of the chisel edge by predrilling a pilot hole of a diameter equal to the chisel edge width [62, 69].

Oxford Jr. [58], conducted an experimental study of the basic mechanics of the drilling process using a quick stop device to freeze the action of the chisel edge during drilling. The work reveals that the deformation at the center of the chisel edge acts like an indenting punch, while the remaining part of the chisel edge is that of a cutting action with a very high negative rake angle. A similar result was observed by Shaw [70], with two distinct types of chips observed in a sudden stop test performed to determine the chip form at the drill point by comparing the chips produced at the cutting edges and that of the chisel edge. It was done by filling a pilot hole on a brass block with lead. The size of the pilot hole is equal to that of the web thickness of the large drill used. The observed result shows chip form by cutting at the cutting edges, and a combination of both cutting and extrusion at the chisel edge. In-line with their earlier work and further investigation, Shaw and Oxford Jr. [60], later derived equations for computing torque and thrust when using dimensional analysis and other techniques.

Williams [71], developed a chip formation and an indentation model for the chisel edge region of a twist drill to predict the shape of the wear zone on the chisel edge. Equations were derived for the computation of the torque and thrust produced by the chisel edge given the drill point geometry, the cutting condition, and shear stress factor for the work material. Based on the experimental observation by Oxford Jr. [58], an assumption that two models (i.e., an indentation model and a model of chip formation) are required for

the study of the basic mechanics of the chisel edge was arrived at. However, the influence of the drill feed velocity on the chisel edge geometry has been considered to develop the model used to analyze the process mechanics at the chisel edge. Williams further expanded on this work by including the cutting edges to developed two chip formation models and an indentation model for simulating the action of the drill point of a twist drill [72]. From these models, equations were derived for the prediction of the total torque and thrust given the cutting condition, drill geometry, and an empirical factor that is related to the work material. The main cutting edges and portion of the chisel edge were treated as orthogonal cutting and extrusion at the center region of the chisel edge. The challenges associated with the accuracy of the model for predicting the forces and torque is not only dependent on the validity of the many simple assumptions made in the three models, but also on the magnitude of the empirical shear stress factors used.

Armarego and Cheng [73, 74], developed a thin shear zone cutting analyses based on oblique cutting models for predicting reasonable deformation and the force distributions along the cutting lips of a modified flat rake face drills. The model accounts for the variation in the twist drill geometry and gives reasonable trends when numerically tested. The thin shear zone cutting model was considered in drilling so that at any point on the cutting lips, the chip velocity is the resultant of the relative velocity between the drill and the work material and the shear zone velocity. However, a similar analysis for conventional twist drill fails to give acceptable trends, which implies a further work is needed to study the curved rake face tools. Notwithstanding, using statistical technique the deformation and thrust force and torque equations based on the geometrical similarity concept was experimentally verified for both the conventional and modified flat rake face twist drills.

Armarego and Wright [75], later developed predictive models for drilling torque and thrust and compared these models for three drill flank configurations (viz. plane flank, conical flank, and clearance planes flank) based on the mechanics of cutting analyses, fundamental machining data such as the shear stress and chip length ratio, and flank configuration that influences tool angles. The models resulted in a comparable thrust and torque predictions when numerically tested over a wide range of drill point feature values and showed a good correlation between predicted and experimental data. Furthermore, simpler empirical thrust and torque equations were obtained for all flank configurations, which indicate that the approach can be successfully applied to predict the torque and thrust, without resorting to the more complex drill flank geometrical analysis, provided the basic geometry at the cutting edge of the drill can be adequately modeled.

Watson [76-79], work also implemented the oblique cutting model in developing a torque and thrust predictive model in metal drilling at the cutting lips. The model assumed that a pilot hole would eliminate the region to be machined by the chisel edge, leaving the material being machined by each individual lip to be considered as a number of individual elements. The experimental results show a significant difference between drilling with a pilot hole and predictive model results. However, accounting for the integrity of the chips (i.e. taking the chip as one piece rather than a series of individual elements) gave a closer correspondence between predicted and experimental results at the cutting lips. By observing through a transparent model of the chisel edge drilling into modeling clay, a predictive model was developed for the chisel edge. This model shows region of extrusion and oblique machining with working rake angle ranging from positive to a very large

negative value. However, adding the chisel edge model and the cutting lip model does not give a good correspondence with the predicted result when drilling without a pilot hole.

### **2.3.5 Problems Associated with Metal Drilling Processes**

Metal drilling is a highly dynamic machining process. The performance of the process is influenced by the drill point geometry of the drilling tool and controlled by the process parameters. The efficiency of the process is a synergy of the process performance, and the quality of the hole created. Over the years, several attempts have been made to improve the twist drill design and the drill point geometry through analysis and mathematical modeling of the drill geometry [38, 41-43, 46, 47, 53, 54, 80-84], modeling of the grinding wheel profile [48-50], process parameters optimization [85-88], and the use of cutting fluid or minimum quantity lubrication (MQL) [89-93], all geared toward improving the efficiency of the process and surface integrity of the hole created. Metal drilling induces significant surface damage and microstructure change that could be attributed to plastic deformation resulting from mechanical stresses and elevated temperature from the continuous drilling process [94]. The thermo-mechanical fields resulting from cutting processes impact the surface quality of the workpiece.

## **2.4 Burr Formation**

During chip formation, the plastic flow resulting from the shearing process can lead to an undesirable projection of material at the end of the cut. This undesirable projection of plastically deformed material is known as a burr. Most often, burrs are partially formed chips left on the workpiece from the chip formation process. Burr has also been defined as all material extending past the theoretical intersection of two adjacent surfaces where such material was the result of plastic deformation by a chip-making cutting tool [95]. Over the years, only a few researchers have attempted studying the burr formation mechanism in machining and specifically drilling.

### **2.4.1 Mechanism of Burr Formation in Metal Cutting Process**

A general study of the mechanisms of burr formation by Gillespie and Blotter [1] showed that burr formation occurs in three distinct ways. The first involves a lateral flow of material (Poisson burrs), which results from the material's tendency to bulge at the sides due to compression from the cutting tool until plastic deformation occurs. The second is the rollover burr, which is essentially partially formed chips pushed out of the path of the cutter rather than being sheared. This burr type forms in operations where the principal cutting force passes over a free edge. The third is the tear burr, which is the result of material tearing from the workpiece rather than shearing. Nakayama and Arai [96], used a different approach where the cutting edges which are directly involved in the burr formation, and the mode and direction of the formation were the essential system for classifying the burr formation. Using these two systems, most of the burrs formed in various machining

operations were designated. The rollover burr type proposed by Gillespie and Blotter was dealt with as a specific case of the chip formation process in the final stage of cutting by Ko and Dornfeld [97]. With the assumption that the deformation consists of shearing and bending deformation in a burr formation when no fracture occurs, they proposed a burr formation model that characterized the burr formation by three parts: initiation, development, and the formation of the burr. The model has based on the observation of the behavior of workpiece material during the orthogonal cutting of commercial plasticine. It has assumed that the burr formation begins at a transition point where the steady-state chip formation stops as the cutting tool edge approaches the end of the cut. At this transition point, the natural chip formation stops, and plastic deformation begins below the plane of the machined surface in the cutting direction, as illustrated in Figure 2.23. The model is only applicable to cutting conditions, tool geometry and the workpiece material that do not exhibit fracture along the negative shear plane during the orthogonal cutting process. The deformation is not concentrated along this negative shear plane as it is in the shear plane, and the strain hardening effect is not as severe as in chip formation.

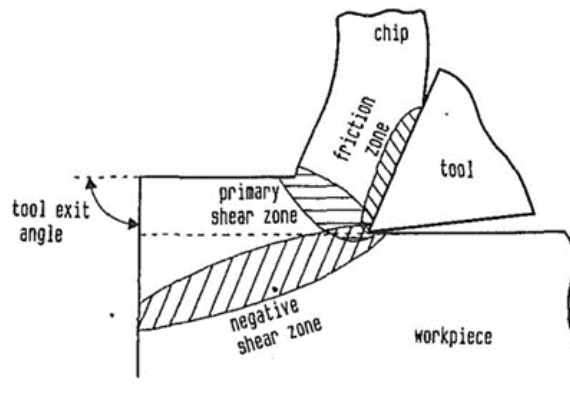


**Figure 2.23: Schematic illustration at transient cutting state [97].**

By direct observation, it has been found that the negative deformation plane begins to form when the steady-state chip formation stops as the tool approaches the end of the cut in an orthogonal cutting process [97-99]. The reports show that when burr formation begins, fracture causing chip separation initiates in the direction of the shear angle during the steady-state chip formation. Plastic bending and shearing of the negative deformation plane contribute to the burr formation. Whereas, if edge breakout occurs instead of burr formation, a crack propagates along the deformation plane to cause the breakout, as shown in Figure 2.24. Two modes of progress on the negative deformation plane were observed—edge breakout caused by plastic bending and slip along the negative deformation zone by the shear stress. The fracture mechanism has been revealed by fractography to be due to a shear rupture. This contributes to edge breakout and is dependent on the ductility of the workpiece material. The formation of burrs in various machining processes could be the result of one or more of the burr formation mechanisms reported by Gillespie.

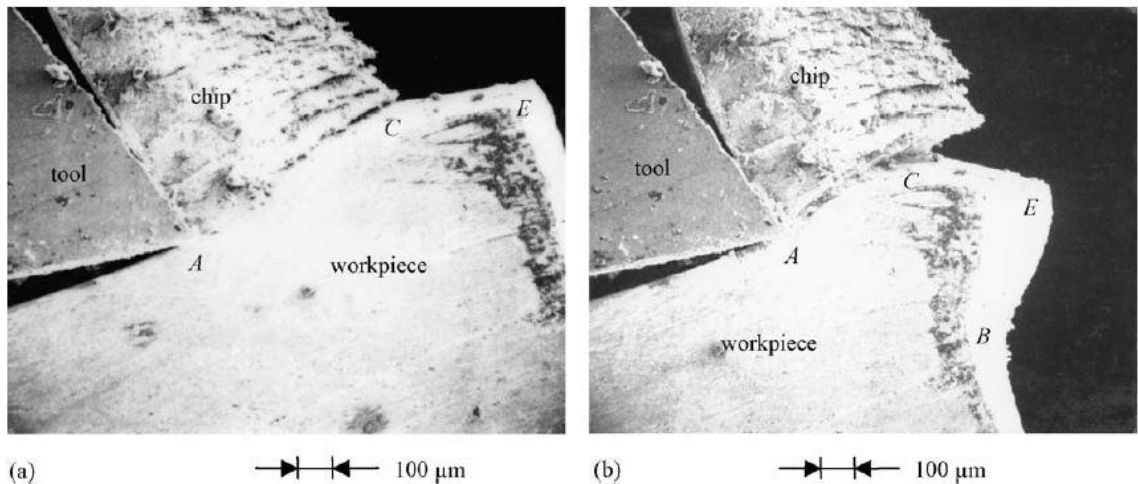


**Figure 2.24: SEM photomicrograph of annealed copper sample due to (a) fracture causing chip separation and (b) development of burr formation [99].**

## 2.4.2 Mechanism of Burr Formation in Metal Drilling Process

Metal drilling is one of the most common machining operations in industries, and in spite of its importance, most of the researches are focused on reducing burr formation in metal drilling through tool geometry design, process and parameter optimization, or the use of some form of control chart [4, 8, 100-108]. Only a few studies have been done which investigate the mechanisms of burr formation in metal drilling at tool breakout. One of the earliest studies which attempt to explain the mechanism of burr formation in Ti-6Al-4V alloy has been reported by Dornfeld et al. [7]. The study investigates the effects of tool geometry and process conditions on exit burr formation during metal drilling using a split-point and helical point drill. Based on the cross-section shape created under different machining conditions, burrs formed in dry cutting were categorized into four burr types, as shown in Figure 2.25. Type I has a uniform height and thickness. Type II is similar to Type I but has a leaned-back cross-section. Type III has a severe rolled-back shape, while Type IV is also a roll-back with a widened exit and has relatively small burr height.

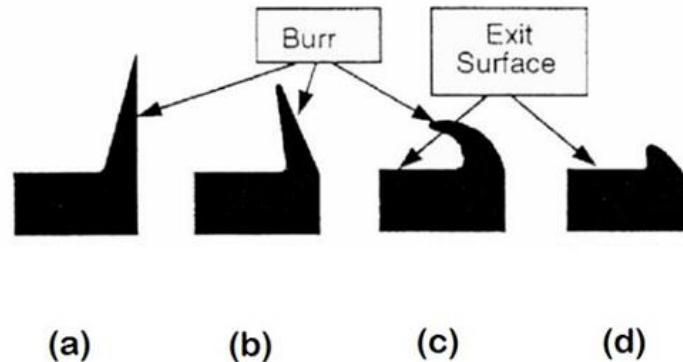


**Figure 2.25: Burr types formed in dry drilling of Ti-6Al-4V alloy (a) Type I (b) Type II (c) Type III (d) Type IV [7].**

The roll-back phenomenon at tool breakout during the drilling of Ti-6Al-4V has been illustrated in Figure 2.26. This shows that during the breakout from (a) to (e), as the drill approaches the exit surface, the material begins to deform under the chisel edge. This plastic deformation zone expands from the center to the edge of the drill, and one of the cutting edges will cause separation of the cap from the hole perimeter. And depending on the drill point geometry, initial rupture may occur near the center of the remaining material. The remaining material at the hole perimeter is then pushed out to form a burr with a cap at the final stage of the drilling process. At this stage, there is no further chip formation, which means the energy generated has no way of dissipating. This material tends to inhibit heat dissipation due to low thermal conductivity. Therefore, causing a localized increase in temperature at the inner surface of the burr, and consequently, the thermal expansion believed to be the principal cause of the lean-back and roll-back phenomenon observed in the burr formation process.

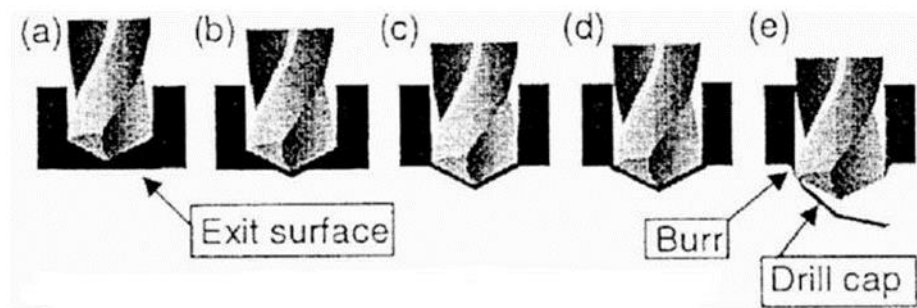


**Figure 2.26: Burr formation with drill cap [7].**

Analysis of the drilling burr formation mechanism when drilling with a conventional drill and a new-concept drill has been performed with the goal of increasing

accuracy and productivity in drilling operations. A burr formation scheme has been suggested by Ko and Lee [103], considering the drill geometry and the cutting condition. The breakout burrs were classified into three types: Type A (no cap by fracture), Type B (burr with cap), and Type C (burst burr without cap), as shown in Figure 2.27. Based on experimental observation, they showed that the burr formation is the result of plastic deformation and fracture. The fracture location is determined by the fracture strain of the material and the tool geometry. This involves comparing the strain at the drill point with that along the exit edge of the hole. Hence, most burr formation is highly dependent on the material properties, the drill geometry, and the cutting condition.

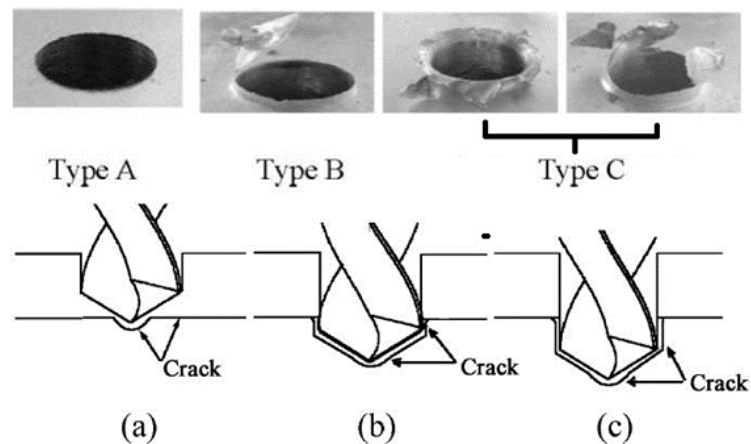


**Figure 2.27: Classification of drilling burr formation and location of the crack at breakout [103].**

It was observed that as the feed per revolution increases, the burr changes from Type B to Type C for each spindle speed when using an HSS drill. These changes were also notable when the spindle speed increases for each feed. This means that the location of fracture initiation moves from the exit edge of the hole to the drill point or some points

on the cap. The reason why a conventional HSS drill produces type C burr in many cases as compared to the new concept drill was ascribed to the dependency of the fracture on the twist drill geometry. Hence, for a small point angle drill, the strain at the drill point is much larger than that along the exit edge of the hole. However, for a larger drill point angle, the strain at the drill point is less than that along the exit edge of the hole. Therefore, tensile stress increases at the part along the exit edge as the drill advances and fracture occur, producing type B uniform burr with a cap.

A model that describes the mechanism of burr formation in drilling of metal has been reported by Saunders and Mauch [109], in an attempt to develop a simplified burr formation model. The model extends the burr formation mechanics in orthogonal cutting to a complex drill geometry, and also includes the effect of temperature in the analysis. The material in front of the drill point was modeled as an axisymmetric circular plate with varying thickness. The drilling thrust force was modeled as a pressure on the top surface of the plate. The force produced at the chisel edge was modeled as indentation near the center and an orthogonal cutting at the outer edge, while at the cutting lips region, it was modeled as oblique cutting. Failure leading to exit burr formation was described in two cases, as shown in Figure 2.28. The case I describes the condition prior to tool breakthrough. That is, as the drill point progresses toward the exit surface, material in front of the drill point is reduced, thereby increasing the overall level of stress of the material. If the Von Mises stresses exceed the ultimate strength of the material, breakthrough occurs. Else, the drill advances until the material in front of the drill point fractures at the failure point at some radius,  $r$ . Case II, on the other hand, gives the condition at breakthrough. That is, if the material in front of the drill point continues to support the thrust force and

cutting continues until the stress at point B reaches the ultimate stress, failure would occur at point B, leaving the remaining material to be bent over forming a burr. The feed-rate was shown to have the dominant effect on the burr formation, and the model also supports the theory that the temperature effect would be greatest at low feed-rate.

A 2D finite element model has been developed by Saunders [110] to address the limitations of the classical models. The model examines the stress state at each load step based on applied thrust force to the material in front of the drill during drilling. If the set failure criterion for the material in front of the drill is satisfied, the simulation stops with the assumption that no further cutting takes place, and the remaining material bends out to form the burr with a burr height  $R_f$ , as shown in Figure 2.28b). This was used to determine the burr height for three feed-rates and to simulate the heat transfer near the exit condition in drilling operations. However, this does not describe tearing burr formation.

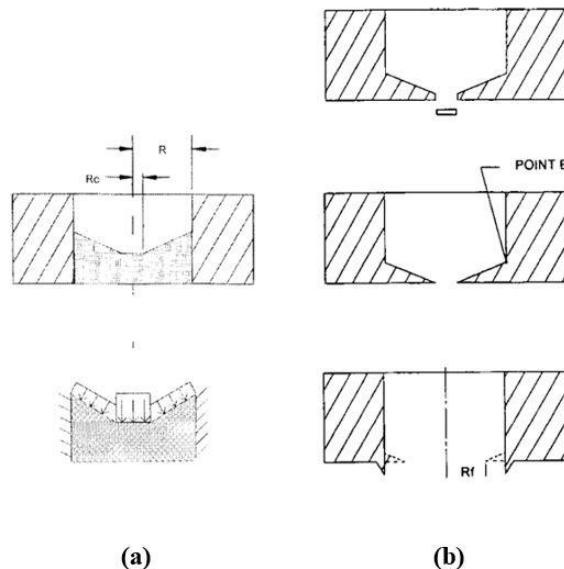


**Figure 2.28: Illustration of (a) Case I, geometry and loading (b) Case II, burr formation sequence [109].**

A 3D finite element model that simulates the dominant role of negative shearing and bending mechanisms in the drilling burr formation process of 305L stainless steel has been developed by Guo and Dornfeld [111]. The model accounts for dynamic effects of mass and inertia, strain hardening, strain rate, automatic mesh contact with friction capability, material ductile failure, and temperature-mechanical coupling simultaneously. The process was simulated in an attempt to understand the burr formation mechanism in the drilling process. By investigating a series of stress contours and progressive deformation at the edge of the work material, the burr formation mechanism was characterized in four stages: initiation, development, pivoting point, and the burr formation stages, as shown in Figure 2.29.

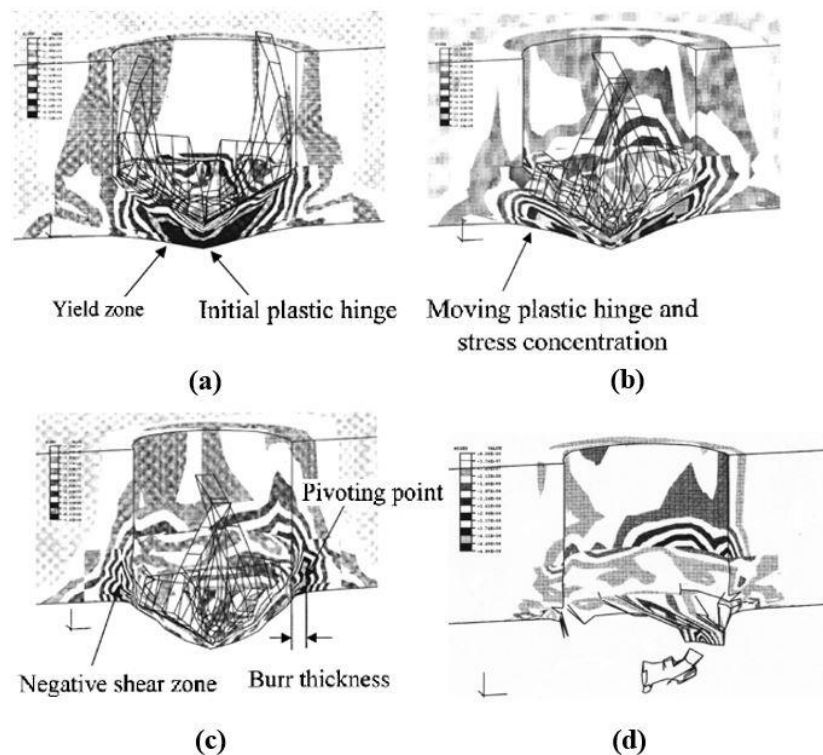


**Figure 2.29: Von Mises stress contour in (a) burr initiation, (b) burr development (c) at pivoting stage (d) burr formation [111].**

The initiation stage begins with the formation of a bulge at the exit surface of the workpiece, due to localized fully plastic deformation as the drill tip approaches the bottom edge of the workpiece. The bulge continues to develop and enlarge; this is the development stage. An unstable chip begins to form as a result of increased material bending, and a transition from cutting to ploughing occurs along the cutting lips of the drill. At the pivoting point, catastrophic bending occurs at the workpiece below the drill point. The interaction between the cutting lips and the material is dominated by a ploughing effect with reduced chip formation. The material in front of the drill tip is stretched, while workpiece material near the workpiece edge is compressed. Finally, the exit burr is formed as the bulge breaks and material stretches, exceeding its maximum fracture strain.

An analytical model for burr formation in metal drilling that holds for ductile materials that produce uniform burr with drill cap has been proposed by Kim and Dornfeld [9]. The model implements the principle of energy conservation and metal cutting theory, and the burr formation mechanism used in the model was based on the observation of the behavior of work material during the drilling of low alloy steel. This uses the Merchant model, which does not account for the cutting speed effects. Hence, the model developed does not account for the cutting speed effects in the drilling burr formation. However, it includes the effect of the drill geometry, material property, and the process condition. An analytical model that is based on the theory of slip-planes has been proposed by Segonds et al. [112], The model was set up based on mechanical and geometrical consideration, and specific for predicting burr type and thickness when drilling ductile work material. Bu et al. [113] also developed an analytical model for predicting the exit burr height and thickness during drilling. The model considered the impact of process parameters such as

the cutting force, spindle rotational speed, feed rate, and temperature effect in the analysis and implemented the drill geometrical factors such as the point angle, helix angle, chisel edge, and web thickness in order to improve the practicability of the application.

### **2.4.3 Burr Minimization and Deburring Approach**

The need to maintain appropriate surface integrity is a requirement for efficient manufacturing. It has been found both by an experimental and theoretical approach that machining burrs cannot be prevented by changing machining parameters alone, but can be minimized by the use of appropriate machining parameters [1]. The work material property and tool sharpness also influence the burr formation. The workpiece ductility and strain hardening exponent are directly linked to the burr size, as such, large burr does not form on brittle materials [95]. Material with high shear strength has been found to form thicker burr than material with low shear strength, while dull cutting tool that may result from tool wear tends to increase cutting force, and consequently thick burr formation. The burr height and root thickness could be minimized by decreasing undeformed chip thickness, decreasing the shear strain of the chip (attained by high rake angle, high cutting speed, cutting fluid and cold working of the work material), increasing tilted approach angle and turning the direction of cutting force toward the workpiece [96]. However, in metal drilling processes, the approach implemented to minimize burr formation could vary due to the complex nature of the cutting tool geometry. In this section, we will go over some of the research work put forth to investigate the burr minimization technique and deburring schemes in metal drilling processes

#### **2.4.4 Burr Minimization Scheme in Metal Drilling**

Reducing burr formation in metal drilling processes has become a continuous research problem. Hole quality is related to the drill geometry and cutting conditions [114]. Several researchers have focused on burr minimization approach by investigating the effect of the process parameters on the burr formation and the hole quality in drilling [115-117], while others have looked into burr minimization scheme that uses a step drill has been proposed [105], the influence of the drill point geometry [118], and process parameter control and optimization [4, 107, 119].

One of the early research that investigate the effect of workpiece material structure and drill diameter on burr formation has been reported by Sugawara and Inagaki [10]. In an attempt to investigate the burr size reduction and improved cutting ability in micro-drilling, the workpiece of various microstructures was drilled with drill bits of various diameters to observe the grain size effect. The tests performed on the workpiece having granular structure and relatively large crystals showed a reduction in the grain boundary in the drilling region, as the feed-rate decreases. They ascribed the major factor causing improvement in the cutting ability that leads to a reduction in the burr formation principally to the workpiece structure and cutting at a reduced feed-rate.

Pande and Relekar [100], approached the problem of reducing burr formation in metal drilling in two fronts. First, an experimental approach based on response surface methodology technique and mathematical models were planned and used to correlate the response parameters (burr size) to the drilling process parameters( viz. the feed, drill diameter, length to diameter ratio of the hole and the work material hardness) to investigate

the influence of process parameters on the burr formation. The feed was observed and identified as the most significant parameter which governs the sizes of burr and optimal process conditions that minimize the sizes of burr. Finally, an attachment was developed, which provides a continuous modification of feed during drilling.

The use of drilling burr control chart (DBCC) has been designed to obtain a reasonable range of operating conditions for metal drilling derived from experimental data on burr formation carried out at varying feeds and speeds [8, 120-122]. By normalizing the data obtained, a range of drill diameter can be covered. The charts aid in the prediction and control of drilling burr formation under given cutting conditions. Thus, a selected cutting parameter would generate a minimized burr or preferred burr shape for an application. This application can also be used across similar work materials (e.g. carbon steel). Based on reports by Kim et al. [120], which developed a DBCC for stainless steel, AISI 304L, and low alloy steel, AISI 4118, and the DBCC developed by Min et al. [8], for low alloy steel, AISI 4118, when using a split point HSS twist drill, only two and three burr shapes were observed for AISI 304L and AISI 4118, respectively. These were believed to be mainly due to the properties of the materials, relatively high strain hardening coefficient, and ductility. The ranges of the height and thickness of the uniform burrs were observed to be independent of the drill diameter.

#### **2.4.5 Deburring Scheme**

Burrs are a projection of plastically deformed work material or partially formed chips hanging at the edge of machined surfaces. Burrs are by-products of all conventional machining operations and are non-value adding conditions to component parts. A burr-free

machined part surface is needed to prevent loose burr that could result in injury, poor part assembly, and jamming of mechanism. Deburring operations are needed to obtain burr-free surfaces. They are costly and time-consuming processes and could be achieved through hand deburring and other deburring processes. Deburring processes must be based on the burr characteristics together with the part properties [2]. The burr characteristics are described by properties such as the length, thickness, shape, or hardness.

The burr sizes generated during machining processes depend on the tool geometries used, the speeds and feeds, and the work material properties, while the burr removal cost is directly related to burr size and location [95]. In several cases, the deburring cost of precision miniature parts approaches the cost of machining due to close tolerances, minute part sizes, and large burr sizes. The following facts are essential in the selection of deburring processes:

- a) The burr size to be removed (thickness and height).
- b) The amount of stock loss that can be tolerated from the deburring process.
- c) The surface finish required.
- d) The required edge condition (how large a radius or chamfer is allowable or required).

Other important features to consider are the part size, part material, and the burr location. A list of deburring processes has been presented, which grouped deburring processes into the six major categories: viz. abrasive processes, mechanical processes, thermal processes, chemical processes, and electrochemical processes [123].

Deburring and machining costs can be minimized by appropriate changes in the workpiece and tooling design [95].

## **Chapter 3: Analysis of PCM and Fault Identification**

The need to optimize production efficiency in manufacturing processes has led to a great deal of research in process condition monitoring (PCM) of machining processes. This has drawn attention to different techniques and applications for monitoring either individual machine tool components such as a spindle motor or an entire machine tool. Over the years, there has been a growing development of reliable and effective devices or sensors for monitoring machining operations, ensuring the design of unmanned machining, tool condition monitoring, etc. to ensure efficient metal removal rates and taking adequate action in the event of tool failure. Torque, forces, and power are basic process variables that depend exclusively on the conditions of the cutting process and/or the cutting tool condition [124]. A survey of commercially available sensors used in unmanned machining applications has been reported by Tlustý and Andrews [125], which are implemented in dimension monitoring, force monitoring, power monitoring, and acoustic emission monitoring. However, for the purpose of this thesis, our focus is on the implementation of force and power monitoring in PCM and fault identification in machining operations.

### **3.1 Force Application in PCM and Analysis**

The forces in machining operations are measured using a dynamometer. The device comes in a variety of different configurations that make it possible to mount them at different points on different types of machine tools. As an example, dynamometers can be mounted to a tool post on a CNC lathe or a table for milling and drilling work or built into a spindle bearing, and they are ideal for evaluating cutting forces as the spindle motor current,

voltage and speed vary [125]. Cutting forces and torque data are obtained in real-time and used as an indirect method for tool wear monitoring as compared to direct observation [126]. Tool wear is an undesirable feature associated with machining processes and adversely affects the cutting mechanics, and ultimately the cutting tool life. In general, cutting forces and torque increase as wear progresses, and the ratio of cutting and feed force components are usually a good indication of tool wear and failure [127-129]. For tool breakage monitoring, the results from force dynamometers can be analyzed to look for specific signal patterns in the force signal [130, 131]. Force signals are also processed for the detection of chatter that can occur when cutting parameters coincide with a natural frequency in the machining system. The cutting forces are also implemented in the adaptive control of the machining process [132].

### **3.2 Power Application in PCM and Analysis**

Energy-aware manufacturing is gaining attention in process condition monitoring. This could be attributed to its low-cost and reliability in its implementation. Power monitoring is obtained by continuously keeping track of the voltage, current and power factor of the spindle or drive motor, from which the consumption is being evaluated [125]. A study carried out to investigate the feasibility of motor power and current measurement for adaptive control of the cutting process has been reported by Mannan et al. [133], in which measured power and current signals from the spindle and feed motors of an NC lathe and machining center were analyzed for the response of the current and power variations due to process changes. It was found that the tool wear and tool breakage are successfully detected using power and current signals. A relationship between wear and experimental

cutting power data has been described by Cuppini et al. [134], and an inexpensive and reliable technique for drill fracture detection have been developed by Liu et al. [135]. By monitoring the instantaneous stator current and setting a threshold on the demodulated stator current signal, drill fracture features can be extracted. Drill wear monitoring using spindle motor and feed motor current was also investigated [136]. In more recent research by Simoneau and Meehan [137], a direct power measurement technique was used to identify process conditions and potential process outcomes during metal cutting. The characteristics of the machine and process power consumption were assessed using a direct measurement technique to measure the peak power of a 3-axis CNC milling machine. The spindle speed and total machine power were obtained for the machining of a standard test part using varying cutting parameters and ultimately used to characterize the machine tool for different cutting processes.

Power and Energy monitoring in production systems are essential for the evaluation of efficiency and overall machining performance as it relates to the finished parts. In view of power monitoring on the overall machine tool components, several researchers have focused on quantifying the energy demand for machine tools with an attempt to optimize energy usage. An energy framework that shows the electrical energy requirements for manufacturing processes has been presented by Gutowski et al. [138]. Their analysis shows that the specific energy requirement for a manufacturing process is not constant and that manufacturing processes are becoming more energy-intensive, with process rate as the most important variable for estimating energy requirement. The reduction of energy consumption footprint through optimization of the cutting process parameters in the machine tool is an ongoing process with the goal of minimizing the energy consumption

footprint [139-144]. Other researches are in areas of energy-aware process planning and scheduling [145-147]. All of them are geared towards obtaining an efficient manufacturing process.

### **3.3 PCM Summary**

We have dedicated this small section in the thesis to PCM in order to introduce the concepts of force and power monitoring at a very high-level. Both will be used extensively throughout the experimental work, which will be illustrated in the next chapter of the thesis.

## **Chapter 4: Experimental Work**

The following chapter lays out the experimental work that was conducted throughout the research. Starting with a hypothesized breakdown of the through-hole drilling process, the chapter presents the experimental setup, workpiece material, and ultimately all the drilling experiments that were conducted. The results and discussion of the experiments will be covered in Chapter 5 and Chapter 6, respectively.

### **4.1 Hypothesized Deep-Hole Drilling Zone Classification**

The interaction between the cutting tool and workpiece material as the tool breaks through the exit surface of the workpiece material leads to the formation of an exit burr. Burr formation is an undesirable projection of plastically deformed material. The process is highly dependent on the work material properties, drill geometry and the mechanics and conditions of the cutting process [103].

Unlike any previous research on the formation of through-holes in drilling operations, it is being hypothesized that the deep-hole drilling process from start to finish consists of 3 distinct zones. Determining how and where the through-hole should be separated into individual zones is based on how the drilling process affects hole quality at different stages of the deep hole drilling operation. These proposed zones are illustrated in Figure 4.1. This classification is based on, and emphasizes the challenges encountered in various regions of through holes created during the drilling of engineering components and parts.

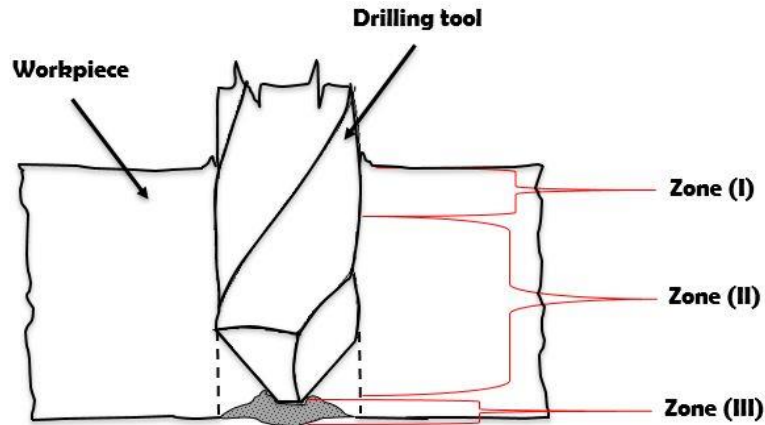


**Figure 4.1: Classification of the zones in a through-hole drilling processes.**

The first zone (Zone I) illustrates the entrance phase of the drill point as the tool engages the workpiece. The cutting edges of the twist drill are not fully engaged, and the cutting forces rises as the tool feeds into the workpiece. The possible challenges encountered in this zone occurs in the centering of the cutting tool into the workpiece which could lead to poor positioning or eccentricity of the hole. This can be avoided by adding a second machining operation using a center drill. Researchers have investigated the initial cutting conditions that influence position deviation, when the drill approaches the workpiece [148-150], and the dynamic behavior that influences the hole tolerance and shape at initial penetration [151, 152]. It has been shown graphically and statistically that hole location errors increase with feed [153]. Fast penetration of the cutting tool through the work material increases hole deflection and vibration in the cutting tool which subsequently results in higher circularity errors [154]. Therefore, reducing hole location and circularity errors could be achieved using small feeds at hole initiation. Another challenge in this zone is the formation of an entrance burr as the tool drills into the work material. This is formed either as a result of a bending action followed by clean shearing

or the result of a Poisson action from the plastic flow of the material in a normal direction of the applied force [155]. The entrance burr occurs at the corners of the twist drill as it feeds into the workpiece and is usually small and almost immeasurable. However, as the cutting edges wear from continuous use, the size of the bulge becomes more pronounced.

In the second zone (Zone II), the cutting lips of the twist drill are fully engaged. In this zone, hole quality is affected by the interaction between the chip that is being formed and the hole surface as chips travel through the flutes during chip evacuation. As the hole-depth to tool-diameter ratio increases, there is an increased tendency for chip rubbing and clogging which leads to increasing difficulties in chip evacuation and an increase in the cutting forces [156, 157]. In precision machining, the rubbing actions resulting from chip evacuation could affect the dimensional accuracy of the hole produced. Oversized hole, angularity error and taper error are some of the detrimental features to the hole quality in this zone.

The final zone (Zone III), involves both shearing and ploughing processes of the workpiece material at tool breakout. It is the combination of these processes that leads to the formation of an exit burr on the workpiece material during drilling. Some of the earlier research into exit burr formation mechanisms and minimization or control strategies in metal drilling has been discussed in Sections 2.4.2 and 2.4.3. It has been found that burr formation cannot be prevented in metal cutting processes [1], however, the need to understand the exit burr formation mechanism in metal drilling is an area of ongoing research. Appropriate knowledge of the mechanisms of exit burr formation could aid in the design of tools that permit accurate burr prediction and process planning that mitigate exit burr formation in metal drilling.

To investigate the phenomenon of the tool interaction with the workpiece material at breakout, drilling tests were performed on extruded Al 6061-T6 material using standard HSS twist drills. The cutting tests were performed without the use of cutting fluid, and the data collected was the thrust force and cutting power of the drilling process. The investigation aims to combine data analysis, optical microscopy and material hardness testing in the study of the burr formation during tool breakout at the exit surface of work material. This includes analysis of the feed and cutting power data, the observation and analysis of the photomicrograph and the microhardness test values of material directly below the drill point of the twist drill prior to tool breakthrough at the exit surface of work material leading to exit burr formation. The analysis is geared to present a better understanding of the breakout burr formation mechanism and identify changes in process mechanics during the drilling process and the onset of the burr formation process. This introduces the use of energy analysis in identifying process changes and changes in the mechanics of drilling and the machining processes in relation to the process and material.

## **4.2 Workpiece Material**

Aluminum 6061-T6 has been used for all the drilling experiments conducted in this study. Aluminum alloys are commonly known for the strength-to-weight ratio and corrosion-resistance. Al 6061-T6 belongs to the 6000 series of aluminum wrought alloys with magnesium and silicon as its principal alloying elements, its chemical composition is shown in Table 4.1. Al-Si alloys are generally used where strength is not an issue. The addition of magnesium and silicon to aluminum produces a compound of magnesium-silicide, which provides this material its ability to become solution heat-treated for

improved strength characteristics. The magnesium addition allows for significant age-hardening through precipitation of the Mg<sub>2</sub>Si in the aluminum matrix, which aids in improving the yield strength of the alloy. It contains 0.8 to 1.2 wt. % magnesium and 0.4 to 0.8 wt. % silicon and other alloying elements with the limits accounting for the overall properties of the alloy. The base aluminum element accounts for a balance of 95.8 to 98.6 wt. % of the alloy.

**Table 4.1: Chemical composition limits of the Al 6061-T6 alloys by wt. % [158].**

Elements	Al	Mg	Si	Cr	Cu	Fe	Mn	Ti	Zn	Others (each)	Others (total)
Min	95.8	0.8	0.4	0.04	0.15						
Max	98.6	1.2	0.8	0.35	0.4	0.7	0.15	0.15	0.25	0.05	0.15

Al 6061-T6 alloy is known for its good corrosion resistance, good machinability, weldability, and increased tensile strength of 45 ksi (achieved by heat treatment and artificial aging). Table 4.2 gives the typical mechanical properties of the alloy such as good toughness and finishing characteristics, that make it useful in structural, automobile and aerospace applications.

**Table 4.2: Typical mechanical properties of Al 6061-T6 alloy.**

Tensile strength		Yield strength		Shear strength		Hv	Elongation, %	
MPa	ksi	MPa	ksi	MPa	ksi		1.6 mm (1/16 in.) thick specimen	13 mm (1/2 in.) diam specimen
310	45	276	40	207	30	107	12	17

Aluminum 6061-T6 alloys typically have a coarse equiaxed grain structure with an average grain size of 18 μm as shown in Figure 4.2. The alloy consists of a high density of

needle-shaped precipitates and a low density of  $\beta$ - $Mg_2Si$  precipitate. The structure contains an uneven distribution of the precipitate in the matrix.

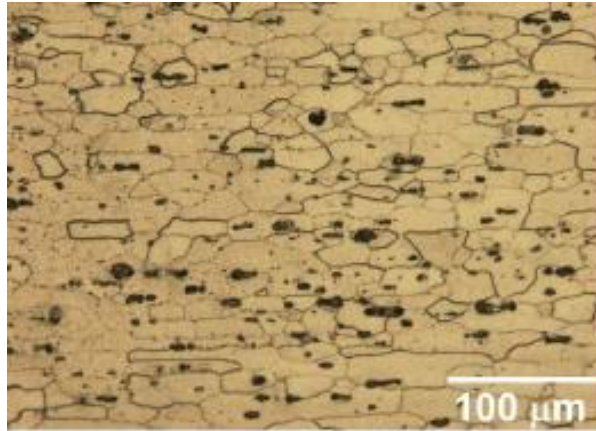


**Figure 4.2: Micrograph of undeformed Al6061-T6 alloy [159].**

### **4.3 Experimental Setup – Data Acquisition**

Metal drilling experiments were performed using an Okuma OSP U100M CNC milling machine. The machine tool is a 3-axis milling machine type ES-V4020 with a 3-phase power supply source, rated capacity of 23 KVA, supply voltage of 220 V, and a frequency of 60 Hz. The power requirement of the CNC milling machine tool is presented in Appendix B. The cutting power measurements were obtained from a PH-3A power cell transducer mounted onto the 3-phase lines of the spindle motor of the CNC machine, with analog output of 0-10V and rated at 10A, 230V network. The spindle power accounts for the cutting and spindle rotational power of the cutting tool during drilling. Simultaneously, thrust force measurements were taken using a KISTLER 9255B dynamometer mounted onto the workbench of the machine tool. The force and power signals were passed through

a DAQ system with the force signal going through a KISTLER type 5010 dual-mode amplifier. An illustration of the setup is shown in Figure 4.3. A final connection is made from the DAQ to desktop computer unit equipped with LabVIEW. The data collected were analyzed using a lowpass filter to filter potential noise that may result from chatter vibration and low frequency whirling before using data for further analysis. It is important to note that the uncertainty associated with the PH-3A power cell transducer measurement is  $\pm 0.5\%$ , while the uncertainty associated with the dynamometer measurement is  $\pm 1\%$ .

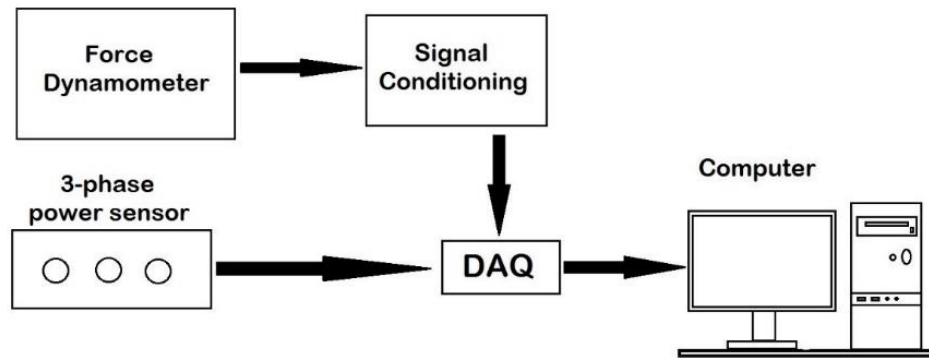


**Figure 4.3: Experimental setup for the drilling process.**

#### **4.4 Experimental Drilling Tests**

All the metal drilling experiments fall into one of three categories: preliminary drilling tests, through-hole drilling experiments and stepped through-hole drilling experiments. The preliminary tests were conducted for two reasons. The first is to confirm the presence of the hypothesized three zones presented in Section 4.1. The second reason is to ascertain any boundary conditions, criteria and constraints that might be required for the primary

drilling experiments particularly as they pertain to drill diameter and workpiece material thickness relationships. By using preliminary drilling tests to understand and model the behavior of the deep-hole drilling process, an appropriate workpiece thickness for steady-state cutting in relation to the tool point geometry and tool diameter could be obtained. As part of the preparation for the primary through-hole drilling experiments, the workpiece thickness must be such that the thrust and cutting power data are maintained in the steady-state region of drilling. This will eliminate any cutting force effects that may result from chip-flow resistance or chip clogging. Essentially, by confirming the existence of the hypothesized 3 zones, the preliminary experiments could be used to determine the workpiece thickness for all subsequent drilling experiments.

The second category is through-hole drilling experiments. An overall view of the complete through-hole drilling experiment is summarized in the flow chart shown in Figure 4.4. The premise behind the workpiece thickness selection and the constraints used in this experimental work is based on findings from the preliminary tests and the position of the critical depth obtained by Iruikwu and Simoneau [160], during deep hole drilling of Al 6061-T6 alloy. This second set of experiments is the foundation of the analysis of the research.

The final set of drilling tests were the stepped through-hole drilling experiments. These tests are used to physically observe and validate findings from the previous through-hole drilling experiments. These tests were also used to examine the stepped burr breakout of the workpiece material, photomicrography, and microhardness testing of the workpiece material through-hole cross-sections.

In all the drilling experiments, thrust forces and cutting power data were collected for analysis. The thrust and cutting power data analysis will ultimately be used to introduce a novel approach that uses cutting energy analysis in the form of feed power from the thrust action and cutting power or the specific cutting power, to identify critical points of interest for further study. Details of the experimental procedures are presented in Section 4.4.1 to 4.4.4.

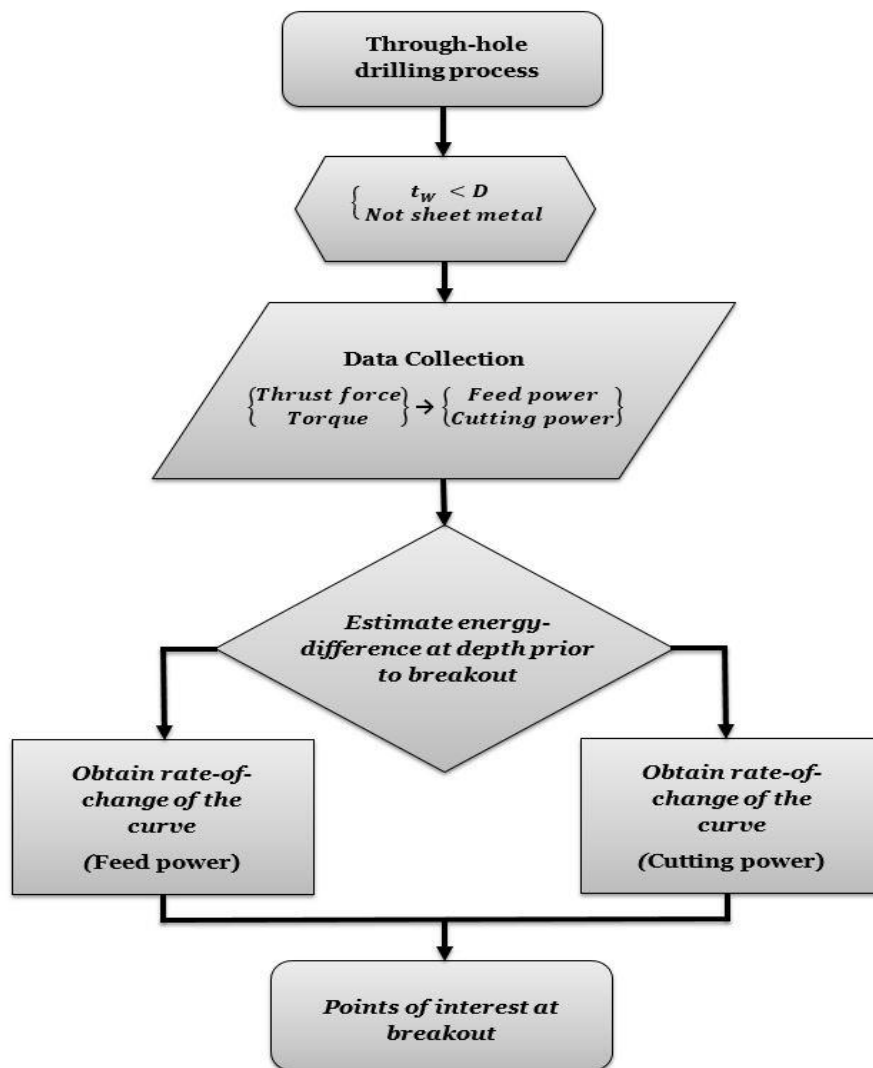


Figure 4.4: Flow chart of experimental procedure.

#### **4.4.1 Preliminary Drilling Test Procedure**

A series of pre-drilling experiments were performed and the spindle power during drilling measured, recorded and analyzed as the cutting tool made a through-hole in a 1-inch (25.4 mm) thick, 6061-T6 aluminum workpiece. The drilling tool used was a 19/64-inch (7.5 mm) black-oxide coated standard HSS twist drill. Spindle speeds of 2573 rpm, 3217 rpm and 3860 rpm were used. This was all done for five different feeds ranging from 0.05 mm/rev to 0.25 mm/rev. The results of the pre-drilling test conducted are presented in Section 5.1.

#### **4.4.2 Experimental Drilling Test Procedure**

The primary through-hole drilling experiment for this study was performed based on findings from the analysis of the pre-drilling experiments described in the previous section (the results and discussion of the pre-drilling experiments are presented in later chapters). Two standard twist drill types with size 3/8-inch (9.52 mm) in diameter and point angle of  $118^\circ$  were selected for the actual drilling experiment. This belongs to the medium size tool range and the cutting edges of the tool point are clearly designed. The experimental parameters used in the main drilling experiment are shown in Table 4.3. All cutting tests were performed without the use of cutting fluid and the cutting parameters were within manufactural recommended values for the drilling of Aluminum alloys. The cutting edges of the twist drill were inspected after each drilling tests and cleaned up using sandpaper to remove potential build-up edge or sticky chips material to ensure that the twist drills used are sharp and in good condition throughout the drilling experiments. The thrust and cutting

power data used in this investigation were obtained by taking the average of three test data from three different drilling tests performed for each cutting parameters.

Table 4.3: Drill test parameter for workpiece material thickness,  $t_w = 8.9$  mm.

Drill Type	Spindle Speed (rpm)	Feed (mm/rev)			
A	2037	0.05	0.10	0.15	0.20
	2547				
B	2037				
	2547				
	3056				

The drill type *A* is a black-oxide HSS standard twist drill with a helix angle  $\delta$ , of about  $29^\circ$ , while drill type *B* is uncoated HSS standard twist drill with  $\delta$  of about  $35^\circ$ . It was assumed that the cutting edges are sharp throughout the cutting process, there is no runout, and the workpiece material properties are homogeneous throughout the stock.

#### 4.4.3 Stepped Drilling and Photomicrograph Procedure

The final set of deep-hole drilling experiments was the stepped through-hole drilling tests. This set of drilling tests involved drilling a through-hole at incremental depths as shown in Figure 4.5. Part of the aim of this set of tests is to obtain photomicrographs of the workpiece material below the drill point and within the third and final zone – Zone III as previously described in Section 4.1. The photomicrographs will include images of the microstructure of the workpiece material at selected hole depths prior to tool breaking through the workpiece exit surface and just after tool breakout. The tests were performed at fifteen different hole-depths using the twist drill type *A* as illustrated in Figure 4.5. This was done at a spindle speed of 2037 rpm, using feeds of 0.05 mm/rev and 0.20 mm/rev respectively.

The samples were sectioned, cold mounted, polished and etched to obtain the photomicrographs. Photomicrographs samples were selected at hole depths prior to and after the tool breaks through the exit surface of the workpiece material.

To investigate the behavior of the workpiece material and the mechanism of burr formation during tool breakout when drilling Al 6061-T6 alloy, fifteen different depths were machined into the work material. The first three depths fall within the deformation zone region (Zone III), prior to the tool point breaking through the exit surface of the workpiece material. The third hole-depth is just on the 8.9 mm plane of the exit surface. The drill point depth increment for each hole depth is  $d_{inc} = 0.286$  mm. Some of the cross-sections are shown in Figure 4.6 to help illustrate the procedure.

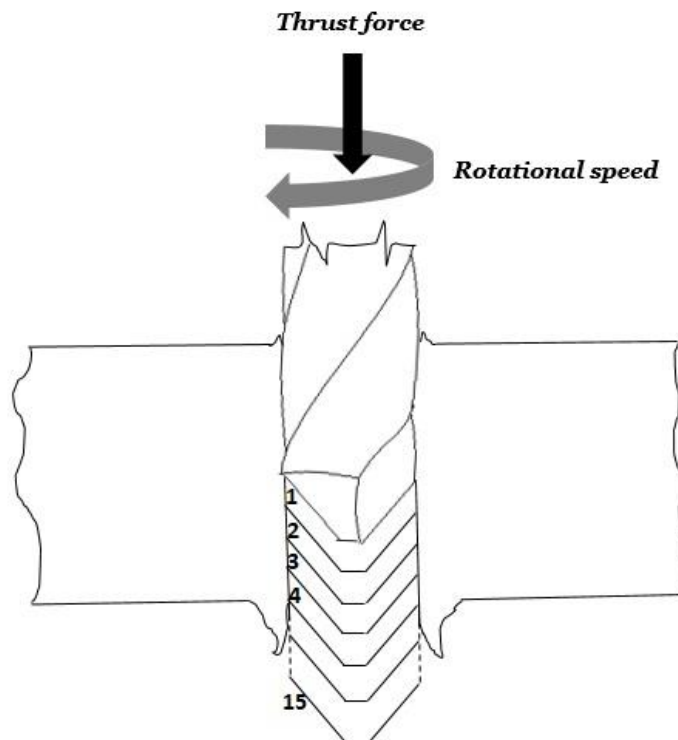


**Figure 4.5: Through-hole for 15 different hole-depths.**

The workpiece samples were sectioned, cold mounted, polished, and etched. The etching was done by applying the Keller's reagent for 30-50 seconds, followed by a Weck's reagent which helped to reveal the grain boundaries.



(a)



(b)

**Figure 4.6: Cross-section of the drilled samples at depths 1,2,3,5,6,8,9,14 &15 at spindle speed of 2037 rpm at feeds (a) 0.05 mm/rev, (b) 0.20 mm/rev.**

#### 4.4.4 Hardness Test Procedure

A Vickers hardness test was performed to study the changes in the physical property of the material below the chisel edge of the cutting tool prior to tool breakout leading to exit burr formation. This would enable us to investigate the changes in the physical properties of the work material leading to breakout burr formation. The drilling of the work material was done using the twist drill type  $B$ , and the test was performed using the cutting parameters given in Table 4.3. For each cutting parameter used, the work material was drilled to three different hole-depths known as the breakout distance or breakout depth,  $t_{Br}$ . The breakout depth is an indication of the distance measured from the chisel edge to the exit surface of the workpiece. The positions of the breakout depth were selected based on positions of critical points of interest derived from the analysis of the thrust force and cutting power data at tool breakout. Detailed analysis of the thrust force and cutting power data leading to identifying critical points of interest and the breakout depth,  $t_{Br}$  used in this investigation are discussed in Section 6.2.

The drilled workpiece samples were sectioned, cold mounted, and polished. This is the preparation phase of the workpiece sample before performing the hardness test. This preparation phase of the experiment is necessary to keep the sectioned workpiece sample in a tight region thereby maintaining the physical properties of the material close to the edges of the sample and it is necessary in order to obtain accurate microhardness test results. Next, the Vickers hardness test was performed on the workpiece samples at the region below the chisel edge of the deformation zone of the work material as shown in Figure 4.7. The spacing between indentations and from the edges of the work material was

performed in accordance with the standard ASTM E92-17 [161]. The indentations created were measured and recorded, and the hardness values computed. The breakout depth used in this study and the results of the Vickers hardness ( $HV$ ) test are presented in Section 5.3.2.

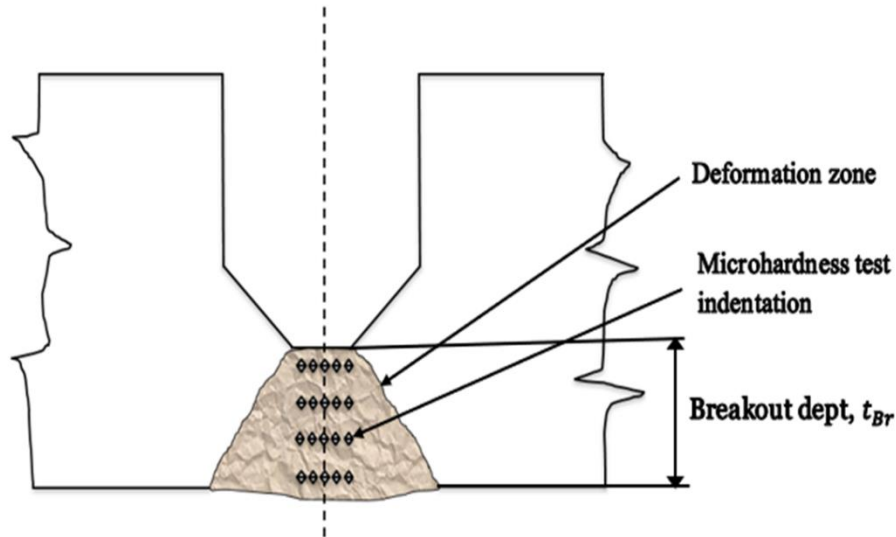


**Figure 4.7: Illustration of Vickers hardness test indentation on workpiece sample.**

## 4.5 Summary

The chapter began with the introduction of a new and novel approach to classifying the problems associated with metal drilling processes. The approach splits the through-hole drilling process into three zones, with emphases laid on the possible challenges. These zones have been labeled zones I, II and III. However, it is Zone III that is of primary interest in this research since it is believed that it is this zone exclusively, that is linked to the breakout burr formation process. The workpiece material, cutting parameters and all drilling tests along with the rationale for the tests were presented in detail.

## **Chapter 5: Experimental Results**

In the previous chapter, we have discussed the various experimental tests conducted in this research work to investigate the exit burr formation mechanism in metal drilling processes. In this chapter, results from the pre-drilling test, the primary drilling experiment, and other experimental works conducted will be presented. The thrust force and cutting power data were observed and recorded for each drilling tests conducted. For the purpose of data processing and analysis, it has been noted that the uncertainty associated with the force and power measuring devices are  $\pm 1\%$  and  $\pm 0.5\%$ , respectively.

### **5.1 Preliminary Drilling Test Results**

The preliminary drilling test results show a pattern in the total spindle power signal that indicates the behavior of the power expended during drilling processes. The total spindle power accounts for the sum of the power expended in the shearing of the work material during chip formation (specific cutting power) and the spindle rotation during the drilling process. The process begins with a power rise as the chisel edge of the cutting tool engages the workpiece surface to the point of full engagement of the cutting edges or lips of the twist drill. As the tool drills further into the work material, steady power is maintained until a hole depth that is approximately the size of the tool diameter. As the hole-depth to diameter ratio increases further, an increase in the power signal continues and later becomes erratic. The cutting power signal becomes more unstable at this depth as the feed or feedrate is increased as shown in Figure 5.1. This agrees with the work by Ke et al. [156], which shows that in deep-hole drilling operations the thrust force and torque begin

to increase at some critical depth. The unprecedented power rise accounts for other factors that constrain the chip evacuation process in deep-hole drilling, such as, chip-flow resistance and chip clogging effect.

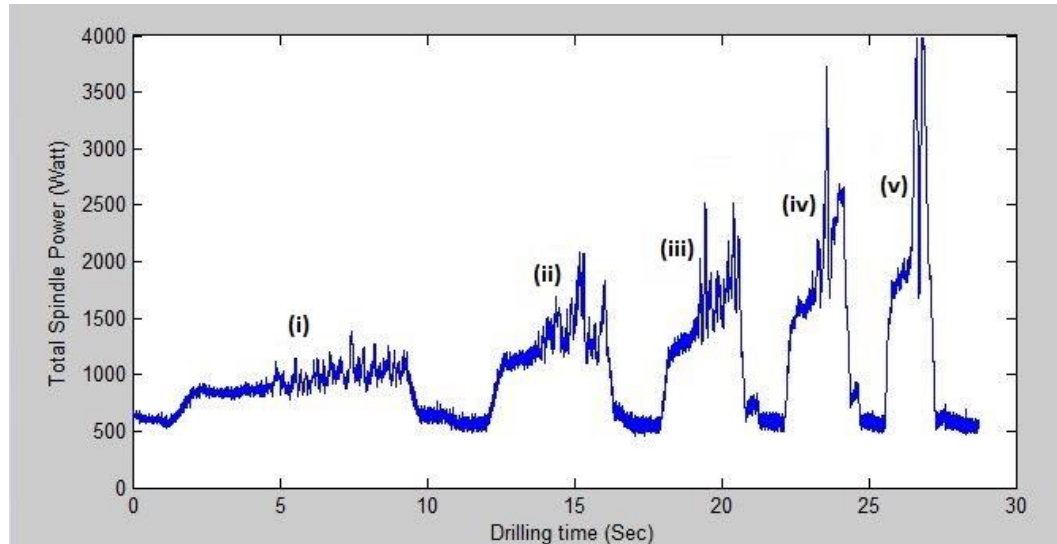


**Figure 5.1: Drilling a 25.4 mm thick Al6061-T6 workpiece using 7.5 mm black-oxide HSS standard twist drill at 3860 rpm and feeds: (i) 0.05mm/rev (ii) 0.10 mm/rev (iii) 0.15 mm/rev (iv) 0.20 mm/rev (v) 0.25 mm/rev.**

For the pre-drilling tests conducted at a spindle speed of 3860 rpm, additional power rise of about 200 Nm/s was observed from the steady-state at a feed of 0.05 mm/rev for case (i), a rise of about 800 Nm/s at 0.10 mm/rev for case (ii) and a maximum peak power rise of additional 2500 Nm/s for case (v) at 0.25 mm/rev; which is more than the steady-state cutting power of the process. This shows that as the depth-to-diameter ratio of the drilling process increases, so does the additional power due to chip-flow resistance and the chip clogging effects. The onset of the spindle power rise from the steady-state was observed at hole depth greater than the tool diameter for the workpiece material and tool type used in this study.

## **5.2 Experiment Drilling Test Results**

The data obtained during the actual experimental work using the cutting parameters given in Table 4.3 are presented in this section. These results show the thrust force and cutting power obtained by taking the average of three test data from three different drilling experiments performed for each cutting parameters during the drilling of Al 6061-T6 workpiece samples.

### **5.2.1 Thrust Force Results**

The thrust force data were obtained for the drilling test performed on Al 6061-T6 alloy having a workpiece thickness 8.9 mm when using a type *A* twist drill and machining at a spindle speed of 2037 rpm and 2547 rpm respectively. The cutting tests were performed at feed range 0.05 mm/rev to 0.20 mm/rev. The thrust force data measured at a spindle speed of 2037 rpm gave a mean thrust force of about 434 N at full penetration when cutting at a feed of 0.05 mm/rev, 851 N at a feed of 0.10 mm/rev, 1061 N at a feed of 0.15 mm/rev and at 0.20 mm/rev, a mean steady-state thrust force of 1348 N was obtained. Figure 5.2 shows the thrust force data obtained during the drilling process at the lower and upper feed limit studied when machining at a spindle speed of 2037 rpm. The data obtained show a proportional increase in the thrust force as cutting feed increase, as expected. This trend was also observed when machining at a spindle speed of 2547 rpm, with a mean thrust force of 528 N observed at a feed of 0.05 mm/rev, 918 N at a feed of 0.10 mm/rev, 1145 N at a feed of 0.15 mm/rev and a mean thrust force of 1313 N at a feed of 0.20 mm/rev. These results also show an increase in the thrust force as the spindle speed is increased, however,

the feed or feedrate has shown the most impact on the thrust force during the drilling process.

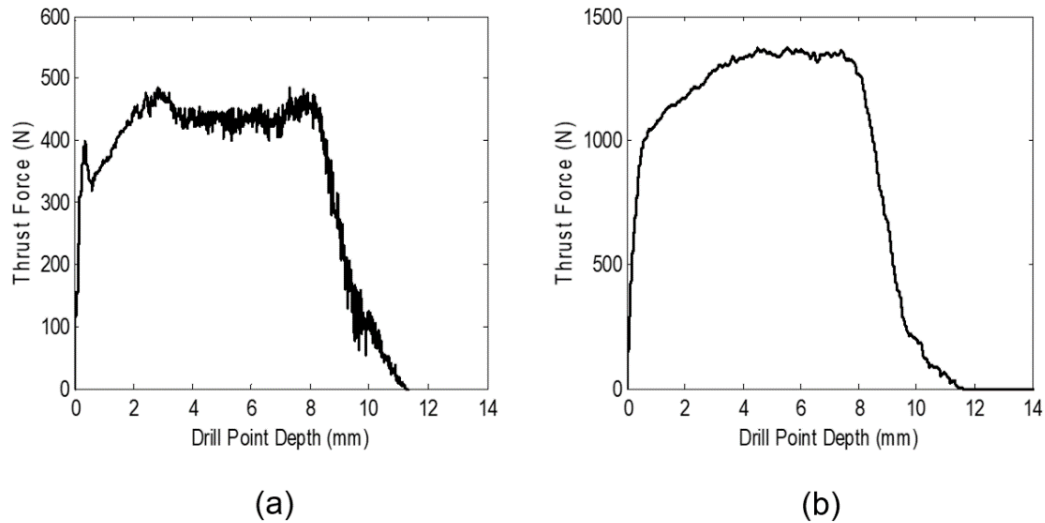


**Figure 5.2: Thrust forces in the drilling of Al6061-T6 workpiece of thickness 8.9 mm using standard twist drill type A at 2037 rpm, (a) 0.05 mm/rev (b) 0.20 mm/rev.**

The thrust force data obtained during the drilling tests performed when using the type B twist drill show a similar trend to the results of twist drill type A. The drilling tests were conducted using the same range of feeds, and three spindle speeds (i.e., 2037 rpm, 2547 rpm and 3056 rpm) during the drilling test performed when using the standard twist drill type B. All drilling test parameters used are shown in Table 4.3.

The thrust forces data measurement for the drilling tests performed when drilling an Al 6061-T6 work material of workpiece thickness 8.9 mm using a type B twist drill at a spindle speed of 2037 rpm gave a mean thrust force of about 259 N at full penetration when cutting at a feed of 0.05 mm/rev, 510 N at a feed of 0.10 mm/rev, 849 N at a feed of 0.15 mm/rev and a mean thrust force of 1053 N at a feed of 0.20 mm/rev. The mean thrust

force increases with increasing feed in all cases of spindle speed tested. This is similar to the trend observed during the test conducted using the type *A* twist drill, however, a considerable reduction in the thrust force was observed when drilling with the type *B* twist drill of the same drill size when drilling on the same stock material and thickness using the same set of drilling parameters. This could be attributed to the twist drill design, as a slight variation in the tool design and geometry of the same drill size could pose a significant impact in the cutting mechanics due to the complex nature of the process and the tool geometry. The thrust force data obtained at spindle speed 2037 rpm using the feed 0.05 mm/rev and 0.20 mm/rev are shown in Figure 5.3. The results show a considerable reduction in the thrust force when compared to Figure 5.2, which could be due to the increased helix angle and variation in other features of the drill point geometry such as the web thickness, rake angle, etc.

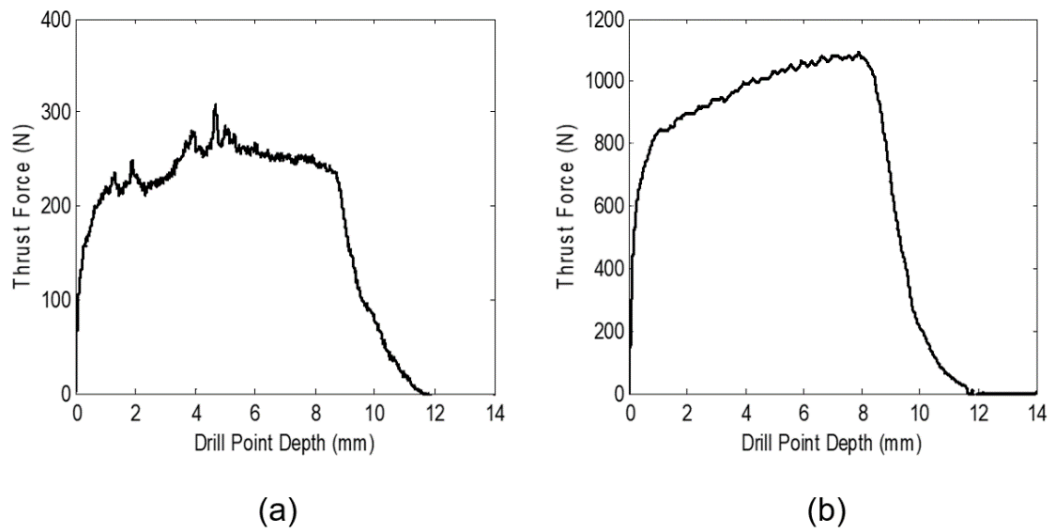


**Figure 5.3: Thrust forces in the drilling of Al6061-T6 workpiece of thickness 8.9 mm using standard twist drill type *B* at 2037 rpm, (a) 0.05 mm/rev (b) 0.20 mm/rev.**

The observed results also show that although the cutting parameters have a great influence on the thrust force data, the tool design and geometry are too important to be ignored in metal drilling processes. A complete representation of the mean thrust force data for the two standard HSS types used in this experimental work is shown in Figure 5.4. The results show increasing thrust force as the feed increases, while the spindle speed shows only a slight increase in thrust force from 2037 rpm to 2547 rpm and a substantial increase at 3056 rpm. Nonetheless, the influence of these cutting parameters on the breakout burr formation would require further analysis of the thrust force data prior to tool breakout at the exit surface of the work material for an understanding of the breakout burr formation phenomenon.

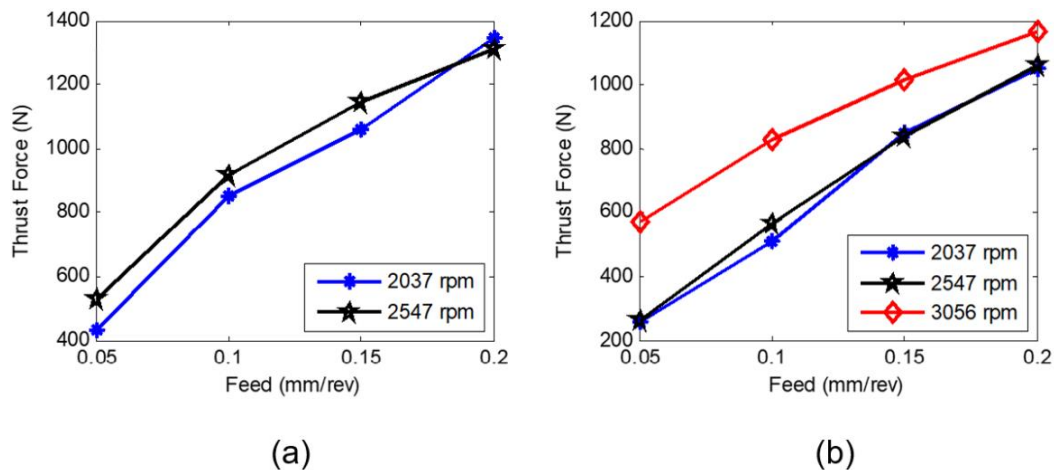


**Figure 5.4: Thrust force data during the drilling of 8.9 mm Al6061-T6 stock thickness using standard twist drill (a) type A, (b) type B**

### 5.2.2 Feed Power Results

The goal of this thesis is to introduce an innovative approach that uses energy analysis to investigate breakout burr formation mechanisms and to identify critical points of process

change leading to the exit burr formation during metal drilling processes. The complex geometry of the cutting tool makes direct use of the thrust force, cutting forces and torque data a challenge. This accounts for the absence of a simplified model for the analysis of the process. However, the power due to thrust force is required for the investigation of the breakout burr mechanism. This is given as the feed power consumed and has been computed using equation (6.3), as discussed in Section 6.2. The computation is made possible since the feed-rate is constant across the cutting lips of the twist drill in the feed direction along the axis of the rotating cutting tool. On the other hand, the cutting speed in the cutting direction varies across the cutting edges on the drill point which makes direct use of the cutting forces or torque a challenge. The computed thrust force results for feeds 0.05 mm/rev and 0.20 mm/rev when drilling Al 6061-T6 of stock thickness 8.9 mm at a spindle speed of 2037 rpm when drilling with the types *A* and *B* twist drills are shown in Figure 5.5 and Figure 5.6.

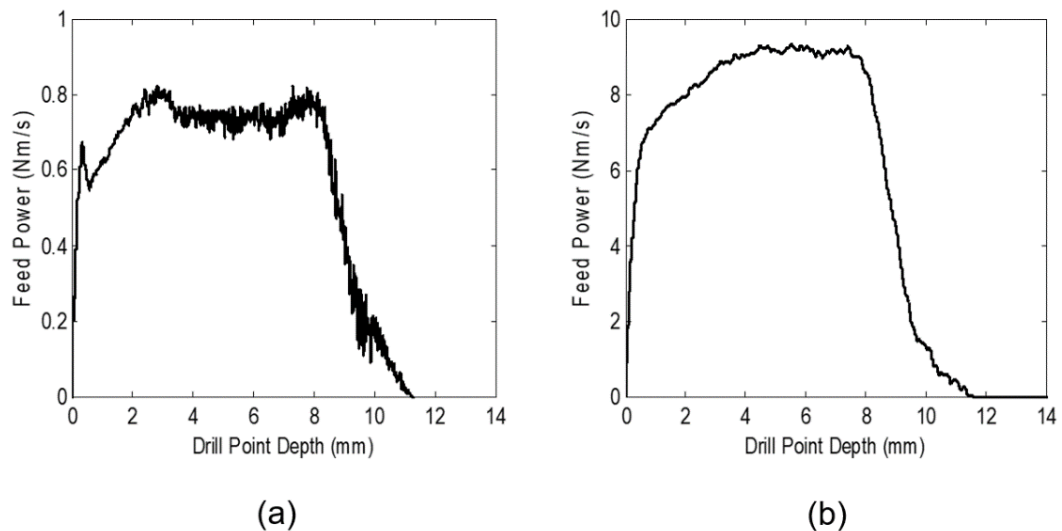


**Figure 5.5: Feed power in the drilling of Al6061-T6 workpiece of thickness 8.9 mm using standard twist drill type *A* at 2037 rpm, (a) 0.05 mm/rev (b) 0.20 mm/rev.**

The feed power accounts for the power expended due to the thrust force acting on the workpiece material as the twist drill feeds into it. A mean feed power of about 0.7 Nm/s and 9.2 Nm/s was obtained at feeds 0.05 mm/rev and 0.20 mm/rev when cutting at 2037 rpm using the type *A* tool. These values reduce to about 0.4 Nm/s and 7.1 Nm/s respectively, for the drilling tests performed using the standard HSS twist drill type *B* at the same spindle speed and feed. The feed power is negligible and has always been neglected in the analysis of metal cutting processes, yet, its importance in the analysis of breakout burr formation during metal drilling processes cannot be overemphasized. It is also important to note that the feed power share similar characteristics as the thrust force with respect to the variation in the spindle speed and feed, but the feed power is a more reliable and required tool in the analysis of the exit burr formation in this study.

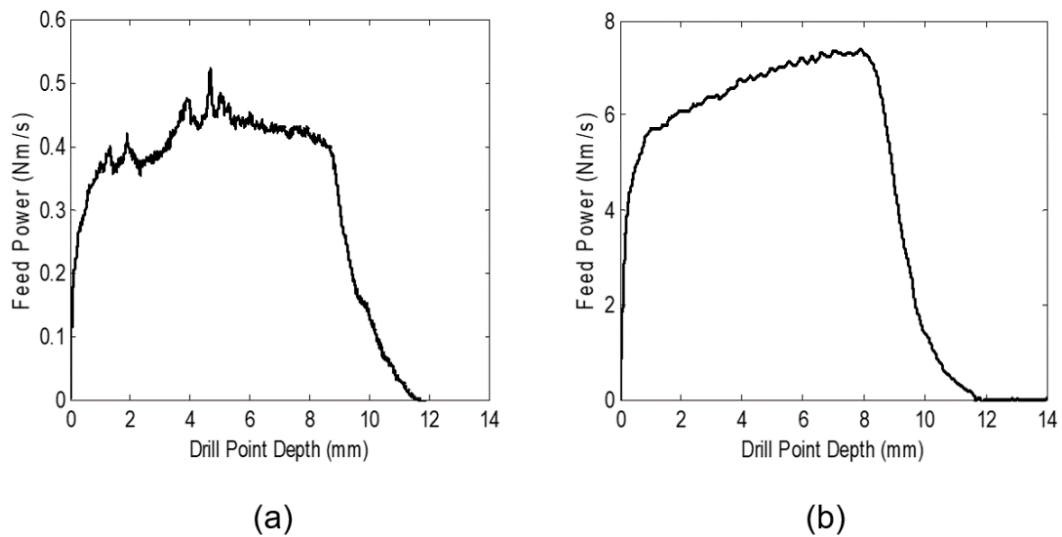


**Figure 5.6: Feed power in the drilling of Al6061-T6 workpiece of thickness 8.9 mm using 3/8-inch un coated HSS standard twist drill type *B* at 2037 rpm, (a) 0.05 mm/rev (b) 0.20 mm/rev.**

### 5.2.3 Cutting Power Results

The cutting power data is also a requirement used to investigate the burr breakout phenomenon as it accounts for the energy expended in the shearing of the workpiece material during the chip formation process. Keeping in line with the results of the thrust force and feed power presented for the upper and lower limit of feed studied. At full penetration, mean cutting power of 295 Nm/s and 710 Nm/s were observed at feeds 0.05 mm/rev and 0.2 mm/rev when drilling at a spindle speed of 2037 rpm using the type *A* twist drill as shown in Figure 5.7. These results show an increase in cutting power as the cutting feed increase. This makes sense as increasing feed increases the amount of material being shear at the cutting edges and thus the material removal rate.

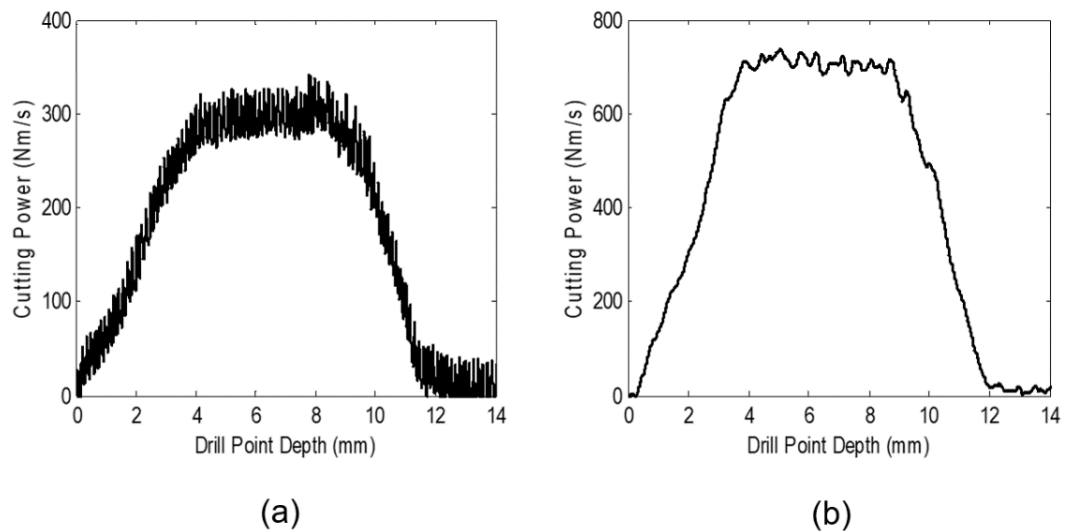


**Figure 5.7: Cutting power in the drilling of Al6061-T6 workpiece of thickness 8.9 mm using standard twist drill type *A* at 2037 rpm, (a) 0.05 mm/rev (b) 0.20 mm/rev.**

The cutting power data when cutting with the type *B* twist drill also shows an increase in cutting power as the feed increases. At a spindle speed of 2037 rpm, the mean

cutting power observed was about 180 Nm/s when cutting at a feed of 0.05 mm/rev. The mean cutting power increases to 667 Nm/s at a feed of 0.2 mm/rev as shown in Figure 5.8. The cutting parameters have a significant influence on the energy expended in the shearing of the Aluminum 6061-T6 stock during the drilling process. Results show a considerable increase in the cutting power as feed increase for all the cases studied. The mean cutting power increases from 295 Nm/s at 0.05 mm/rev, 450 Nm/s at 0.10 mm/rev, 563 Nm/s at 0.15 mm/rev, to 710 Nm/s at 0.20 mm/rev when cutting at 2037 rpm using drill type A. The results obtained at the same spindle speed when drilling with the type B standard twist drill gives 180 Nm/s at 0.05 mm/rev, 361 Nm/s at 0.10 mm/rev, 519 Nm/s at 0.15 mm/rev and 667 Nm/s at 0.20 mm/rev.

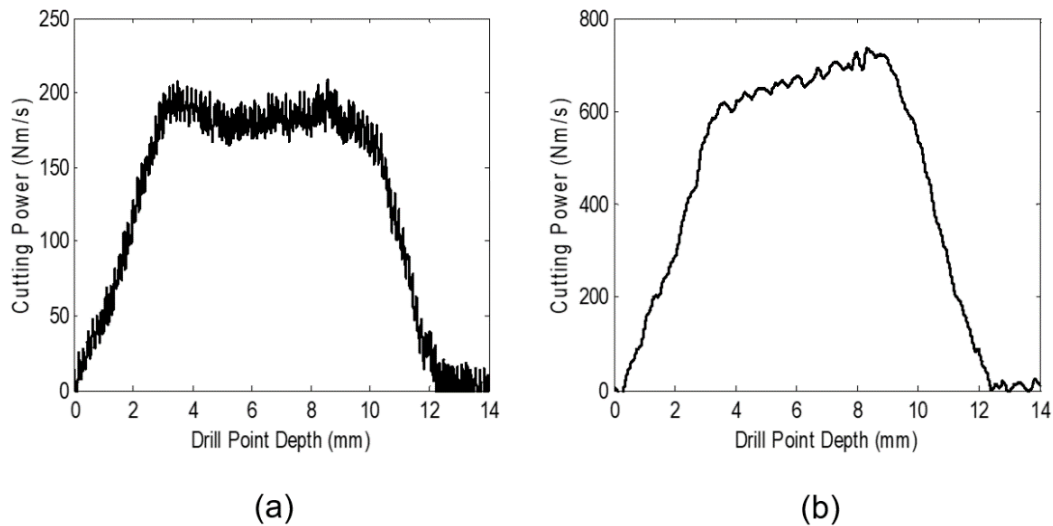


**Figure 5.8: Cutting power in the drilling of Al6061-T6 workpiece of thickness 8.9 mm using standard twist drill type B at 2037 rpm, (a) 0.05 mm/rev (b) 0.20 mm/rev.**

Increasing spindle speed also yields a considerable increase in the cutting power output, which is expected. This increases the material removal rate and the rate of strain at the cutting edges of the tool. The results show an increase in the mean cutting power from

295 Nm/s to 370 Nm/s for drilling performed at 2037 rpm and 2547 rpm respectively when machined at a feed of 0.05 mm/rev using the type *A* standard HSS twist drill. These results are shown in Figure 5.9 for the drilling test performed on an 8.9 mm Aluminum 6061-T6 work thickness. A similar trend was observed during the drilling test performed using the type *B* twist drill at a spindle speed of 2037 rpm and 2547 rpm for all feeds.

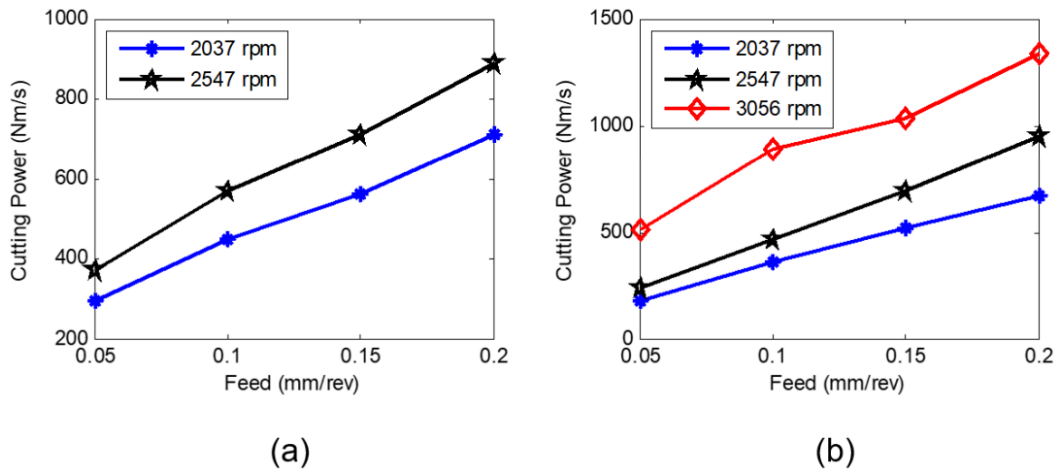


**Figure 5.9: Cutting power data during the drilling of 8.9 mm Al6061-T6 stock thickness using standard twist drill (a) type *A*, (b) type *B*.**

For the drilling tests performed using the type *B* twist drill, at a feed of 0.05 mm/rev at full penetration, a mean cutting power of 180 Nm/s was observed at a spindle speed of 2037 rpm and increases slightly to 235 Nm/s at a spindle speed of 2547 rpm. Furthermore, increasing spindle speed to 3056 rpm increases the mean cutting power by a significant amount to 509 Nm/s. This considerable increase was observed across all feed investigated, however, as the feed increases the amount by which the cutting power increases when cutting at 2037 rpm to 2547 rpm becomes substantial. This could be attributed to the higher material removal rate and tool-workpiece interaction leading to high temperature and

consequently friction. Aluminum alloys are prone to stick at high temperatures when machining at higher cutting speed and increasing the feed increases the shear area and consequently the material removal rate. This directly affects the cutting mechanics during the process as it impacts chip flow resistance and friction raising the overall cutting forces during the chip formation process.

Another notable feature observed is the significant reduction in the overall cutting power expended during the drilling of Aluminum 6061-T6 stock using the type *B* standard HSS twist drill when compared to the power data obtained for the drill type *A* standard HSS twist drill for all cutting parameters studied. This reduction can be attributed to the tool design and variation in the helix angle, web thickness, rake angles, chisel angle, etc. The reduction was also observed in the thrust force data obtain which makes sense since increased helix angle decreases torque and thrust force [59, 60]. It should be noted that even with the same tool size standard HSS twist drills with a drill point of  $118^\circ$ , a variation in the drill point geometry and helix angle has a significant effect on the process output.

### **5.3 Deformation Zone Test Results**

To better understand the breakout burr formation phenomenon, an investigation of the changes that occur in the microstructure level of the workpiece material as the cutting tool breaks through the exit surface of the workpiece material is a necessity. To do this we have conducted a drilling test to capture the photomicrograph of the workpiece at various stages as the cutting tool drills through a hole. Furthermore, Vickers hardness tests were also performed on the workpiece samples. This would aid in understanding how the process

changes affect the physical property of the workpiece at tool breakout. The procedures implemented to study the breakout burr formation mechanism and behavioral characteristics of Aluminum 6061-T6 at tool breakout during drilling are presented in Section 4.4.3 and 4.4.4.

### **5.3.1 Photomicrographs of Breakout Burr**

The microstructure of the workpiece samples below the drill point of the Aluminum 6061-T6 work material was observed. The effect of the feed can be seen on the material behavior as shown in Figure 5.10, as the cutting tool breaks through the exit surface of the work material of thickness 8.9 mm. Observing Figure 5.10 A), for a drilling operation conducted at a feed 0.05 mm/rev, no bulge was observed at the first drilled hole depth (8.328 mm), but a material bulge was observed below the chisel edge at the second hole depth (8.614 mm). This shows that at a feed of 0.05 mm/rev, the material begins to bulge after the first hole depth, whereas when drilling at a feed of 0.2 mm/rev the material bulge occurs before the first hole depth tested (at 8.328 mm) as shown in Figure 5.10 B). This shows that a change in the feed causes a change in the position of the deformation zone boundary from the exit surface.

Another interesting finding is the initiation of crack or tear at the grain boundaries of the bulged workpiece material directly below the chisel edge of the twist drill. This phenomenon was observed in all cases studied. It should be noted that the depth at which the crack initiates varies slightly with feed, i.e., as the feed increases so do the onset of the crack on the work material below the chisel edge of the twist drill. The position of the crack

initiation impacts the burr type formed since uncut work materials below the drill point are pushed out to form exit burr.

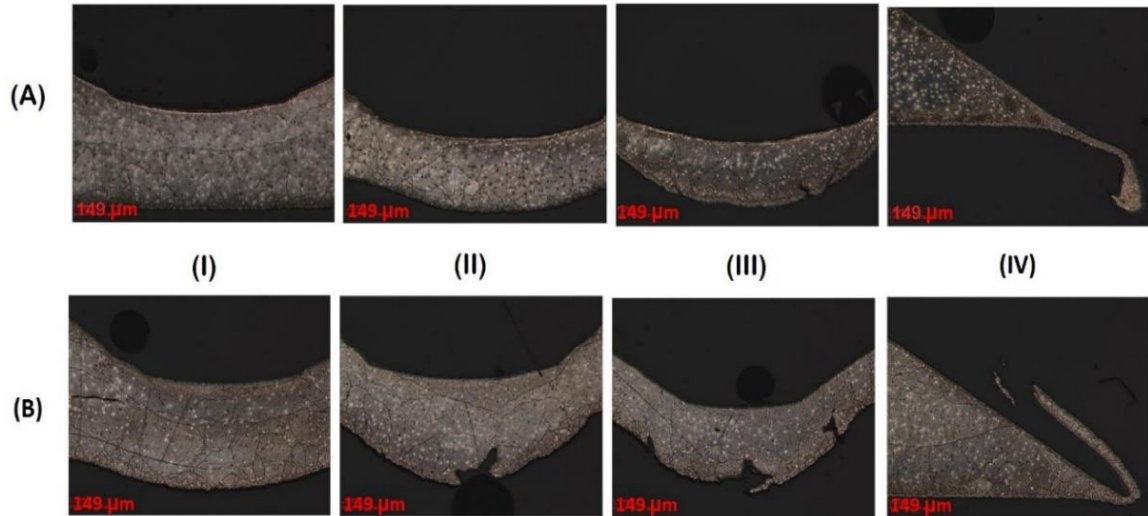


**Figure 5.10: Micrograph of samples drilled to depths (I) 8.328 mm, (II) 8.614 mm, (III) 8.90 mm & (IV) 10.616 mm, at rotation speeds of 2037 rpm (A) feed of 0.05 mm/rev & (B) feed of 0.20 mm/rev**

### 5.3.2 Hardness Test Results

To further investigate the effect of the breakout phenomenon on the physical properties of the work material, Vickers hardness tests were performed using positions of the points of interest identified in the analysis of the thrust force and cutting power data. The analysis of the thrust force and cutting power data and the technique implemented in the assessment of critical points of interest that identifies the changes in the process mechanics and material prior to tool breakout during the drilling process are discussed in detail in Section 6.2. The points of interest derived from the activity of the thrust force are the position of breakout initiation, P1 and the deformation zone depth, P2. These points have been

identified in this study as the points of onset of the change in the cutting mechanics and material physical properties leading to the exit burr formation. The material cut and its hardness are of prime importance to the specific cutting energy. The hardness value of the work material is closely akin to the specific cutting energy [60]. The hardness value of the workpiece section below the chisel edge of the twist drill is used here to further investigate the work material characteristic in the deformation zone during breakout burr formation.

The microhardness test was performed on workpiece material between the chisel edge of the twist drill and the exit surface before tool breakout as illustrated in Figure 4.7. The distance from the position of the chisel edge to the exit surface measured around the deformation zone is known as the breakout distance or breakout depth,  $t_{Br}$ . It is measured from the origin at the chisel edge to the exit surface of the workpiece directly below the cutting tool as shown in Figure 5.11. The work material was drilled to three different breakout depth ( $t_{Br_1}$ ,  $t_{Br_2}$  and  $t_{Br_3}$ ) using the twist drill type *B* and the test parameters as presented in Table 4.3. However, the results of the drilling test performed at a spindle speed of 2037 rpm and feed of 0.15 mm/rev are presented for this analysis.

The first breakout depth,  $t_{Br_1}$  should occur at hole-depth position few micrometers before the position of the breakout burr initiation P1, the second  $t_{Br_2}$ , occurs at a hole-depth position between P1 and P2, while the third breakout depth  $t_{Br_3}$  should be at a hole-depth between P2 and the exit surface of the work material. Hence, three approximate breakout depth positions (1.5 mm, 0.8 mm and 0.5 mm) were selected for all test cases of  $t_{Br_1}$  to  $t_{Br_3}$ . These values were used based on the position of P1 and P2 obtained from the thrust force data when cutting at the upper limit cutting speed and feed parameter, which

result in the most deformation zone depth and also cause the burr initiation to occur earlier. It should be noted that the breakout depth dimensional difference observed between the NC machine input data and the machined workpiece sample data was negligible.

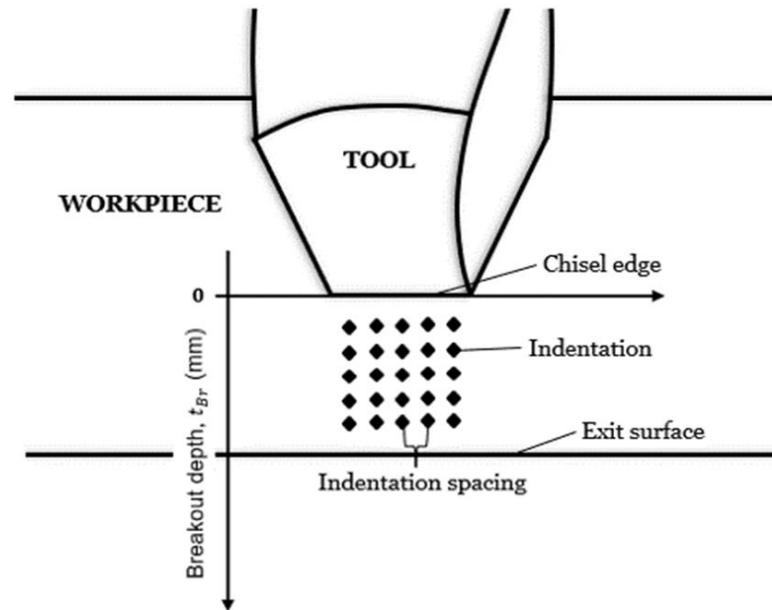


**Figure 5.11: Illustration of data representation for hardness test values.**

The Vickers hardness test results for test samples machined at a spindle speed of 2037 rpm and a feed of 0.15 mm/rev for the three breakout depth examined are shown in Figure 5.12 to Figure 5.14. The spacing between the indentations was carried out in conformity to the microhardness testing standards, ASTM E92-17. The test force applied on the cold mounted and polished workpiece sample is 2.01 N (205 gf). The indenter is brought into contact with the test specimen, in the direction normal to the workpiece surface, and allowed to dwell for 30 sec. The diagonals of the indentation are measured, and the Vickers hardness value estimated. It should be noted that the  $HV$  of undeformed Al 6061-T6 is at about 107  $HV$ .

The results show a drop in the overall  $HV$  values around the edges and midway of the deformation zone depth for tests performed at breakout depth of 1.5mm. Similarly, lower  $HV$  values were also observed near the exit surface. However, higher values up to 112  $HV$  were observed at about 0.3mm from the chisel edge and 113  $HV$  at 0.3mm to the exit surface of the drilled workpiece. The microhardness values for the drilling test performed at 2037 rpm and feed 0.15 mm at the breakout depth,  $t_{Br_1}$  is shown in Figure 5.12. The higher  $HV$  values are sparsely distributed and prominent at the indentation at 0.3mm from the free surfaces (i.e., from the chisel edge and the exit surface of the drilled sample).

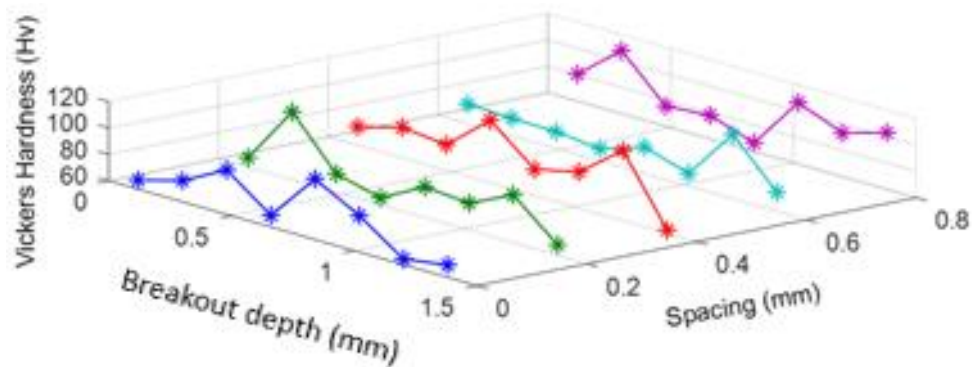


**Figure 5.12: Vickers hardness values of Al6061-T6 at breakout depth,  $t_{Br_1}$  of 1.5 mm to exit surface, using drill type  $B$  at feed 0.15 mm/rev and speed 2037rpm.**

As the twist drill feeds through P1, at breakout depth,  $t_{Br_2}$  the overall microhardness value reduces further below that of the undeformed aluminum alloy. This can be seen in Figure 5.13. The  $HV$  values show that the work material directly below the chisel edges is subjected to plastic deformation that accounts for the energy expended in the shearing process leading to thermal softening due to high strain, high strain rate, and

temperature rise and due to the compressive stress that results from the thrust action. This causes a transition in the material property below the chisel edge of the deformation zone and weakens the material thus reducing the hardness property of the material. At this stage, the higher  $HV$  values are noticeable close to the free edges at the chisel edge and exit surface. However, a high  $HV$  value was observed within this mixed, which could be due to an uneven distribution of the beta-magnesium silicate precipitate in the matrix and inhomogeneity in the hardness distribution.

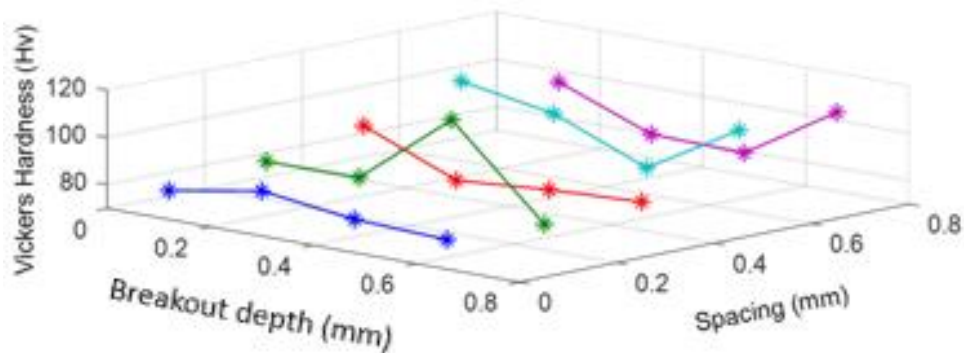


**Figure 5.13: Vickers hardness values of Al6061-T6 at breakout depth,  $t_{Br_2}$  of 0.8 mm to exit surface, using drill type  $B$  at feed 0.15 mm/rev and speed 2037rpm.**

As the cutting tool drills further within the deformation zone to  $t_{Br_3}$ , the work material is subjected to a combination of shearing, ploughing and pushing effect causing the workpiece to bulge. This causes regions of compression around the middle of the chisel edge and tensile stress around the periphery of the chisel edge. This causes the material hardness values to respond accordingly as shown in Figure 5.14. At the periphery of the chisel edge, low  $HV$  values were observed. The reverse occurs toward the exit surface, as the material is subjected to compressive stress around the periphery of the chisel edge.

Pushed work material around this region is subjected to bending stress and tensile stress and reduced  $HV$  values at the exit surface directly below the chisel edge center.

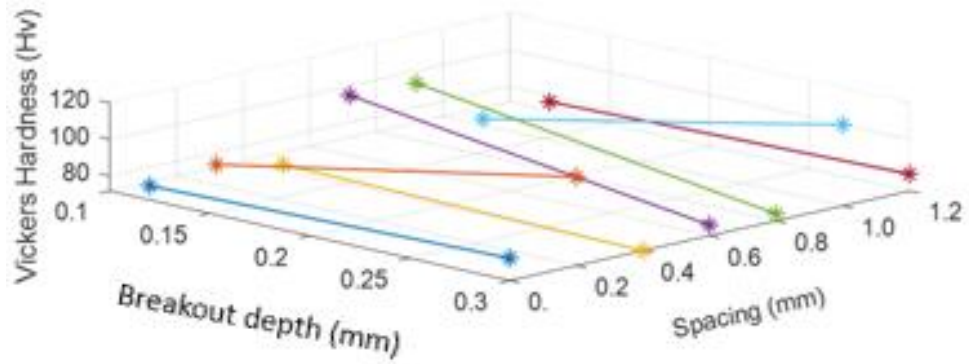


**Figure 5.14: Vickers hardness values of Al6061-T6 at breakout depth,  $t_{Br_3}$  0.5 mm to exit surface, using drill type  $B$  at feed 0.15 mm/rev and speed 2037rpm.**

## **Chapter 6: Discussion of Results**

The research focus of this thesis is centered around zone (III) of the through-hole classification introduced in Section 4.1, and is aimed at investigating the burr formation mechanism in metal drilling. The choice of work material is Al 6061-T6 known for its weight-to-strength property and good machinability, which makes it one of the most used Aluminum alloys in structural, automobile, aerospace and general-purpose application. However, it generates crown burrs when machined at high feeds and speeds due to its ductility and sticky property at high temperature which dwindles the performance and efficiency of the machining process. Unlike stainless steel, Al 6061-T6 has no relationship between the exit burr thickness and burr length [155], which makes it an important work material to investigate the breakout burr formation mechanism in metal drilling processes. This chapter will present a detailed analysis of the experimental data obtained in Chapter 5. The technique implemented and observation will be presented. The findings and contributions of the approach used in this analysis and its implication to the study of breakout burrs in metal drilling processes will be addressed.

### **6.1 Discussion of Preliminary Test Results**

The results of the pre-drilling tests show that at a depth that is just about the size of the tool diameter, the spindle power signal begins to experience an increase in the cutting power signal. Therefore, in deep-hole drilling operations, the thrust force and torque begin to increase at some critical depth. On account of this observation, the workpiece thickness was machined from 25.4 mm (1-inch) to 8.9 mm in preparation for the actual drilling

experiment with the intent to limit the thrust force and cutting power signal within the steady-state operation as a constraint for the study.

Based on the observations of the cutting power from the preliminary tests, the model shown in Figure 6.1 was proposed to illustrate the cutting force and cutting power signal characteristics in deep-hole drilling operations. The proposed model reveals that the metal drilling processes begin with steady-state cutting of the workpiece. As the drilling process continuous, when a critical depth,  $t_{wc}$  is reached, a rise in the cutting force and power occurs. This critical depth has been found to be approximately equal to the drill tool diameter when machining the Al6061-T6 workpiece. This model is applicable to drilling processes for a standard twist drill, other drill types may behave differently depending on the tool design and drill point geometry.

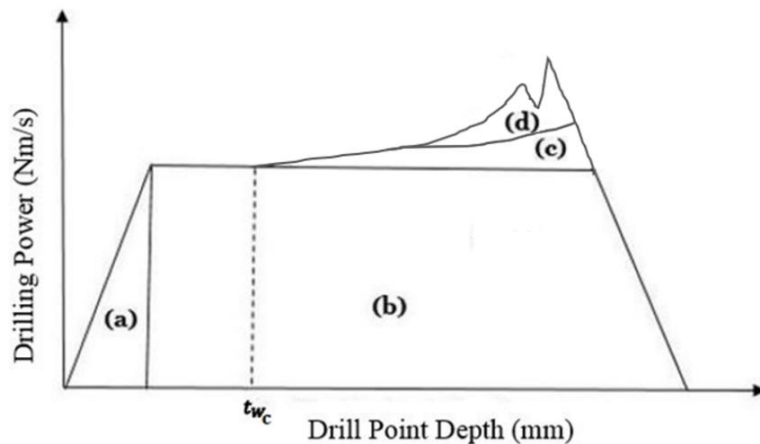


**Figure 6.1: Schematic illustration of deep-hole drilling Power data.**

The segment labeled (a) in Figure 6.1 is the cutting area represented by zone (I) from Figure 4.1. This involves penetration of the drill point into the workpiece at the start of drilling. It accounts for the cutting process from the point at which the chisel edge

touches on the workpiece surface to the point at which the drill point is completely engaged in the workpiece material, starting from the center of the chisel edge to the periphery of the cutting edges. The segment labeled (b) accounts for the continuous chip formation process as the cutting edges are completely engaged in the process. It begins with a steady-state cutting until a depth is reached and resistance from chip evacuation and chip clogging causes a rise in the forces and power signal. The segment labeled (c) accounts for the resistance to chip flow due to chip rubbing action on the tool-flute and hole-wall interface as the chips are evacuated from the drilled hole. This resistance to chip flow increases with an increasing depth-to-diameter ratio. The final segment labeled (d) accounts for the chip clogging problems that result in chip evacuation in deep-hole drilling. At this depth, the power signal becomes inconsistent, changing drastically with increasing feed-rate. This was seen in the pre-drilling test shown in Figure 5.1. The result shows a drastic rise in the total spindle power as feed is increased. This agrees with work done by Ke et al. [156], who investigated the effect of the chip thickening in deep-hole drilling of AISI 1045 steel using a 6.4 mm HSS drill.

Therefore, the total power expended during deep-hole metal drilling processes can generally be expressed as

$$u = u_{cut} + u_f + u_{cl} \quad (6.1)$$

where  $u_{cut}$  is the specific cutting power due to shearing of workpiece material at the cutting edges,  $u_f$  is the power due to chip flow resistance and  $u_{cl}$  is the clogging effect. The unit for the estimated power consumption is given in Nm/s. The drilling power consumed during a through-hole must be equal to the specific cutting power to maintain a steady-state drilling process.

Aluminum Al6061-T6 alloy is a ductile material with good machinability, forming continuous chips during the shearing process. Chip formation begins as a spiral after full engagement of the drill lips and translates into a string shape at a certain depth. The chip at the exit of the flute flows at about the same rate as the rotational speed of the cutting tool, but at the cutting edge the chip is limited to the cutting speed at the cutting edges. When the rotating force effect at the chip exit exceeds the cutting action and chip-flow resistance, the spiral chip stretches into a string, or the chip fractures at the cutting edge and is evacuated. This phenomenon continues until more of the string chips form leading to difficulty in the chip evacuation. This phenomenon was investigated by Ke. F. et al. [162], where the chip removing motions and forces were analyzed. On this account, it has been inferred that maintaining the formation of a spiral chip is necessary to obtain steady chip evacuation and minimal chip-flow resistance. Therefore, cutting fluid is recommended in deep-hole drilling of aluminum alloys. This material sticks at high temperatures and forms built-up-edges at low cutting speed. The use of cutting fluid would increase cutting efficiency and tool life, but in turn, increases the overall machine tool energy usage and pose some environmental and health concerns.

For the deep-hole drilling the chip-flow resistance and chip clogging begin to have an effect at a hole-depth greater than or equal to 5 times the tool diameter. For this workpiece material, it was observed that the rise in the drilling power during a drilling operation initiates at a hole-depth approximately equal to the twist drill tool diameter, hence it is expedient that we select a workpiece thickness that is less than the tool diameter to avoid the effect of chip-flow resistance or chip clogging that could result during chip evacuation, and consequently eliminate any additional force effects that could alter the

power and force signals used in identifying the critical points of the burr formation mechanism at tool breakout. The chip-flow resistance forces may be present at this hole-depth, but they are negligible.

An additional condition that was accounted for in the preparation of the actual experimental test, is that the workpiece must not be sheet metal. It has been shown experimentally that the thrust and torque in sheet metal drilling are at its peak when the drill lips are completely engaged at full penetration, after which there is a drop in the forces signal as the drill breaks through the sheet metal. The thrust and torque of a metal drilling operation consist of transient signals necessitating the evaluation of the influence of drill point geometry on the basis of peak signal levels in sheet metal drilling [114]. As such, the geometry of the drill point is reflected in the patterns of the cutting force signals. Thus, the workpiece diameter for this study must meet the condition

$$0.3d < t_w \leq d \quad (6.2)$$

where  $d$  is the standard twist drill diameter and  $t_w$  is the workpiece thickness. It should be noted that the standard twist drill attains full penetration at approximately  $0.3d$ . This parameter varies for different twist drill types depending on the drill point design and geometry. Thus, keeping to a workpiece thickness less than the critical depth  $t_{wc}$  at full penetration would help maintain a steady state cutting power during the drilling processes. This approach has been investigated to optimize peck depth in the deep-hole drilling cycle by Iruikwu and Simoneau [160]. Therefore, based on the findings and set constraints an Al 6061-T6 stock of thickness of 25.4 mm was face milled to 8.9 mm and used in the main experimental tests conducted.

## 6.2 Discussion of the Feed and Cutting Power Results

Thrust force and cutting power data were collected for the drilling experiments. The premise for reducing the workpiece thickness below the value of the cutting tool diameter was to limit the cutting power to its steady state of cutting operation throughout the cutting experiment. The vertical axis drive (feed) power expended by the machine tool could not be obtained using a 3-phase power sensor due to some anomalies resulting from the phasing of the vertical drive motor, which posed challenges in obtaining accurate voltage and current signal measurements. However, for the this study the feed power expended by the cutting tool in the drilling test is obtained as

$$u_{th} = F_{th} * f_r \quad (6.3)$$

where  $F_{th}$  is the thrust force measured in newtons (N), and  $f_r$  is the feed-rate of the metal drilling process measured in mm/min.

### 6.2.1 The Energy-difference Approach and Change-rate Curve

The next step requires the introduction and implementation of an original method known as the energy-difference approach (EDA) for further data analysis to investigate the exit burr formation mechanism. The energy-difference is expressed as the differences in the energy expended in drilling a workpiece through successive hole-depths, estimated from a referenced arbitrary point of the steady-state cutting process. It estimates the energy used up in performing a drilling process between successive hole-depth. During a drilling operation, the difference in the energy expended to perform a drilling process from point A to B, as shown in Figure 6.2, taking an initial reference on the entry surface is given by

$$E_{AB} = E_B - E_A \quad (6.4)$$

where  $E_A$  is the energy expended in drilling from the onset to point A (joules),  $E_B$  is the energy expended in drilling from the onset to point B (joules).

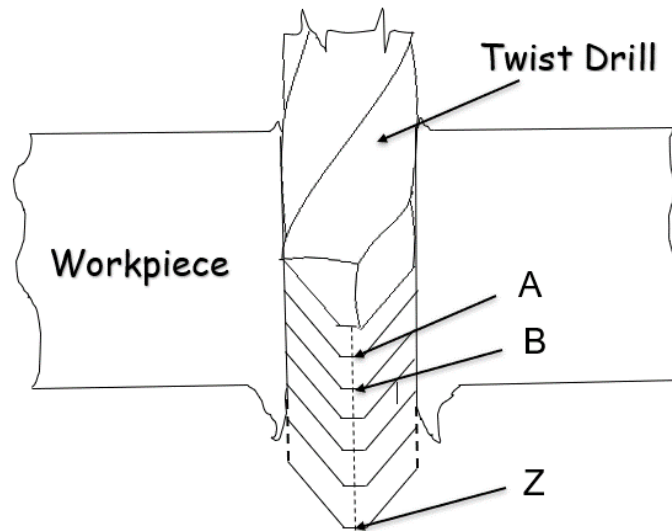


**Figure 6.2: Illustration of successive incremental hole-depth in drilling.**

The energy-difference approach requires an initial arbitrary hole-depth position on the zone of the steady-state cutting operation. It estimates the process energy used up in drilling the workpiece from an arbitrary hole-depth during steady-state cutting to subsequent hole-depth during the drilling operation. It can be used to estimate the energy change due to changes in the process mechanics, as cutting edges shear through the work material, and is used to identify process changes and the change in the work material property, as the twist drill breaks through the exit surface of the workpiece. To obtain good accuracy during the implementation, the arbitrary depth selected must be such that it allows for enough clearance between the chisel edge and the exit surface. The energy-difference

is obtained with respect to a referenced arbitrary depth which was selected to be  $0.65 * t_W$  using the expression

$$E_{diff} = E_n - E_k \quad (6.5)$$

where  $E_{diff}$  is the energy-difference (joules),  $E_k$  is the energy at an arbitrary hole-depth estimated at 65% of the depth traveled in reference to the workpiece thickness  $t_W$ , while  $E_n$  is the energy at an incremental hole-depth. It should be noted that  $E_n > E_k$ .

The curve representation of the energy-difference for a sequence of successive incremental hole-depth is known as the energy-difference curve. Using the energy-difference curve data, a change-rate curve is derived and used to identify unique points of interest that characterize the exit burr formation mechanism in metal drilling processes. This method requires estimating the slope or change-rate curve from the energy-difference curve and identifying the unique points on the curve that correlates with the changes in the chip formation process- including changes in the cutting mechanics that are observable from cutting power data, and changes in the material properties due to deformation and thermal effects observable from the thrust force or feed power data. This would enable us to understand the parameters affecting the formation of various burr types at tool breakout and aid in characterizing the phenomenon involved.

Using feed and cutting power in this investigation, unique points in the metal drilling process at which the steady-state operation maintained during the material removal process is interrupted due to changes in the cutting mechanics and response to workpiece material property are identified. The shearing action on the cutting edges of the twist drill is also affected by the changes in the material properties below the drill point before tool breakout

at the workpiece exit surface. These changes are being captured by the analysis of the feed and cutting power signal using the energy-difference approach.

### **6.2.2 Analysis of the Feed Power**

The feed power accounts for the thrust action that acts on the work material during the drilling process. As the drill approaches the exit surface, a region of plastically deformed work material is formed below the drill point of the twist drill. This region has been labeled zone (III) in the through-hole classification by zones shown in Figure 4.1. The distance from the point of the start of the deformation zone to the exit surface is mainly dependent on the thrust force [9]. Therefore, in this analysis, real-time thrust force data is converted to the feed power data using equation (6.3) as required for the implementation of the energy-difference approach discussed in section 6.2. The feed power values are very low and have typically been ignored in drilling experiments. The horsepower due to thrust has been found to be as low as 0.44 % of the total power during the drilling of S.A.E 6150 steel [63]. Notwithstanding, its relevance in this study cannot be overemphasized.

Through the implementation of the EDA on the feed power data, the feed energy-difference (FED) curve was obtained for all drilling tests conducted using standard HSS twist drill type *A* and type *B*, as shown in Figure 6.3 and Figure 6.4. The results show that as feed increases (keeping spindle speed constant), the feed power increases, indicated by the increasing slope of the straight-line portion of the curve. The feed causes the drill point to penetrate the workpiece causing the work material to deform and flow around the chisel edge and cutting lips of the twist drill. Therefore, as the feed increases, the workpiece material removed per revolution also increases. The energy-difference curve accounts for

the change in the energy requirement during full penetration and occurs at a constant rate during continuous drilling operation until interrupted by any change in the process mechanics, material property, or process parameter. Further analysis of the FED curve results would aid in identifying the points of change in the process mechanics and work material physical property that characterizes the onset of the deformation zone (III) and the exit burr formation mechanism during through-hole drilling.

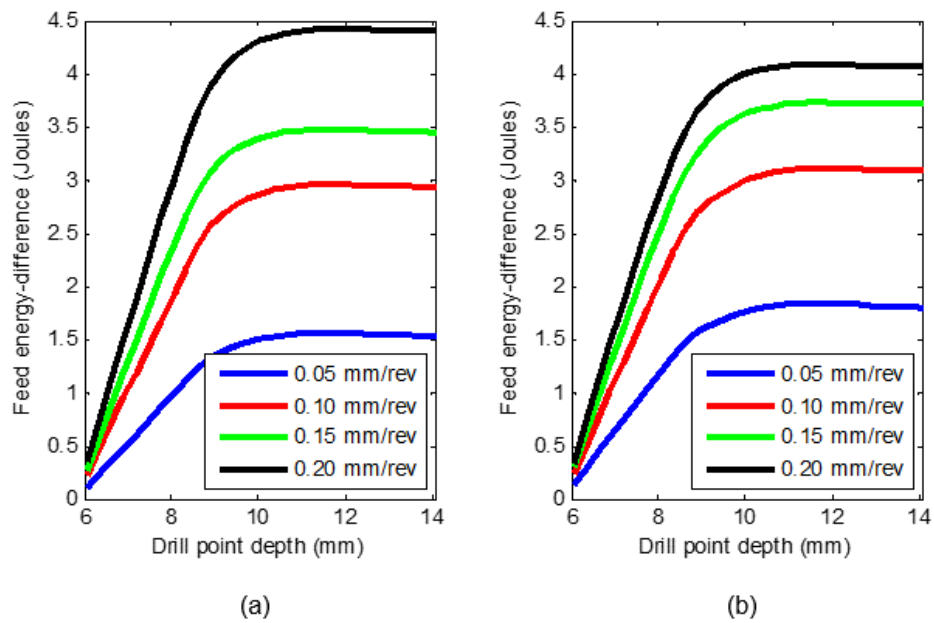


**Figure 6.3: FED curve in the drilling of Al6061-T6, workpiece thickness 8.9 mm using standard twist drill type A, at (a) 2037 rpm (b) 2547 rpm.**

The results show a common trend in the FED curves, starting with a straight-line plot for all cases tested, which is an indication of the constant feed power or thrust force applied during the steady-state drilling operation. As the tool feeds into the deformation zone of the workpiece, the straight-line transitions into a curve, showing changes in the power requirements. These are indications of change in the process mechanics resulting

from changes in the physical property of the workpiece and occur at points of interest that characterize the breakout burr formation mechanism and are identified by estimating the slope or change-rate curve of the feed energy-difference curve.

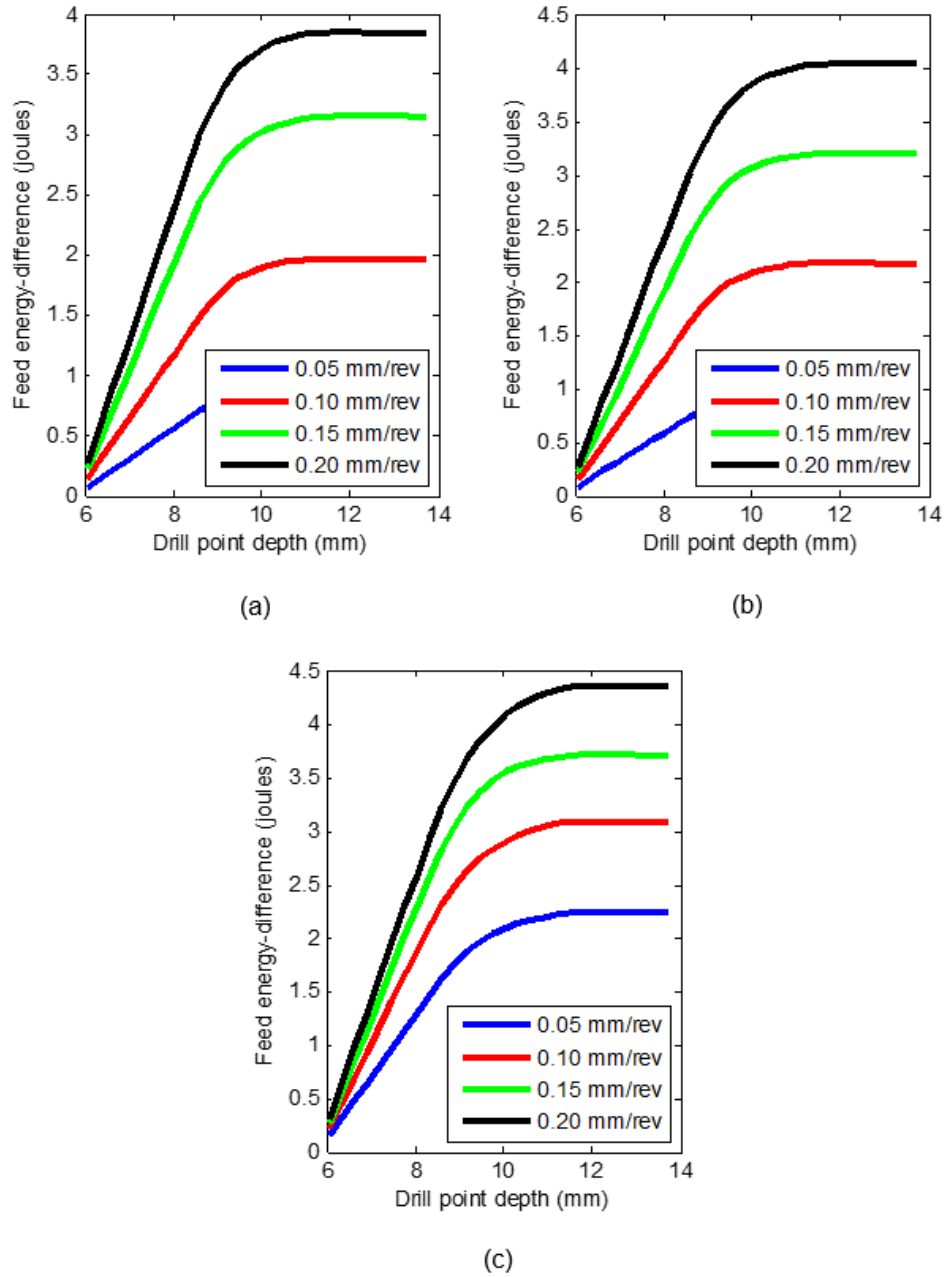


**Figure 6.4: FED curve in the drilling of Al6061-T6, workpiece thickness 8.9 mm using drill type B, at (a) 2037 rpm (b) 2547 rpm (c) 3056 rpm.**

The change-rate (slope) curve for the feed energy-difference has been obtained, with the points of interest identified, as shown in Figure 6.5. The curve describes the rate at which the energy-differences curve changes. It is used to investigate points of process change as the twist drill breaks through the exit surface of the workpiece. The peak on the change-rate curve labeled P1 is known as the breakout burr initiation, which is the onset of the burr formation mechanism. The second position of interest labeled P2 is known as the deformation zone depth. The change-rate value at deformation zone depth matches that of the steady-state drilling process on the change-rate curve and occurs after the breakout burr initiation on the change-rate curve.

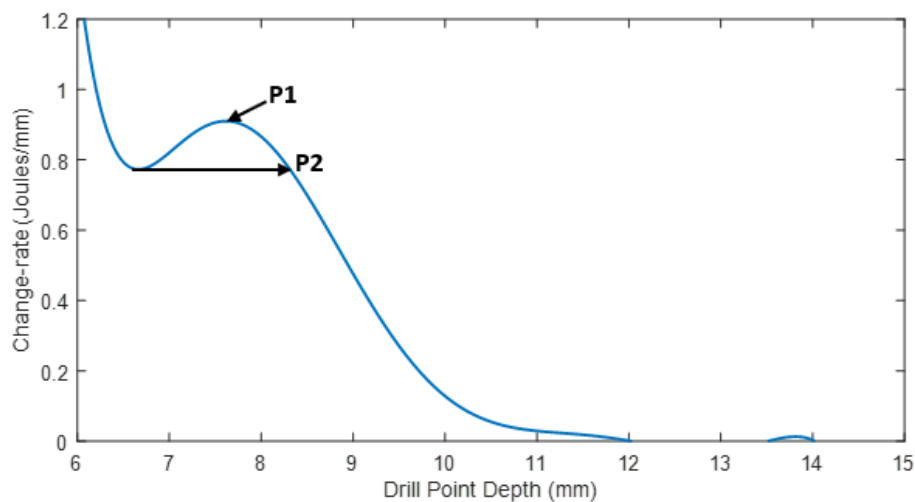


**Figure 6.5: Points of interest on the change-rate curve for FED data.**

The implementation of the EDA has made possible the identification of the onset of the burr formation mechanism, P1, which corresponds to the zone (III) of the through-hole classification, and the deformation zone depth, P2 using the change-rate curve. The change-rate curve of the feed energy-difference for all drilling tests performed using the

standard twist drills type *A* and *B* are shown in Figure 6.6 to Figure 6.10. The results show similar curve characteristics, which make sense since the drilling processes were performed on the same workpiece material at a fixed feed-rate and spindle speed in each instance.

The formation of the deformation zone during breakout burr formation in the metal drilling process is due to a combination of the work done in shearing, which results in high strain, strain rate, and rapid rise in temperature, and plastic flow due to the thrust force. A rapid rise in temperature has been shown to occur at the exit surface of workpiece material during drilling [163]. The temperature increase at the tool-workpiece interface is dependent on the amount of work done and the quantity of material passing through flow-zone [164]. As the twist drill approaches the exit surface of the work material, the volume of material to cut reduces with the material removal rate, and since the rate of plastic flow at the tool-workpiece interface is sufficiently high, enough time is required to conduct the heat generated. Therefore, as the volume of work material below the tool decreases, a point is reached at which the structure of the remaining work material located below the chisel edge becomes thermally weakened and form the deformation zone.

Furthermore, a region of work-hardened workpiece layer form between the chisel edge of the drill point at P1 and the deformation zone depth position at P2. This makes sense since the strain hardening coefficient increases with strain rate [164], and consequently form a work-hardened workpiece layer between the chisel edge and the thermally softened zone. The rise in the change-rate value at P1 is an indication of the additional energy expended to break through the work-hardened layer as the process change from the steady-state operation as it feeds through the work-hardened workpiece region. The thermally softened region is the deformation zone estimated as the breakout distance from P2 to the exit

surface of the work material. As the chisel edge reaches point P2, the workpiece begins to bulge, and the feed energy required to pierce through the material decreases. It is important to note that the point P1 is the onset of the burr formation mechanism and corresponds to zone (III) of the through-hole classification.

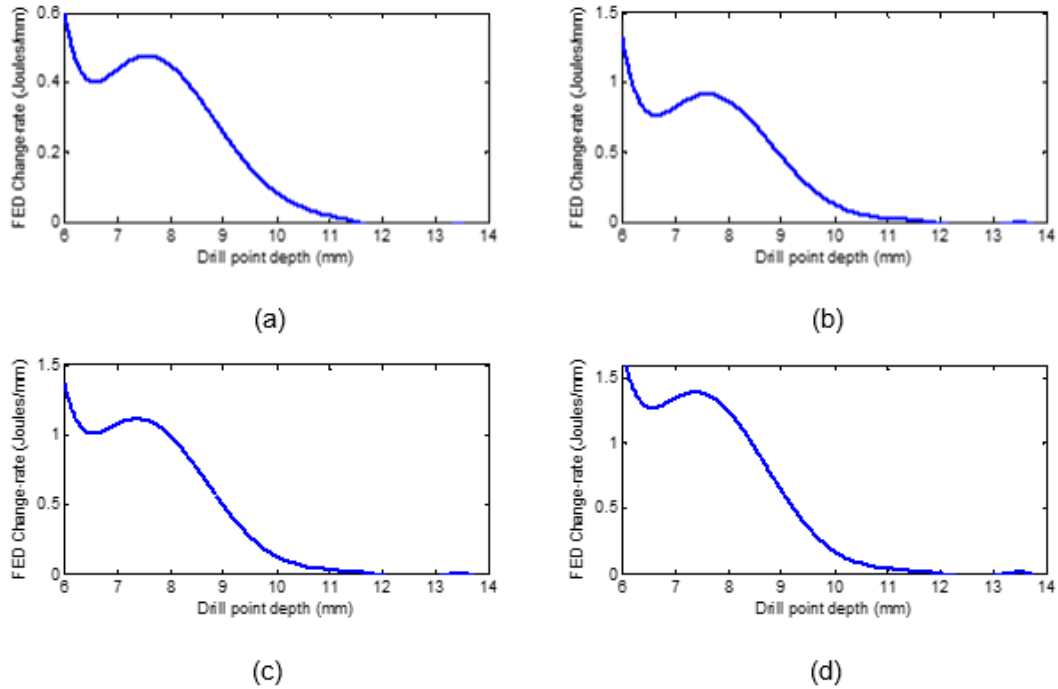


**Figure 6.6: Change-rate curve for FED using drill type A at 2037 rpm and feed (a) 0.05 mm/rev (b) 0.10 mm/rev (c) 0.15 mm/rev (d) 0.20 mm/rev.**

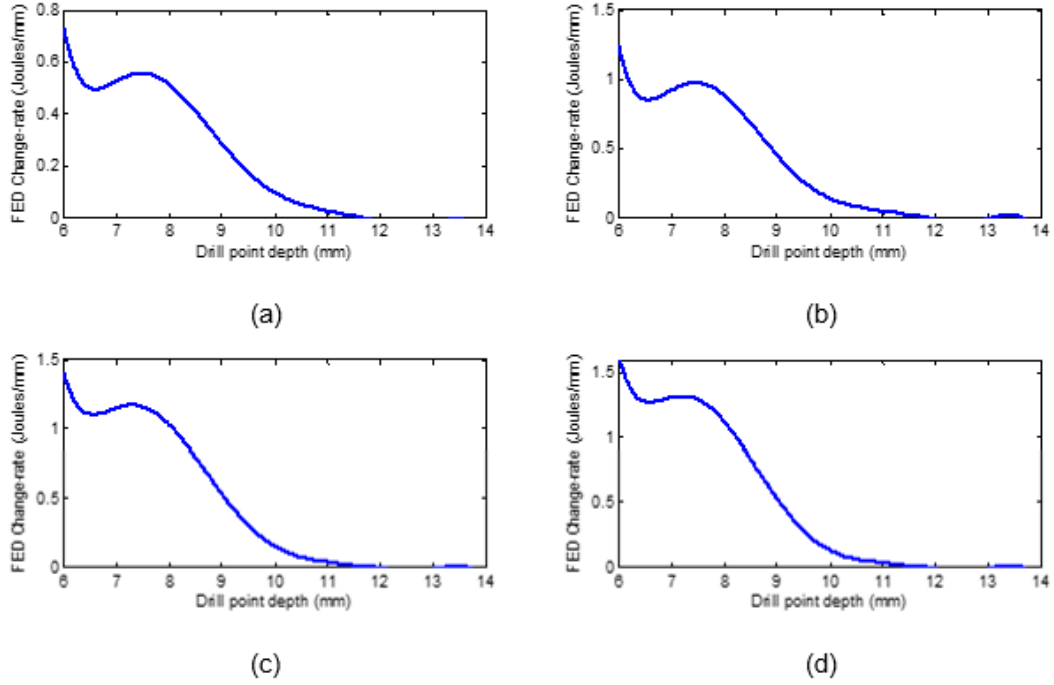


**Figure 6.7: Change-rate curve for FED using drill type A at 2547 rpm and feed (a) 0.05 mm/rev (b) 0.10 mm/rev (c) 0.15 mm/rev (d) 0.20 mm/rev.**

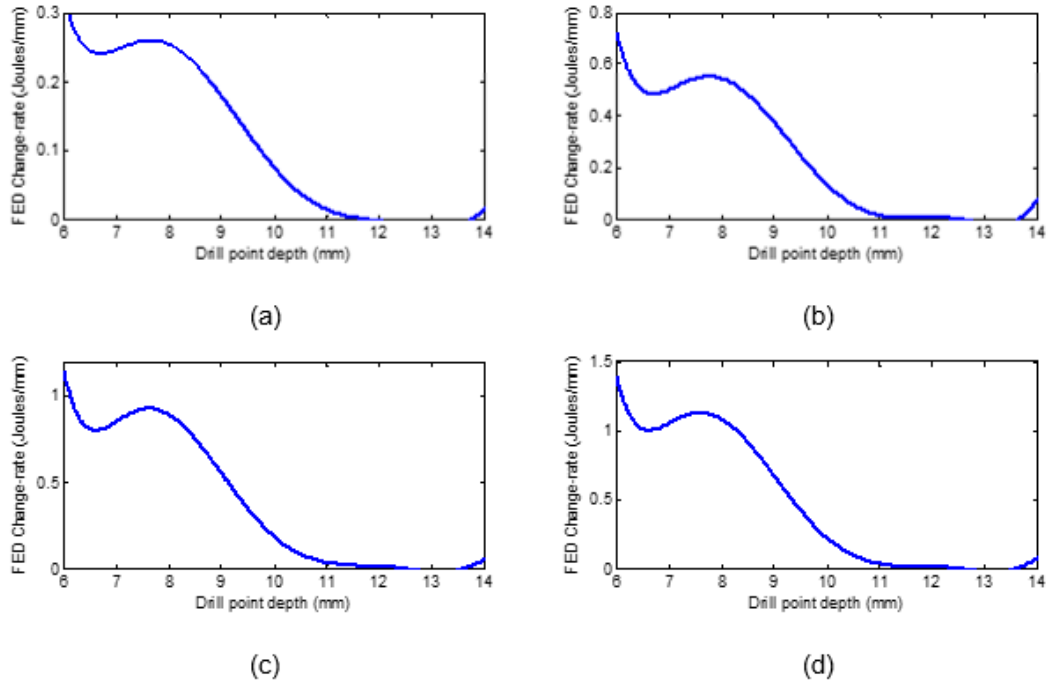
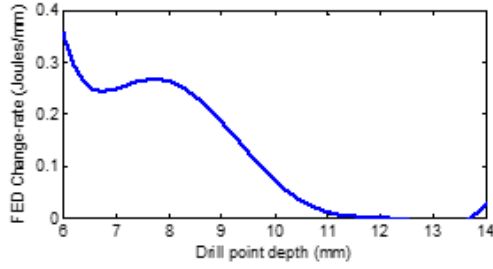
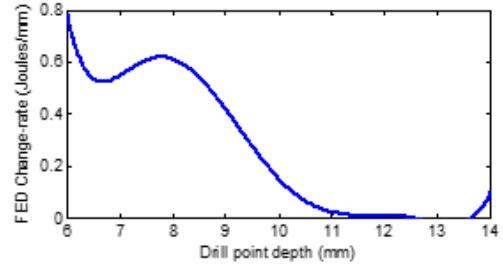


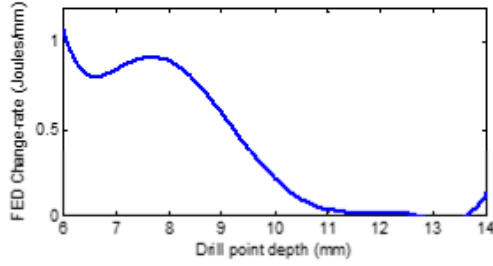
**Figure 6.8: Change-rate curve for FED using drill type B at 2037 rpm and feed (a) 0.05 mm/rev (b) 0.10 mm/rev (c) 0.15 mm/rev (d) 0.20 mm/rev.**



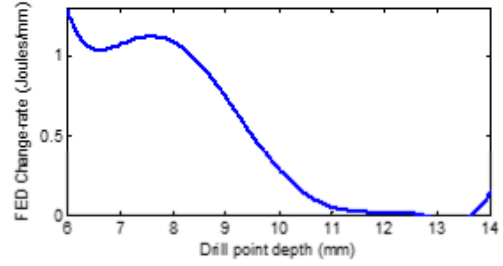
(a)



(b)

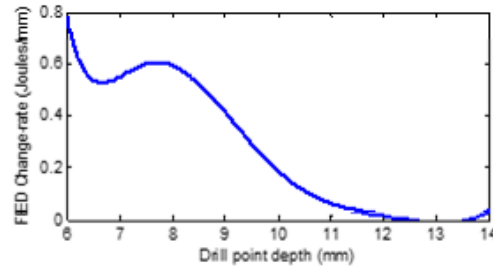


(c)

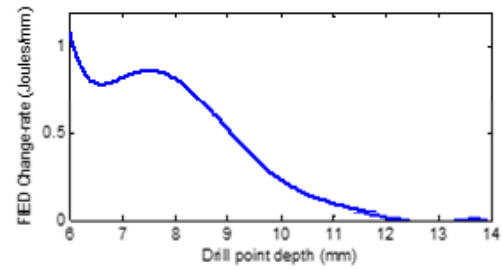


(d)

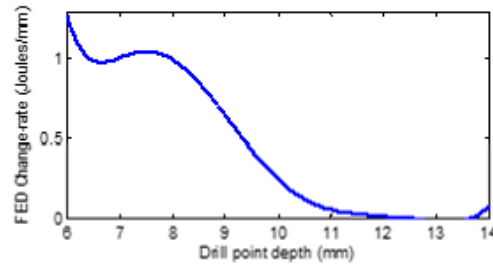
**Figure 6.9: Change-rate curve for FED using drill type *B* at 2547 rpm and feed (a) 0.05 mm/rev (b) 0.10 mm/rev (c) 0.15 mm/rev (d) 0.20 mm/rev.**



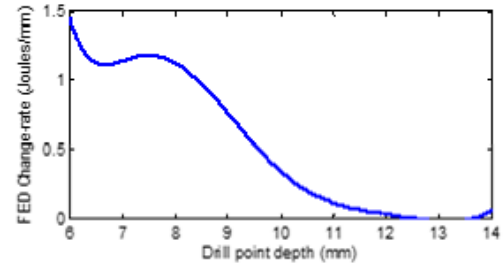
(a)



(b)



(c)



(d)

**Figure 6.10: Change-rate curve for FED using drill type *B* at 3056 rpm and feed (a) 0.05 mm/rev (b) 0.10 mm/rev (c) 0.15 mm/rev (d) 0.20 mm/rev.**

### 6.2.2.1 Breakout Burr Initiation and Deformation Zone Depth

The results of P1 and P2 for all drilling experiments conducted and obtained through the implementation of the energy-difference approach on the feed power data are shown in Figure 6.11 and Figure 6.12. For the drilling tests performed using the twist drill type *A* at a spindle speed of 2037 rpm, P1 was observed at a breakout length of 1.33 mm to the exit surface at feed 0.05 mm/rev. This drop slightly to 1.27 mm at 0.10 mm/rev and then increase to 1.49 mm at 0.15 mm/rev and 1.49 mm at 0.20 mm/rev as shown in Figure 6.11a). During drilling at 2547 rpm, slight variation in the value of P1 was also observed at feed 0.05mm/rev (i.e., from 1.41 mm to 1.44 mm), however, a considerable decrease to 1.18 mm was observed at 0.15 mm/rev before a significant rise to 1.70 mm at 0.20 mm/rev.

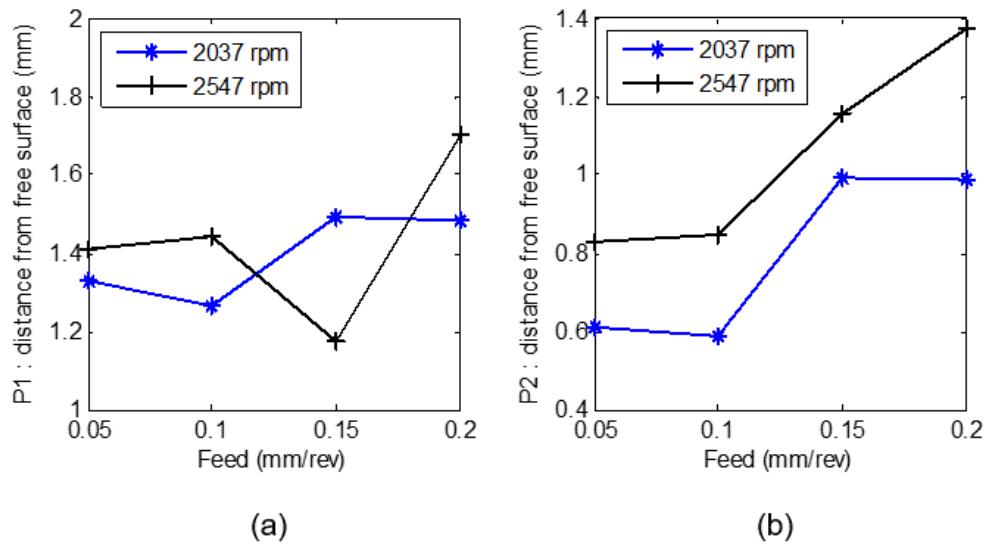


**Figure 6.11: Chisel edge positions at breakout (a) breakout burr initiation, P1 (b) deformation zone depth, P2, during the drilling of 8.9 mm thick Al6061-T6 workpiece using twist drill type *A*.**

The values of P1 are expected to vary slightly as feedrate and speed increases since the drilled hole-depth is shallow and less than the twist drill diameter. This has been observed in the results obtained using the type *B* twist drill as shown in Figure 6.12a). The position of the breakout burr initiation, P1 varies slightly during the drilling conducted at 2037 rpm and 2547 rpm across all feed. However, an increase in P1 was observed as spindle speed increases from 2547 rpm to 3056 rpm for feeds 0.10 mm/rev to 0.20 mm/rev, while at 0.05 mm/rev the position of P1 only varies slightly for the three spindle speeds tested. The slight variation in P1 for all spindle speed and feed could be the result of the shallow workpiece thickness and hole-depth. In deep-hole drilling, these values may vary considerably as the temperature increases with depth, however, it will be difficult to implement the EDA in deep-hole drilling, since forces due to chip flow resistance and chip clogging are present in the cutting and thrust force data.

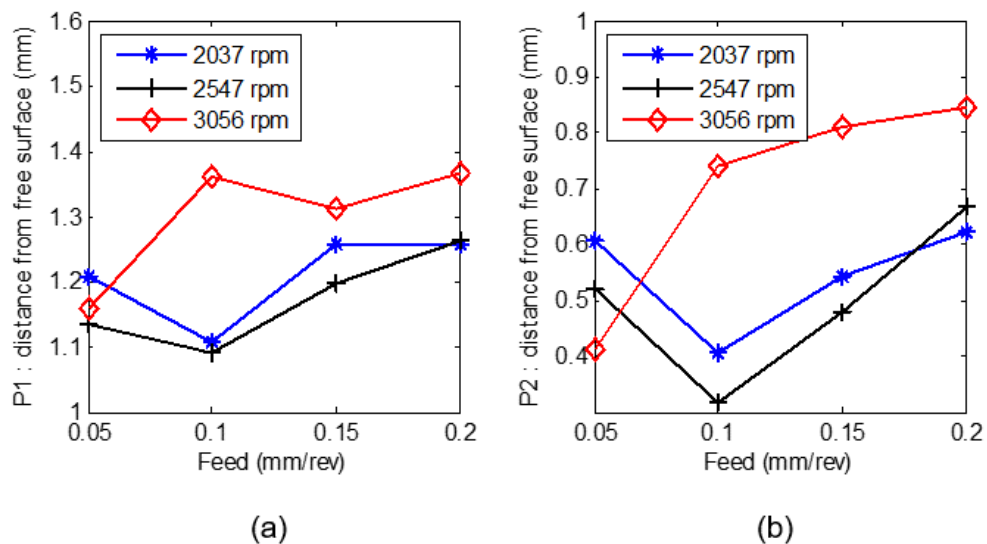


**Figure 6.12: Chisel edge position at breakout (a) breakout burr initiation, P1 (b) deformation zone depth, P2, during the drilling of 8.9 mm thick Al6061-T6 workpiece using twist drill type *B*.**

The deformation zone depth, P2 accounts for the region of the thermally softened workpiece material below the chisel edge of the twist drill. The results obtained for the drilling test performed using the twist drill type *A* shows an increase in P2 as feed increases for both spindle speed tested as shown in Figure 6.11b). Lower values of P2 was observed at feeds 0.05 mm/rev and 0.10 mm/rev. This is followed by an increase as the feed increases to 0.15 mm/rev and 0.20 mm/rev for both spindle speed investigated. This could be attributed to the increase in the work done in shearing as the material to shear per revolution increases, thereby increasing strain, strain rate, temperature and consequently P2. The lowest values of P2 occur at feed 0.10 mm/rev when machining at a spindle speed of 2037 rpm. In addition, the results also showed that the spindle speed has considerable influence on the position of P2 when cutting with the type *A* twist drill, causing P2 to increase with spindle speed for all feed tested. The increase in P2 as speed increases could be due to a combination of increasing friction and workpiece material sticking at the tool-workpiece interface due to the black-oxide coating on the tool and the lower helix angle which in turn increases the total cutting force and consequently an increase in temperature and the length of the deformation zone depth.

The tests conducted using type *B* twist drill show a reduction in the position of P2 as spindle speed increases when drilling at 0.05 mm/rev. However, there is a reduction in the length of P2 as the feed increases to 0.10 mm/rev when cutting at spindle speeds 2037 rpm and 2547 rpm, after which the breakout length of P2 increases at a different rate as the feed increases for the three different spindle speed tested as shown in Figure 6.12b). The results also show that when cutting using the type *B* tool, the position of P2 is only slightly varied when cutting at 2037 rpm or 2547 rpm, however, increasing the spindle speed to

3056 rpm results to a considerable increase in the length of P2 for feeds 0.10 mm/rev to 0.20 mm/rev. A feature worth paying attention to is the overall reduction in the length of P2 for all drill tests conducted using type *B* compared to the type *A* twist drill. This can be attributed to the uncoated finish of the HSS, the tool geometry design and the higher helix angle, which impacts the friction and work done at the tool-workpiece interface and consequently a reduced temperature and the position of P2. This observation is an indication that the tool design, drill point geometry, helix angle and surface finish play a significant role in the exit burr formation in the metal drilling process.

### **6.2.2.2 Work-hardened Layer Thickness**

A layer of work-hardened Al 6061-T6 is assumed to form between the breakout burr initiation, P1 and the deformation zone depth, P2 before burr formation as the tool breaks through the exit surface of the workpiece. The work-hardened layer thickness,  $t_H$  is estimated as the difference between P1 and P2 measured from the exit surface of the workpiece. This is given as

$$t_H = P1 - P2 \quad (6.6)$$

This layer of hardened work material serves as a boundary separating the undeformed workpiece from a region of thermally softened workpiece material. The change in the physical property of the workpiece material in this region is an indication of a change in the process mechanics. Therefore, as the twist drill encounters the boundary of the work-hardened workpiece layer, additional energy is required to pierce through the workpiece in this region, thereby raising the feed power. This occurs at the peak position

on the change-rate (slope) curve derived from the analysis of the feed energy-difference identified as point P1 in Figure 6.8. The values of  $t_H$  estimated for the drilling tests conducted is presented in Table 6.1, while the positions of P1 and P2 obtained are shown in Figure 6.11 and Figure 6.12.

Table 6.1: Work-hardened layer thickness,  $t_H$  obtain at the breakout burr initiation P1.

Drill Type	Spindle speed	Work hardened layer thickness (mm)			
		Feed			
		0.05 (mm/rev)	0.10 (mm/rev)	0.15 (mm/rev)	0.20 (mm/rev)
A	2037 (rpm)	0.72	0.68	0.50	0.50
	2547 (rpm)	0.58	0.59	0.02	0.33
B	2037 (rpm)	0.60	0.70	0.71	0.63
	2547 (rpm)	0.61	0.77	0.72	0.59
	3056 (rpm)	0.74	0.62	0.50	0.52

The results obtained from the drilling test data show that  $0.5 \leq t_H \leq 0.8$  for the drilling test conducted using the twist drill type *A* and *B*. However, at a spindle speed of 2547 rpm very thin  $t_H$  values of 0.02 mm and 0.33 mm were observed at feeds 0.15 mm/rev and 0.20mm/rev respectively. The reason behind the formation of the thin  $t_H$  layer at these cutting feed and spindle speed is difficult to explain. Further study might be required to understand the effect of process mechanics and material property on the work-hardening layer formed between P1 and P2 of the deformation zone.

### 6.2.3 Analysis of the Cutting Power

The feedrate is known to have the greatest impact on cutting and thrust forces during drilling operations and this has been observed in the thrust and cutting power data. Similar to the analysis of the feed power, the EDA was implemented in the analysis of the cutting

power to investigate its influence on the exit burr formation mechanism during metal drilling processes. This requires applying the energy-difference and curve-rate procedures discussed in section 6.2.1.

First, the energy-difference technique is applied to the cutting power data to derive cutting energy-difference (CED) curves for the drilling experiments conducted. Like the feed energy-difference curve obtained from the analysis of the feed power, the cutting energy-difference curve contains sections of straight-line and points of inflection or points of change in the slope of the curve as shown in Figure 6.13 and Figure 6.14. The straight-line is an indication of steady-state cutting, in which the material removal occurs at a constant rate. The shearing process continues at a constant rate until interrupted by a change in process mechanics and material constrain. Finally, the positions of change in the cutting mechanics at the cutting lips of the twist drill before tool breakout is then identified using the change-rate curve of the cutting energy-difference curve.

Based on the analysis of the cutting power data, the cutting energy-difference curve was derived for all drilling tests conducted using the type *A* and *B* twist drills. The results obtained for the drilling experiment for tests conducted using the type *A* show that as the feed increases, the value of the slope of the straight-line portion of the cutting energy-difference curve is decreased considerably for feeds 0.05 mm/rev to 0.15mm/rev. However, from feed 0.15 mm/rev to 0.20 mm/rev only a slight reduction in the slope value was observed for tests conducted at 2037 rpm and 2547 rpm, as shown in Figure 6.13a) and Figure 6.13b) respectively. However, only a small-scale reduction in the slope was observed as feed decreases for drilling tests conducted using type *B* twist drill at spindle speeds 2037 rpm and 2547 rpm as shown in Figure 6.14a) and Figure 6.14b), while at 3056

rpm, a slope characteristic quite similar to the results obtained for type *A* twist drill was observed, as shown in Figure 6.14c).

The results observed suggest that the breakout burr characteristic and burr form generated for drilling operations performed using type *A* twist drill at spindle speed 2037 rpm and 2547 rpm and that performed using type *B* twist drill at spindle speed 3056 rpm may fall into same burr type category. Similarly, the data shown in Figure 6.14a) and Figure 6.14b) suggest that increasing the feed from 0.05 mm/rev to 0.20 mm/rev only has a small-scale impact on the burr type formed when drilling at spindle speed 2037 rpm and 2547 rpm using the type *B* twist drill. This agrees with the burr type produced during the drilling test.

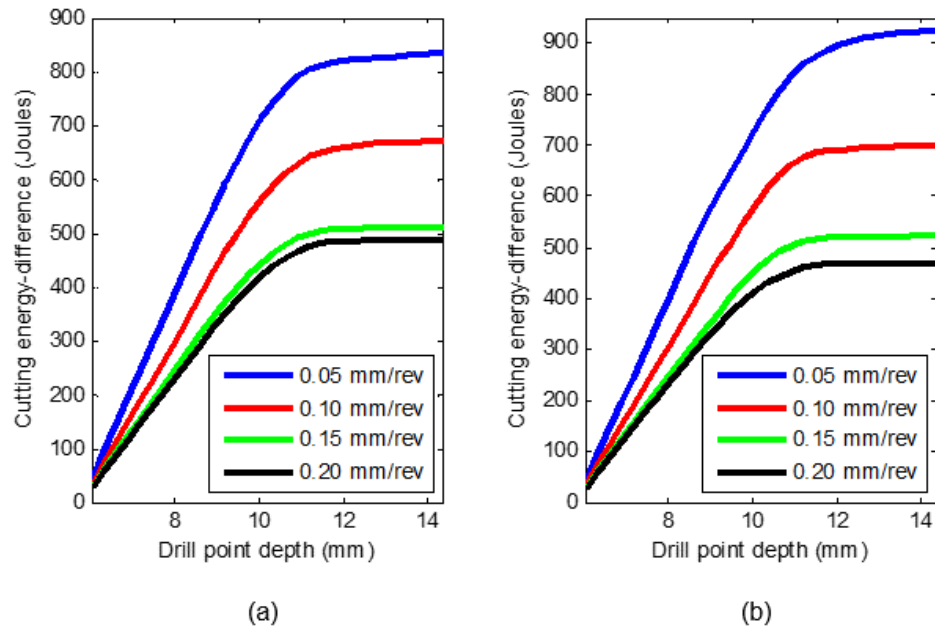
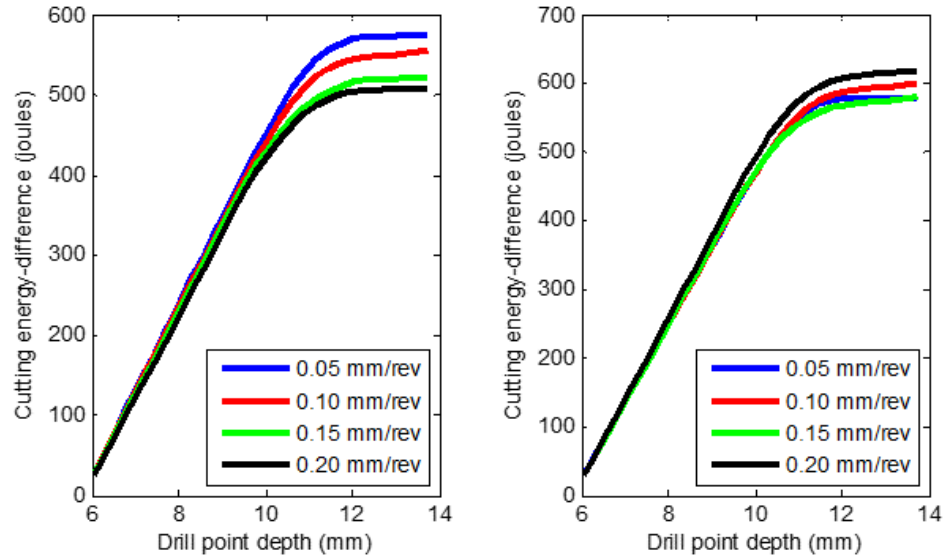


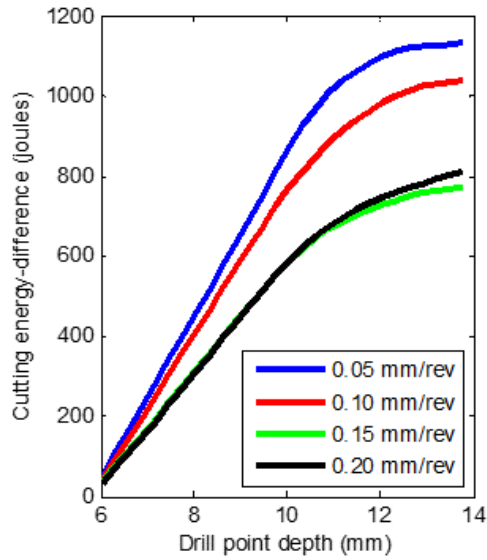
**Figure 6.13: CED curve in the drilling of Al6061-T6, workpiece thickness 8.9 mm using standard twist drill type *A*, at (a) 2037 rpm (b) 2547 rpm.**

Another notable feature is the difference in the slope curve characteristics of the CED curve compared to the FED curve. The slope behavioral characteristic for the CED curve follows a pattern that is reverse to that of the FED curve results shown in Figure 6.3 and Figure 6.4. This implies that in metal drilling processes, the cutting energy expended increases with a decrease in feedrate, while the feed energy expended increases with increasing feedrate. This phenomenon could be attributed to the effect of cutting time, i.e., even though the cutting force is reduced when cutting at low feedrate, the cutting time increases and power accumulates over time giving rise to an overall increase in the specific energy consumption (SEC). In contrast, the feed energy consumption (FEC) increases with increase in the feedrate. This is because as feedrate increases, the rate by which the metal drilling time decreases is a lot less than the magnitude by which feed power increases, but a lot greater than the magnitude by which the cutting power is increased. A detailed analysis of the drilling energy consumption is presented in Appendix A. This shows that feedrate has a direct influence on feed energy and a reverse effect on cutting energy.



(a)

(b)



(c)

**Figure 6.14: CED curve in the drilling of Al6061-T6, workpiece thickness 8.9 mm using standard twist drill type B, at (a) 2037 rpm (b) 2547 rpm (c) 3056 rpm.**

The same approach used to obtain the change-rate curve for the FED curve was also applied here, since they have a similar curve pattern. Hence, the change-rate curve for the CED curve data was estimated. Figure 6.15 shows the points of interest that indicate

the points of process change identifiable on the change-rate curve. The points are known as the point of ploughing initiation, P3, and continuous ploughing, P4. P3 is the onset of ploughing, which alters the shearing of the workpiece across the tool lips, while at P4, ploughing becomes the predominant process across the cutting edges of the twist drill.

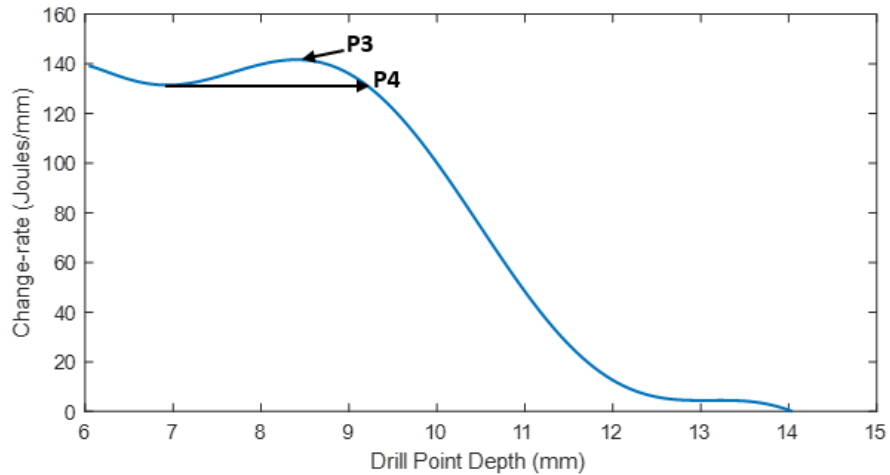
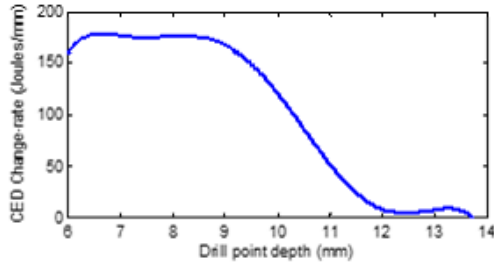
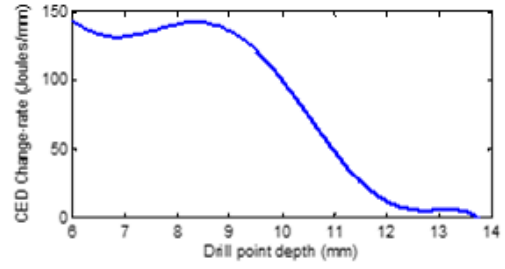


**Figure 6.15: Points of interest on the change-rate curve for a CED data.**

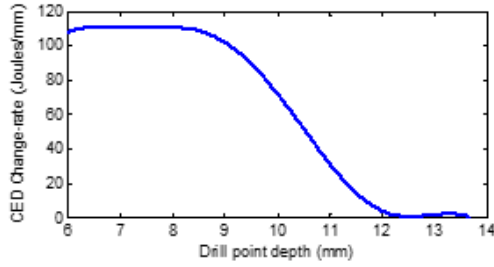
Unlike the curve pattern obtained for all cases tested during the analysis of the change-rate curve for the feed power, the change-rate curve patterns for the cutting power varied slightly, as shown in Figure 6.16 to Figure 6.20. The slight variation in the curve pattern poses some challenges when identifying the critical points of interest. However, to obtain a good approximation of P3 and P4, it was assumed that point P3 occurs as the last peak value on the change-rate curve before the slope value begins to decrease, while P4 match up with the last minimum slope value attained before the peak value at P3, similar to the case in Figure 6.5 and Figure 6.15. But, if no minimum value exists, then the P4 slope value would match up with the slope value at the intersect on the change-rate axis.



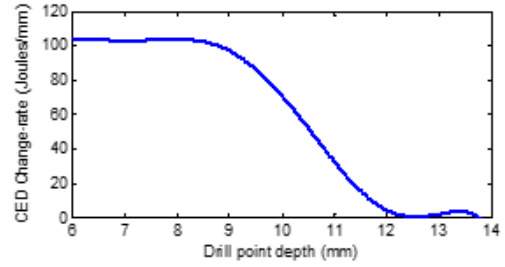
(a)



(b)

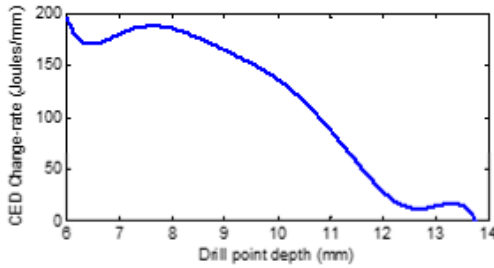


(c)

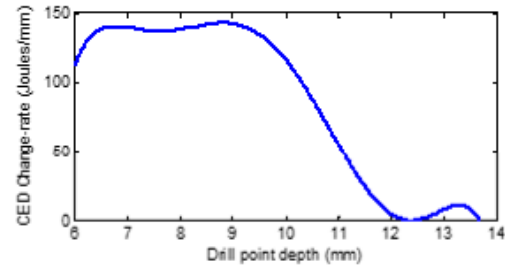


(d)

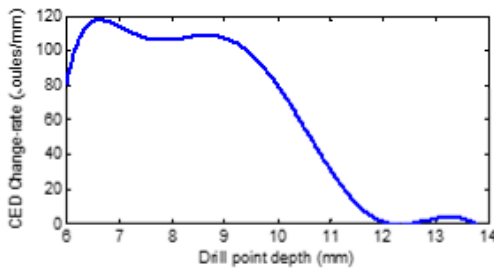
**Figure 6.16: Change-rate curve for CED using drill type A at 2037 rpm and feed (a) 0.05 mm/rev (b) 0.10 mm/rev (c) 0.15 mm/rev (d) 0.20 mm/rev.**



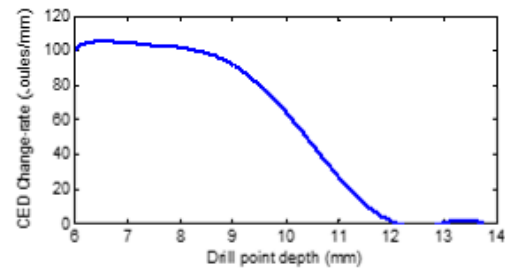
(a)



(b)



(c)



(d)

**Figure 6.17: Change-rate curve for CED using drill type A at 2547 rpm and feed (a) 0.05 mm/rev (b) 0.10 mm/rev (c) 0.15 mm/rev (d) 0.20 mm/rev.**

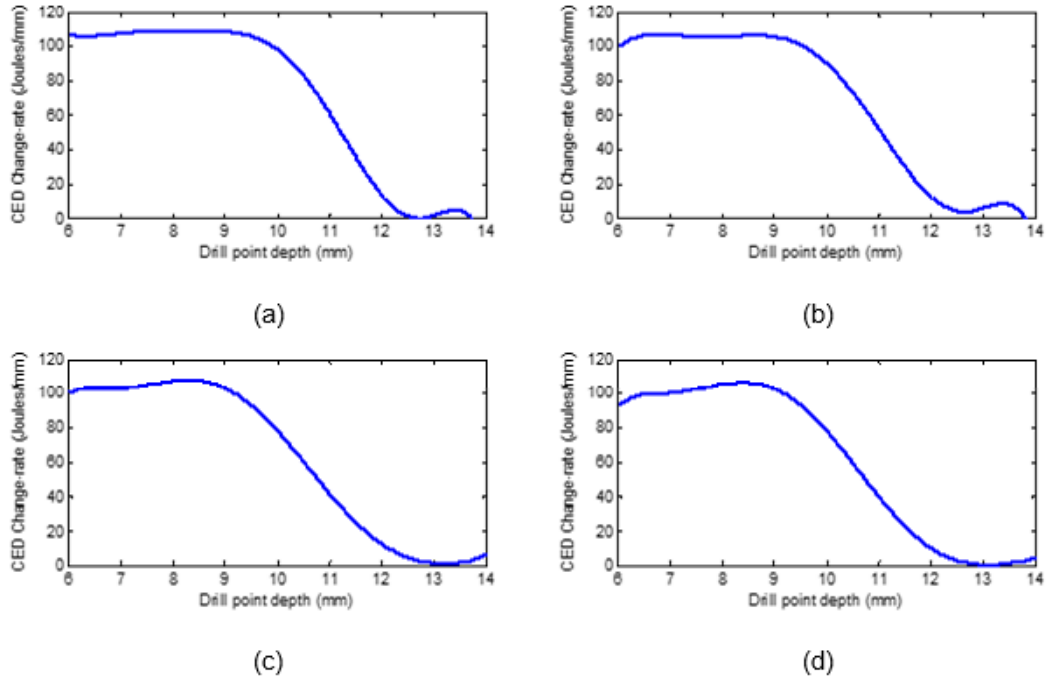


**Figure 6.18:** Change-rate curve for CED using drill type *B* at 2037 rpm and feed (a) 0.05 mm/rev (b) 0.10 mm/rev (c) 0.15 mm/rev (d) 0.20 mm/rev.

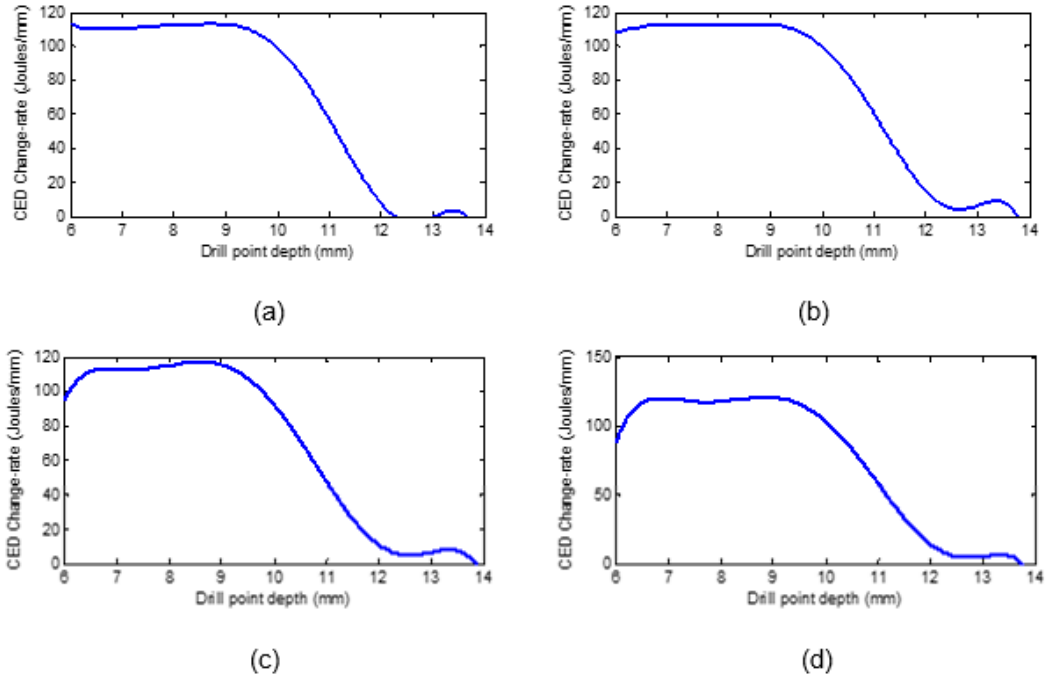


**Figure 6.19:** Change-rate curve for CED using drill type *B* at 2547 rpm and feed (a) 0.05 mm/rev (b) 0.10 mm/rev (c) 0.15 mm/rev (d) 0.20 mm/rev.

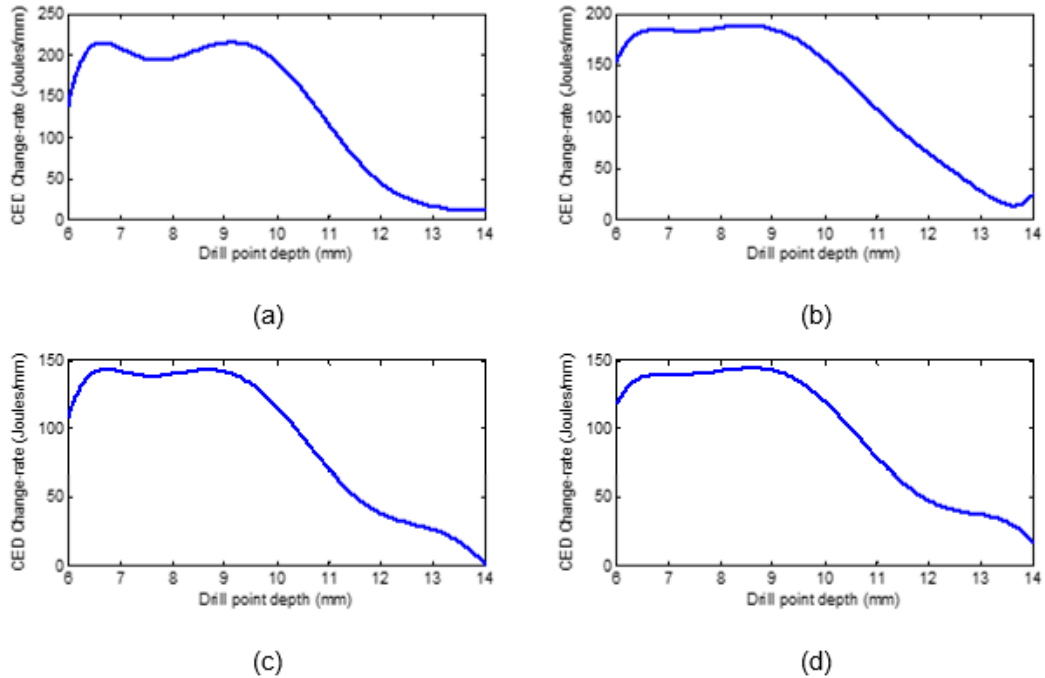


**Figure 6.20: Change-rate curve for CED using drill type *B* at 3056 rpm and feed (a) 0.05 mm/rev (b) 0.10 mm/rev (c) 0.15 mm/rev (d) 0.20 mm/rev.**

Looking at the change-rate curve for the cutting energy-difference, the point P3 identifies the position of the onset of ploughing operation at the tool-workpiece interface. The onset of the ploughing process is due to occur when the chisel edge of the drill point is within the deformation zone depth of the zone (III). Thus, as the cutting edges of the drill point approach the exit surface of the workpiece, a point is reached where the structure of the work material below the chisel edge locally weakened due to high temperature, large plastic strains and strain rate. This forms a region of thermally softened workpiece structure called the deformation zone depth. As the drill point feeds further into this region, a ploughing action begins alongside the shearing of the workpiece material. At P4, ploughing action becomes the predominant process on the cutting edges, and this continues until the remaining workpiece material (if there is any left below the drill point) fractures and/or is

pushed out to form exit burr. P3 is expected to occur within the deformation zone where the physical characteristics of the workpiece material have changed due to plastic deformation and possible thermoplastic effects that may have occurred at the region below the twist drill cutting edges before tool breakout. The importance of the positions identified by the points P3 and P4, in this cutting test is its significance in predicting the thickness and height of burrs formed during metal drilling processes using energy analysis, which have never been done.

### **6.2.3.1 Point of Ploughing Initiation and Continuous Ploughing**

The results of the point of ploughing initiation and ploughing dominance obtained through the analysis of the cutting power data are presented and discussed in this section. During the drilling process using the type *A* twist drill, only a slight variation was observed for the position of P3 when drilling at a spindle speed of 2037 rpm. The onset of the ploughing occurs within a breakout depth of about 0.50 mm for feeds 0.05 mm/rev, 0.10 mm/rev and 0.20 mm/rev and a slight increase to 0.81 mm at 0.15 mm/rev as shown in Figure 6.21a). At a spindle speed of 2547 rpm and feed of 0.10 mm/rev, ploughing begins at the exit surface, which implies that the twist drill just breaks through the exit surface and that some cutting action persists at the cutting edges. At a feed of 0.15 mm/rev, the ploughing begins at 0.25 mm to the exit surface, while at the 0.05 mm/rev and 0.20 mm/rev feeds, the ploughing starts early at about 1.26 mm and 2.22 mm to the exit surface.

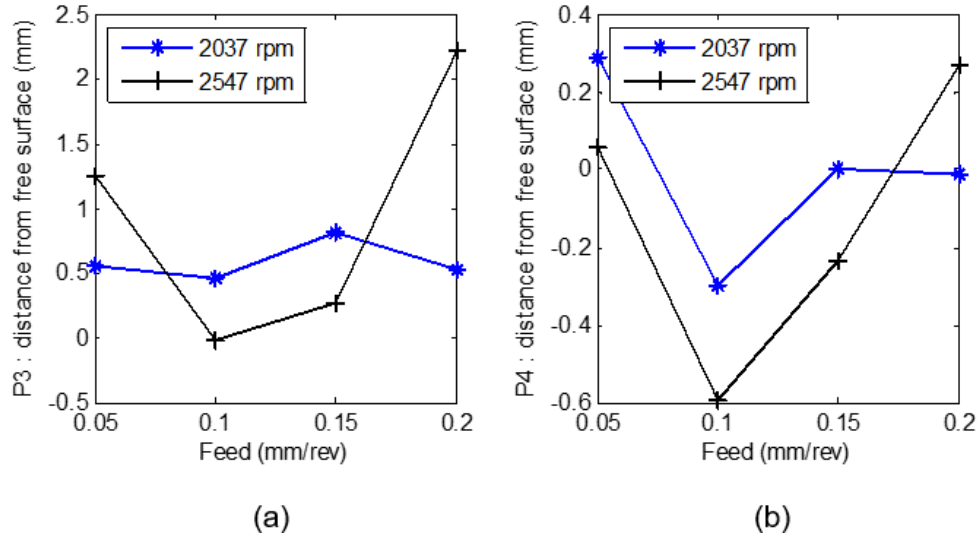


**Figure 6.21: Critical points at breakout (a) ploughing initiation, P3 (b) continuous ploughing, P4, during the drilling of 8.9 mm thick Al6061-T6 workpiece using twist drill type A.**

The analysis of the cutting power data has led to the estimation of the twist drill depth at which the tool-workpiece interaction changes from one of distinct shearing along a plane to predominantly ploughing. The tool ploughing phenomenon is expected to occur after the chisel edge of the twist drill point has drilled through the work-hardened layer and is in operation within the thermally softened region of the deformation zone. However, it was found in some cases to occur after the exit surface has been reached. These were observed in the drilling test performed using twist drill type A at spindle speed 2547 rpm at 0.10 mm/rev, and similarly, the tests conducted using the twist drill type B when drilling at spindle speed 2037 rpm and 3056 rpm at feed 0.05 mm/rev and a spindle speed of 2547 rpm at feed 0.20 mm/rev, as shown in Figure 6.21a) and Figure 6.22a). In general, a reduction in P3 was observed for the drilling tests conducted using type B twist drill for all spindle speed and feed in comparison to the type A tool. This could be attributed to the influence of the twist drill design and drill point geometry on the shearing and plastic-flow

at the tool-workpiece interface. The variation in the tool design features of the twist drill types used has shown to have considerable influence on the thrust and cutting power data and consequently the deformation zone depth.

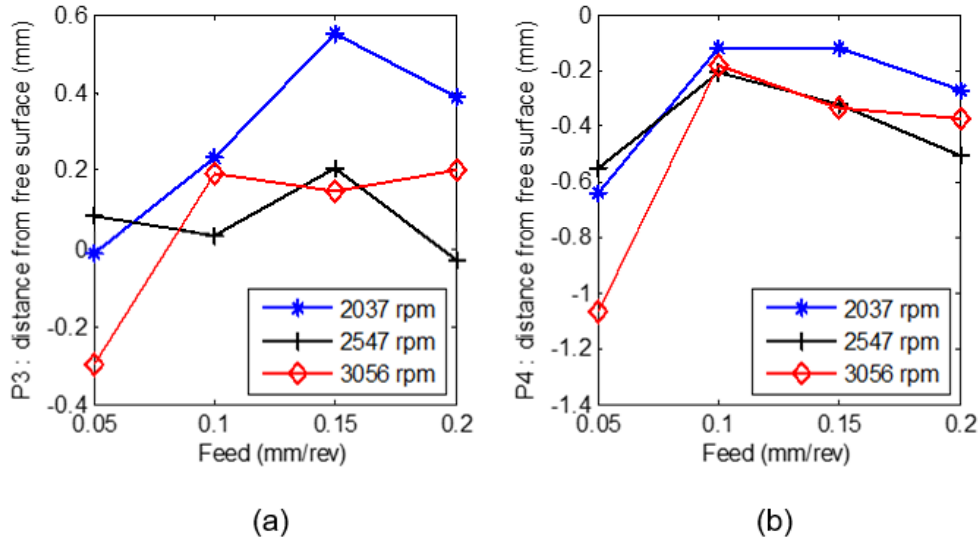


**Figure 6.22: Critical points at breakout (a) ploughing initiation, P3 (b) continuous ploughing, P4, during the drilling of 8.9 mm thick Al6061-T6 workpiece using twist drill type B.**

During the drilling process, after the ploughing initiation, P3, the material removal rate reduces continuously, until ploughing becomes the predominant process at the cutting edges of the tool-workpiece interface. Shown in Figure 6.21b) and Figure 6.22b) are the points of continuous ploughing, P4 for drilling test performed using twist drill type A and type B, respectively. These are expected to occur after the chisel edge of the twist drill has breakthrough the exit surface of the workpiece, however, a large burr type is expected when P4 occurs before the exit surface. The negative position values of P4 is an indication that the tip of the chisel edge has drilled through the exit surface of the workpiece. Based on the drilling scenario and the parameters of the zone (III) obtained in this analysis, the burr

types formed during metal drilling operations could be predicted. From the results of the data shown in Figure 6.21b), a large burr type is expected when drilling with type *A* twist drill at spindle speed 2037 rpm and feed 0.05 mm/rev, and when drilling at spindle speed 2547 rpm and feed 0.20 mm/rev. The dominance of the continuous ploughing action was observed at the exit surface when drilling at 2037 rpm at feed 0.10 mm/rev, while at 2547rpm, this occurs at feeds 0.10 mm/rev and 0.15 mm/rev, respectively.

Based on the drilling tests performed using type *B* twist drill, for all test parameters used, the breakout length at P4 occurs after the exit surface of the workpiece shown by the negative position values indicating the distance from the free surface or the breakout depth, with the least burr type expected to form when drilling at spindle speed 3056 rpm at a feed of 0.05 mm/rev as shown in Figure 6.22b). This would subject the remaining workpiece material around the cutting edges mostly to ploughing and bending action as it is pushed out to form burr rather than shearing. The position value of P4 occurring outside the workpiece material when drilling with the type *B* tool is an indication of a high propensity of the tool to form burr types with miniature burr thickness, but with a small crown, due to the ductile behavior of Al 6061-T6 alloy. It should be noted that the material removal rate as the twist drill proceeds beyond the position of P4 is unprecedented. However, the final piece of work material removed as the twist drill feeds beyond this point during the drilling of Al 6061-T6 alloy is largely dependent on the contact pressure at the tool-workpiece interface, the drill point geometry, and the cutting lips design.

## 6.2.4 Characteristics of the Breakout Burr Formation Mechanism

In section 4.1, a unique method of classifying metal drilling operations has been introduced, which broke metal drilling operations and the subsequent hole being drilled into three zones based on how the drilling process affects hole quality. The three zones emphasize the challenges encountered in various regions of through holes created during the drilling of engineering parts. Hence, the hole created during drilling operations has been separated into three zones (labeled zones (I), zone (II), and (III)), as shown in Figure 6.23. The classification of the zones in the through-hole drilling process is not the focus of the research but emphasizes the area of the research focus classified as zone (III).

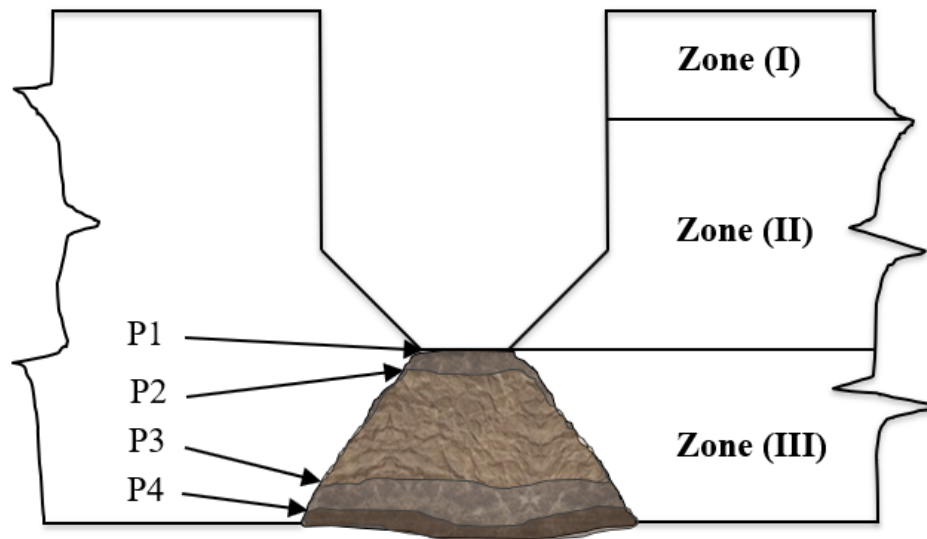


**Figure 6.23: Mechanisms of breakout burr formation and Drilling Zones**

Also derived in this research are the unique points of interest that characterize the exit burr formation mechanism in metal drilling processes. These points have been derived through the analysis of real-time feed and cutting power data using a newly introduced

technique known as the energy-difference approach. Based on the data analysis and investigation conducted, four points or phenomena were observed as the integral features that make up the exit burr formation mechanism, as shown in Figure 6.23, and these are grouped as zone (III) of the through-hole classification.

It has been found that the burr formation mechanism is characterized by these stages in a systematic order, starting from the point of breakout burr initiation, P1 to the deformation zone depth, P2. The position of P1 and P2 are separated by a thin layer of work-hardened work material,  $t_H$  while bulging of work material at the exit surface is an indication that the chisel edge has drilled past the deformation zone boundary at P2. The next phenomenon is the onset of the ploughing process, P3. This continues alongside the shearing of the workpiece during chip formation with a continuous reduction in the material removal rate at the cutting lips of the twist drill. Finally, continuous ploughing dominates the shearing process and becomes the predominant process at P4, while the remaining uncut work material is pushed out or bends to form exit burr. These four stages or the phenomena constitute the breakout burr formation mechanism in the metal drilling process.

### **6.2.5 Summary of Feed and Cutting Power Data Analysis**

This section has focused on the analysis of the feed and cutting power data aimed at investigating the burr breakout mechanism in metal drilling processes. The feed power data has been implemented in place of the thrust force for ease of use. A novel and innovative technique that uses energy analysis to identify unique points of interest that correspond to changes in drilling process mechanics known as the energy-difference approach has been developed. The implementation of the EDA on the thrust force data yields P1 and P2 on

the change-rate curve, where P1 is the onset of the deformation zone formation or the point of breakout burr initiation, and P2 is the deformation zone depth and accounts for the thermally softening region measured from the exit surface of the work material. The work-hardened layer formed between P1 and P2 before tool breakout has also been observed and quantified.

Furthermore, the implementation of the EDA in the analysis of cutting power data also yields two points of interest P3 and P4, respectively. P3 is the onset of ploughing at the cutting lips as the tool drill through the thermally softened region, while P4 is the point of ploughing dominance where the ploughing is assumed to be the predominant process over shearing at the cutting lips, and the uncut workpiece is pushed out to form burr. These points of interest obtained are indications of points of changes in the mechanics and process changes leading to the exit burr formation and describe the burr formation mechanism in the drilling of Al 6061-T6 using a standard HSS twist drill.

### **6.3 Analysis of Material Changes in the Deformation Zone**

In this section, the material change that occurs at the deformation zone leading to exit burr formation, and the characteristic property associated with the burr types formed during the drilling of Al 6061-T6 alloy will be discussed. The analysis of the material changes that occur at the deformation zone during tool breakout will be done in two steps. The first step is through observation of photomicrograph of the workpiece material during tool-workpiece interaction at different stages of the drill point as the tool breaks through the exit surface of the workpiece leading to exit burr formation, while the second step involves the investigation of the changes in the physical property of the workpiece material at three

stages of the burr formation mechanism by observing the microhardness properties of the workpiece below the chisel edge at each stage tested before tool breakout. The findings of this analysis validates the phenomenon of the burr formation mechanism discussed in Sections 6.2 and shows the efficacy of the energy-difference approach in the study of breakout burr formation in the metal drilling process.

### **6.3.1 Microstructure Analysis of the Deformation Zone**

The material behavior of the workpiece in the tool-workpiece interface during drilling is influence by the large plastic deformation imposed on the work material due to high strain, strain rate, and temperature rise due to energy expended in the shearing process and the plastic flow around the tool-workpiece interface. The applied thrust also imposes compressive and tensile stress on a small area of the work material below the chisel edge and its periphery until the material begins to crack or tear at breakout during burr formation. Attempts have been made to capture this phenomenon on the photomicrograph at different stages during the drilling of Aluminum 6061-T6 alloy.

During drilling, near the exit surface, the chip formation process at the cutting zone induces a rapid rise in temperature [163], weakens the workpiece material below the drill point, causing the workpiece to bulge depending on the subjected thrust force during the cutting process as the tool approaches the exit surface of the workpiece. The impact is seen as the feed is varied. High feedrate subjects the workpiece below the drill point to large thrust force, causing the workpiece material to be subject to high compressive action. As the shearing process continues, work material within this region is subjected to high strain, strain rate, temperature rise and is plastically deformed, resulting in a change in the

physical property of material below the drill point. The workpiece material tends to bulge when the hydrostatic stress due to the thrust force exceeds the material yield strength in the region. The application of additional force due to increasing feedrate causes the material to bulge earlier before tool breakout. Thus, influencing the onset of the ploughing process on the cutting edge as it cut through the thermally softened workpiece below the drill point, and less shearing occurs, and subsequently, a reduction in the material removal rate.

Another phenomenon observed is the formation of crack or tear across the grain boundary of the Al6061-T6 work material below the chisel edge of the drill point before tool breakout at the exit surface. The crack initiates across the grain boundary on the free surface just after the workpiece material below the chisel edge bulge. However, this seems to occur earlier when cutting at a high feed. It was found that the feedrate has a direct effect on the tendency of bulging and crack formation on the grain boundary of material directly below the chisel edge of the cutting tool. It has been found that a decrease in feedrate results in a reduction in grain boundary existing in the working region [10], which was also observed. However, the formation of a crack in the grain boundary could mean that the limit of the physical constraints of the grain boundary may be exceeded due to applied load. Thus, as the specific volume of the material below the drill point reduces as more material is removed, the remaining work material is subjected to the high strain rate, stresses, and temperature, which weakens the bound on the grain boundary of the workpiece material in this region. Further investigation may be needed to properly understand the condition of the phenomenon occurring at the microstructure level.

Unlike other harder materials like alloys of steel and titanium, the burr breakout phenomenon during the drilling of Al 6061-T6 alloy has been observed to begin at the

periphery of the chisel edge in all cases observed as shown in Figure 6.24. All samples studied reveal that the work material begins to bulge below the chisel edge, after which crack across grain boundary leading to tearing of the workpiece at the periphery of the chisel edge. At high feed and spindle speed, as the tool drills into the workpiece, the workpiece below the drill point reduces until the physical properties weakened due to the high thrust, temperature, strain, and strain rate. At this point, a combination of shearing and ploughing occurs at the cutting lip until the workpiece no longer shear and the uncut materials are pushed out to form crown burr. At low feed and spindle speed, a similar scenario occurs, however the material removal and shearing occur at a lower temperature, strain rate, and strain. This allows enough workpiece material to be removed after the drill point breaks through the exit surface of the workpiece. At this stage, the material removal rate is unprecedented and depends on the pressure at the tool-workpiece interface and the cutting lips design.

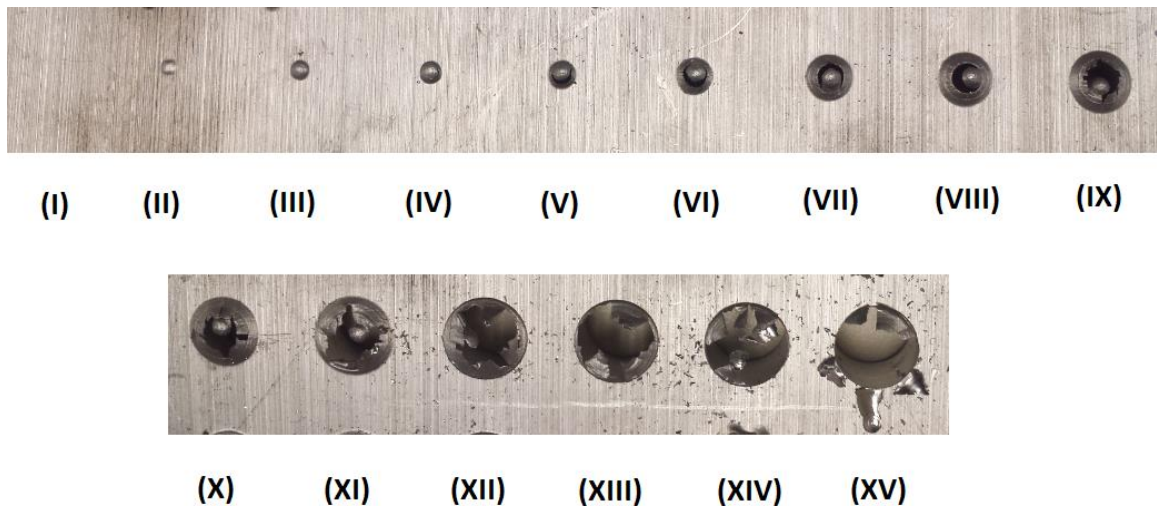


**Figure 6.24: 15 steps drilling of Al 6061-T6 alloy at tool breakout using type A twist drill at spindle speed of 2037 rpm and feed of 0.05 mm/rev.**

At low feed, the low thrust force generated leads to a late formation of a bulge and allows for more workpiece materials to be removed when cutting in the deformation zone, in contrast to high feed, as shown in Figure 5.10. At this stage, a combination of shearing and ploughing continues until a thin layer of material is left uncut at the periphery of the cutting lips, which is pushed out to form burr at the exit surface of the workpiece.

### **6.3.2 Material Hardness Property at the Deformation Zone**

The Vickers hardness results obtained for the analysis of the hardness property of the workpiece material in the zone (III) of the drilling tests performed on Al 6061-T6 stock has been presented in Section 5.3.2. The results show variation in the *HV* values at different points across the work material below the chisel edge region prior to tool breakout. This could result from imperfections in the flow stress at the tool-workpiece interface and inhomogeneity in the strain distribution. However, to better understand these results, the average Vickers hardness distribution across the breakout depth of the test samples has been evaluated for further analysis, as shown in Figure 6.25 to Figure 6.27. The results reveal the hardness distribution across the workpiece from the chisel edge of the twist drill to the exit surface of the workpiece sample. It should be noted that an average *HV* of values less than that of an undeformed Al 6061-T6 alloy was observed across the deformation zone for all samples tested. This may be due to the combined effect of plastic flow and thermal softening due to high strain, high strain rate, and temperature rise on a reduced volume of work material in this zone, causing it to lose its structural integrity and strength.

The average *HV* value obtained for the test sample drilled to a breakout depth  $t_{Br_1}$  of 1.5 mm at a spindle speed of 2037 rpm and feed of 0.15 mm/rev, is shown in Figure 6.25. A look at the average *HV* distribution across the breakout depth shows a rise from 73 *HV* to 90 *HV* at breakout distance 0.15 mm to 0.30 mm and then a drop to 79 *HV* at 0.45 mm from the chisel edge. Similarly, a rise in the average *HV* from 86 *HV* to 95 *HV* was observed at breakout distance 0.45 mm to 0.30 mm to the exit surface and then a drop in the hardness value at 0.15 mm to the exit surface, which is an indication of a work-hardened layer forming around this region. Another observation is the reduced hardness values at about the mid-region of the breakout depth, which may result from stress concentration and temperature effect on the small volume of material in this region. Hence, the workpiece tends to strain-hardened near the chisel edge due to plastic flow, while near the exit surface the impact of the thermal effect is reduced as result of the access to conventional cooling.

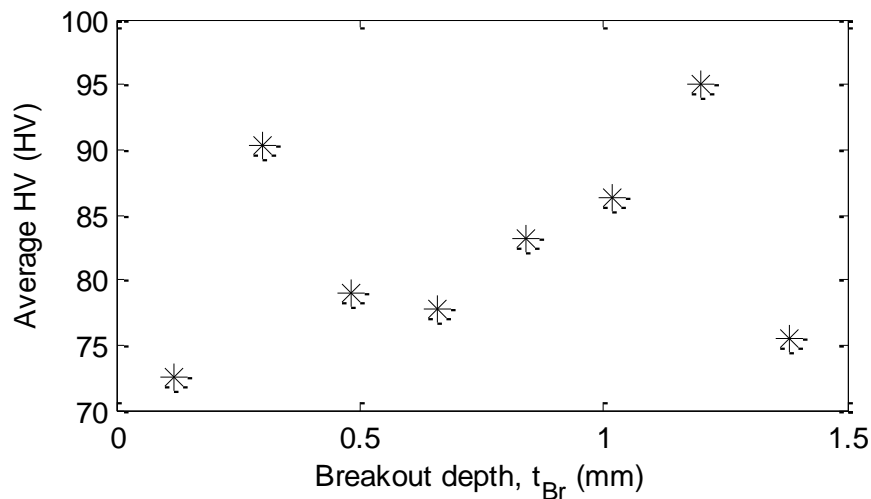


**Figure 6.25:** The average Vickers hardness values of Al6061-T6 at breakout depth,  $t_{Br_1}$  of 1.5 mm to exit surface, using drill type *B* at feed 0.15 mm/rev and speed 2037rpm.

An overall reduction in the  $HV$  values was observed, as the hole-depth increases and the  $t_{Br}$  is reduced to 0.80 mm, as shown in Figure 6.26. However, the higher average  $HV$  value occurred close to the chisel edge and the exit surface respectively, while low  $HV$  value occurred at mid-region of the breakout depth due to thermal softening and stress concentration in this region. The higher  $HV$  value near the chisel edge is an indication of the work-hardened layer formed, which occurs in the breakout distance ( $0.54 \leq t_{Br} \leq 1.26$ ) mm from the exit surface. The higher  $HV$  value near the exit surface could be due to the cooling effect from the surrounding air, thus reducing the effect of thermal softening in this region. This phenomenon was observed in all samples tested and is an indication of the presence of a work-hardened layer formed between the breakout burr initiation, P1, and the deformation zone depth, P2 before tool breakout during the drilling of Al-6061-T6 alloy. These results validate the findings of the analysis performed in Section 6.2.

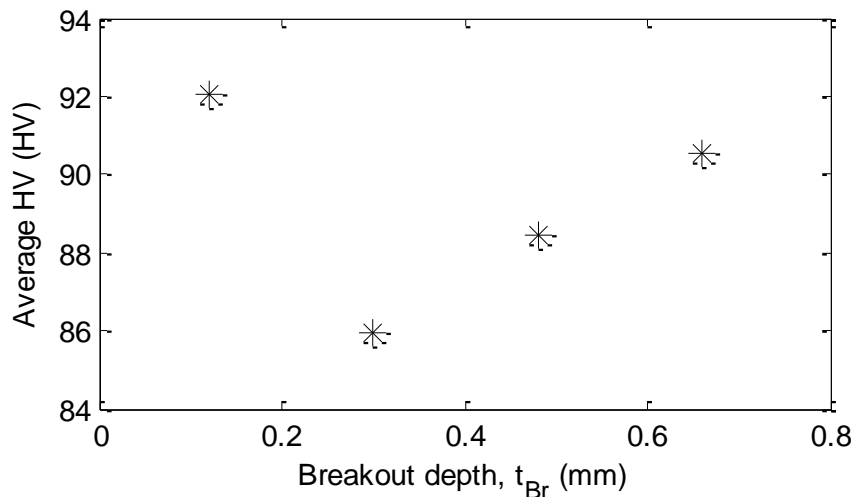


**Figure 6.26: The average Vickers hardness values of Al6061-T6 at breakout depth,  $t_{Br2}$  of 0.8 mm to exit surface, using drill type B at feed 0.15 mm/rev and speed 2037rpm.**

As the drill point feeds further into the workpiece, the work-hardened layer is removed, and the tool cuts into the thermally softened region. This leads to a further reduction of the overall hardness value of the workpiece in this region, as shown in Figure 6.27. The workpiece below the chisel edge begins to bulge subjecting it to regions of tensile and compressive stress, as shown in Figure 5.14, with tensile stresses observed on workpiece near the periphery of the chisel, while compressive stress occurs on work material at the periphery of the chisel edge near the exit surface. A low average *HV* value was observed on workpiece material near the chisel edge due to the tensile stress and bulging initiating and workpiece strain at the periphery of the chisel edge, which weakens the material strength in this region.

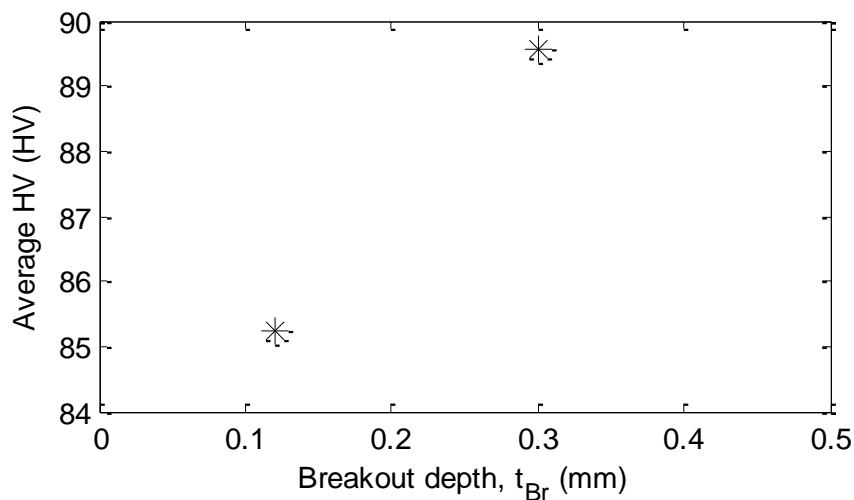


**Figure 6.27: The average Vickers hardness values of Al6061-T6 at breakout depth,  $t_{Br3}$  0.5 mm to exit surface, using drill type *B* at feed 0.15 mm/rev and speed 2037rpm.**

As the drilling process continues, workpiece at the periphery of the chisel edge fractures to initiates the burr formation process. This is in agreement with the 15-step

drilling test shown in Figure 6.24, which shows that the material fracture leading to breakout bur formation during the drilling of Al-6061-T6 occurs at the periphery of the chisel edge. In addition, findings from the photomicrograph observation and microhardness testing and analysis validate the efficacy of the energy-difference approach, as used in determining and analyzing the breakout burr formation during metal drilling processes and the burr formation mechanism derived in Figure 6.23.

### **6.3.3 Summary of the Deformation Zone Material Behavior**

The zone (III) of the drilling process has been investigated through photomicrograph observation and microhardness testing approach. The analysis has presented us with interesting results that confirm the success of the use of the energy-difference approach in the modeling of the exit burr formation mechanism in metal drilling processes. The analysis has also served as a tool that allowed us to confirm the formation of the work-hardened layer and the thermally softened region in the drilling of Al 6061-T6 alloy.

## **Chapter 7: Conclusion**

Burr formation is a common problem in machining and particularly the metal drilling process leading to additional processing and costs in part manufacturing. Since burrs cannot currently be prevented through process control and parameter optimization, it is essential to obtain a better understanding of the mechanism of the burr formation processes in order to develop appropriate models that could help mitigate burr formation in metal drilling processes. However, the complexity of the tool geometry and the dynamic nature of the process poses challenges in the development of even simplistic models for the analysis of the mechanics of the process, consequently, constraining researchers to develop empirical models or alternative methods to approximate the process which are difficult to replicate. As a result, the current research has focused on the development of a drilling technique that uses real-time data to investigate the breakout burr formation mechanism during the metal drilling process.

### **7.1 Summary of Work Done**

The work put forth in this research is the first of its kind to combine using experimental thrust force and cutting power data with the aid of photomicrography observation and microhardness evaluation to characterize the work material behavior below the drill point. Ultimately, the research has allowed for the examination of the entire region below the drill chisel edge at the very onset of the burr formation process. This first in the area of drilling research has allowed for the ability to identify and evaluate the characteristics at critical

points during the burr formation process before and during tool breakout in the drilling of Al 6061-T6 alloy.

Several steps have been put forward to investigate the burr formation process, identify process changes, and better understand the burr formation mechanism in the metal drilling process. These are reflected in the twist drill type and size selection, choice of the work material used, experimental setup, procedure implementation, and the technique used in the data analysis. As part of the investigation, a unique method of classifying through-hole drilling processes has been proposed, separating the length/depth of hole into three zones based on how the drilling process affects hole quality. The proposed through-hole classification as discussed in Section 4.1, aids in narrowing down and helping to focus on specific problems and analysis of metal drilling processes in specific zones, thereby reducing the challenges associated with changes in the process mechanics and material behavior, and subsequent impacts on tool life and workpiece surface integrity. As a result, by classifying the drilled hole into zones, the research was able to focus predominantly on the issues of burr formation by restricting its investigation to zone III of the through-hole classification.

An appropriate experimental setup has been used in this study aimed at collecting real-time thrust and cutting power data simultaneously for further processing and analysis. The experiments have been performed using medium-sized standard twist drill types with a point angle  $118^\circ$  due to the well-defined cutting edges and geometry. The material used is an Aluminum 6061-T6 alloy known for its weight-to-strength property and good machinability, which makes it a commonly used aluminum alloy in structural, automobile, aerospace, and general-purpose application. However, catastrophic burr types and build-

up edges could result in certain ranges of cutting parameters. Unlike stainless steel, with Al 6061-T6, no relationship between exit burr thickness and burr length has been found, and as such, investigating the burr formation and the understanding of the mechanism is of paramount importance.

In preparation for actual drilling tests, a set of constraints was set for the drilling experiment based on the findings from a set of preliminary tests. Established from the analysis is a schematic model of deep-hole drilling power signal which apportioned the process into segments accounting for the different mechanics that constitute and cumulate in metal drilling processes identified on a real-time drilling force and cutting power signal. Thus, the total cutting force or power in deep-hole drilling is expressed as an aggregate of the forces due to cutting, chip flow resistance, and potential chip clogging. These forces are an indication of the complex nature of the drilling process and should be studied separately to develop simplistic models for metal drilling processes.

To investigate the exit burr formation mechanism, an original and innovative method termed the energy-difference approach was developed and utilized. It uses energy analysis to identify points of change in the process mechanics and material behavior that characterize the burr breakout formation mechanism. Applying this technique in the analysis of the thrust force or feed energy has aided in identifying the onset of the deformation zone known as breakout burr initiation - P1, and a thermally softened region known as the deformation zone depth - P2. The application of the approach in the analysis of the cutting power data has also aided in identifying the onset of ploughing - P3 and the point of continuous ploughing – P4, at which point the ploughing process becomes the predominant process over shearing of the workpiece below the drill point as the twist drill

breakout through the exit surface to form burr. A notable feat achieved by applying the EDA is quantifying the length of zone III. Previous research has simply generalized the region under the drill point, referring to it as a deformation zone with no other information. The research presented expands on this body of knowledge significantly. This included identifying regions of the work-hardened layer and thermally softened workpiece before tool breakout. Furthermore, the breakout burr formation mechanism during the drilling of Aluminum 6061-T6 has been developed, and it is an indication of the changes in the process mechanics and material leading to exit burr formation.

Finally, an investigation of the process material characteristics was carried out through observation of the photomicrographs and material microhardness testing of the sectioned, cold-mounted, polished and etched workpiece in zone III of the drilling process classification. The photomicrographs show the microstructure characteristics at different stages of the hole depths as the tool breaks through the exit surface of the workpiece leading to burr formation, while the material microhardness test shows the changes in the physical property due to plastic flow and thermal softening in this region of the work material during tool breakout. In view of the observation, the following findings were made:

(a) the tool breakout begins with tearing process at the periphery of the chisel edge during tool breakout in the drilling of Al-6061-T6 alloy,

(b) a work-hardened layer exists between a region of the work material and the thermally softened region at which point the drilling mechanics is interrupted due to differences in material physical properties, and

(c) the material strength below the chisel edge is continuously reduced as the tool breaks through the exit surface.

These could be the reason why Al 6061-T6 alloys hardly ever form burr caps during metal drilling processes. Observations showed the formation of all burr types as seen by previous influential researchers in the field with the exception of the formation of a burr cap which makes sense since work material tearing and fracture initiates below the chisel edge as the tool continues to plough rather than shear through the workpiece during tool breakout. It is important to note that the hole-depth in all cases observed is less than the tool diameter used which may have considerable influence in the deformation zone depth and the exit burr.

## **7.2 Summary of Results and Findings**

As explained in the previous section, a series of experimental tests and the resulting data analyzed to investigate the exit burr formation in when drilling Al 60661-T6. To achieve the research objectives, several experiments and data analysis were done from which critical points of interest that characterizes the exit burr formation mechanism in metal drilling process could be clearly identified. In addition, these findings were validated through the analysis of photomicrographs observation and microhardness tests of workpiece material below the drill point at tool breakout. A brief summary of the critical steps in the research is summarized below.

- A unique method of classifying through-hole drilling was proposed, discretizing a drilled through-hole into zones based on how the drilling process affects hole quality. The benefit of this is that it narrows the challenges to specific zones, and subsequently, the mechanics and material behavior.

- A set of drilling tests were performed on Al 6061-T6 alloy using two 3/8-inch standard twist drills with the thrust and cutting power data collected for analysis.
- All tests were performed using parameters within the manufacturers' recommendation. This helps maintain a drilling practice that could be easily implemented in the manufacturing industry.
- An original method of data analysis known as the energy-difference approach has been developed and implemented on real-time thrust and cutting power data to predict the onset of exit burr formation, identifying points of changes during the burr breakout process as material behavior and cutting mechanics change.
- Discovery and investigation of four distinct points during the burr formation process that represents changes in the process mechanics.
- Photomicrographs of zones beneath the drill point along with microhardness tests have been conducted on the workpiece material to validate the burr formation process as it moves between critical points, P1 through P4.

As a result of the research work conducted new information in the area of drilling and burr formation were discovered. These new and critical findings are summarized as follows:

- Successful identification of the start of the deformation zone or zone III of a drilling process and subsequently predict the thickness of that zone.
- Identification of the onset of bulging during tool breakout.
- Identification of when ploughing becomes the predominant mechanism over shearing in drilling at the breakout.
- Identification of critical points of interest that characterize the mechanism of breakout burr formation in metal drilling processes.

- Identifying the onset of the tearing process at tool breakout leading to exit burr formation during the drilling of Al 6061-T6 alloy.
- Validation of the energy-difference approach through photomicrograph observation and microhardness testing of the work material behavior at tool breakout.

All of which represent is a first in the area of machining and drilling research.

### **7.3 Contributions**

The research work presented in this thesis has greatly expanded on the existing body of knowledge in through-hole drilling and particularly burr formation at the drill exit point. Using experimental drilling tests, photomicrography observation and microhardness testing, the research has been able to go into a level of detail and understanding regarding the burr formation phenomenon that prior to this work was very general, of a high-level, and lacking any detail.

Based on the research, the following contributions in the area of burr breakout formation in metal drilling processes have been realized.

- Developed a new and innovative method that uses energy analysis in the study of exit burr formation in metal drilling processes.
- Obtained information not previously obtainable during exit burr formation and have confirmed the existence. Thus, the burr formation mechanism has been classified into four stages based on the changes in the process mechanics and material.

- Through this research, 4 critical points in the drilling process have been identified and validated for the first time. These points will be starting points for more research.
- Identification of point – P1, which is the actual onset of the burr formation process.
- Identification of point – P2, which gives the actual depth/size of the deformation ahead of the exit surface.
- Identification of point – P3, which gives the location at which ploughing begins to occur during the drilling process.
- Identification of point – P4, which gives the location at which ploughing is the only process and shearing no longer occurs. It is at this point that any remaining material in the drilled hole will be pushed out as a burr.
- Energy analysis is a cheap and economic way of identifying process changes. This work has introduced a new low-cost alternative to analyzing drilling processes.
- Set the stage for accurate predictive modeling – currently, it is analytical or the use of FEM.

## **7.4 Future Work**

The metal drilling process is a highly dynamic process and greatly influenced by tool design, process parameters and material properties. These parameters are also influential to the exit burr formation mechanism, as such, further investigation would be required to investigate the breakout phenomenon for different tools design and work material. Thus, the following future work would be required.

- Extended drilling tests using various drill designs and sizes.
- Investigate the influence of hole-depth on the deformation zone.
- Develop an empirical relationship between burr size and types based on experimental data.
- Develop a process planning approach to put the results of this work into practice.
- Relationship between deformation zone size and burr size.
- Focus on critical points, specifically P1 and P4. For P1, the focus could be on drilling parameters, and they could be adjusted to move that point. For P4, it is believed that this point relates to the final exit burr that is formed. Therefore, examining and measuring P4 in relation to the exit burr is of interest for future research.

## **7.5 Summary**

A series of experimental tests have been performed on Al 6061-T6 work material using two standard twist drill types to study the breakout burr formation mechanism in metal drilling processes. Data collected for analysis are the thrust (feed power) and cutting power. Although the feed power is on the order of a hundredth of the cutting power, it is expedient and essentially useful in the estimation of the dimension of the deformation zone during the exit burr formation.

Though increasing feed-rate reduces the cutting time and the total cutting energy expended in drilling a hole, the reverse has been observed for the feed energy. This is because, as feed-rate increases, the rate by which the metal drilling time reduces is a lot less than the magnitude by which feed power increases, but a lot greater than the magnitude

by which the cutting power is increased. This shows that the feed-rate directly influences the feed energy and has a reverse effect on the cutting energy.

An original approach has been developed that uses real-time thrust and cutting power data to estimate critical points of interest during burr breakout formation. Using these results, information on the exit burr formation mechanism that was not previously obtainable have been obtained and validated. This has set the stage for accurate predictive modeling of exit burr formation in metal drilling processes.

## Bibliography

- [1] L. K. Gillespie and P. T. Blotter, "The formation and properties of machining burrs," *J. Manuf. Sci. Eng. Trans. ASME*, vol. 98, (1), pp. 66-74, 1976.
- [2] L. K. Gillespie, "Deburring precision miniature parts," *Precision Engineering*, vol. 1, (4), pp. 189-198, 1979.
- [3] N. Ramachandran, S. S. Pande and N. Ramakrishnan, "The role of deburring in manufacturing: A state-of-the-art survey," *Journal of Materials Processing Technology*, vol. 44, (1), pp. 1-13, 1994.
- [4] J. C. Aurich *et al*, "Burrs—Analysis, control and removal," *CIRP Annals*, vol. 58, (2), pp. 519-542, 2009.
- [5] S. A. Niknam, Y. Zedan and V. Songmene, *Machining Burrs Formation & Deburring of Aluminium Alloys*. 2014.
- [6] J. M. Stein and D. A. Dornfeld, "Burr Formation in Drilling Miniature Holes," *CIRP Annals*, vol. 46, (1), pp. 63-66, 1997.
- [7] D. A. Dornfeld *et al*, "Drilling Burr Formation in Titanium Alloy, Ti-6Al-4V," *CIRP Annals - Manufacturing Technology*, vol. 48, (1), pp. 73-76, 1999.
- [8] S. Min, J. Kim and D. A. Dornfeld, "Development of a drilling burr control chart for low alloy steel, AISI 4118," *Journal of Materials Processing Technology*, vol. 113, (1), pp. 4-9, 2001.
- [9] J. Kim and D. A. Dornfeld, "Development of an Analytical Model for Drilling Burr Formation in Ductile Materials," *Journal of Engineering Materials and Technology*, vol. 124, (2), pp. 192-198, 2002.
- [10] A. Sugawara and K. Inagaki, "Effect of workpiece structure on burr formation in micro-drilling," *Precision Engineering*, vol. 4, (1), pp. 9-14, 1982.
- [11] D. A. Stephenson and J. S. Agapiou, *Metal Cutting Theory and Practice*. (2nd ed.) 2006.
- [12] M. E. Merchant, "Mechanics of the metal cutting process. I. Orthogonal cutting and a type 2 chip," *J. Appl. Phys.*, vol. 16, (5), pp. 267-275, 1945.

- [13] M. E. Merchant, "Mechanics of the metal cutting process. II. Plasticity conditions in orthogonal cutting," *J. Appl. Phys.*, vol. 16, (6), pp. 318-324, 1945.
- [14] E. H. Lee and B. W. Shaffer, "The Theory of Plasticity Applied to a Problem of Machining," pp. 405, 1951.
- [15] R. Hill, "The mechanics of machining: A new approach," *Journal of the Mechanics and Physics of Solids*, vol. 3, (1), pp. 47-53, 1954.
- [16] G. Boothroyd, "Effect of Surface Slope on Shear Angle in Metal Cutting," *Journal of Engineering for Industry*, vol. 92, (1), pp. 115-118, 1970.
- [17] M. Choi, "A study of shear angle relationships in shearing process on the shear plane and the rake face in orthogonal cutting," *KSME Journal*, vol. 9, (3), pp. 385-391, 1995.
- [18] W. B. Lee *et al*, "Effect of material anisotropy on shear angle prediction in metal cutting—a mesoplasticity approach," *International Journal of Mechanical Sciences*, vol. 45, (10), pp. 1739-1749, 2003.
- [19] M. C. Shaw, "The size effect in metal cutting," *Sadhana*, vol. 28, (5), pp. 875-896, 2003.
- [20] P. L. B. Oxley, "A strain-hardening solution for the "shear angle" in orthogonal metal cutting," *International Journal of Mechanical Sciences*, vol. 3, (1), pp. 68-79, 1961.
- [21] P. L. B. Oxley, "Mechanics of metal cutting," *International Journal of Machine Tool Design and Research*, vol. 1, (1), pp. 89-97, 1961.
- [22] P. Oxley, "Shear angle solutions in orthogonal machining," *International Journal of Machine Tool Design and Research*, vol. 2, (3), pp. 219-229, 1962.
- [23] P. L. B. Oxley and A. P. Hatton, "Shear angle solution based on experimental shear zone and tool-chip interface stress distributions," *International Journal of Mechanical Sciences*, vol. 5, (1), pp. 41-55, 1963.
- [24] P. L. B. Oxley, "A new approach to the mechanics of metal cutting," *Production Engineer*, vol. 43, (12), pp. 609-614, 1964.
- [25] E. Usui, K. Kikuchi and K. Hoshi, "The Theory of Plasticity Applied to Machining with Cut-Away Tools," *Journal of Engineering for Industry*, vol. 86, (2), pp. 95-104, 1964.
- [26] S. P. F. C. Jaspers and J. H. Dautzenberg, "Material behaviour in metal cutting: strains, strain rates and temperatures in chip formation," *Journal of Materials Processing Technology*, vol. 121, (1), pp. 123-135, 2002.

- [27] H. Ernst, "Fundamental aspects of metal cutting and cutting fluid action," *Ann. N. Y. Acad. Sci.*, vol. 53, (4), pp. 936-961, 1951.
- [28] E. J. A. Armarego and R. H. Brown, *The Machining of Metals*. 1969.
- [29] W. B. Palmer and P. L. B. Oxley, "Mechanics of Orthogonal Machining," *Proceedings of the Institution of Mechanical Engineers*, vol. 173, (1), pp. 623-654, 1959.
- [30] R. H. Brown and E. J. A. Armarego, "Oblique machining with a single cutting edge," *International Journal of Machine Tool Design and Research*, vol. 4, (1), pp. 9-25, 1964.
- [31] M. E. Merchant, *Basic Mechanics of the Metal-Cutting Process*. 1944.
- [32] M. Kronenberg, *Grundzüge Der Zerspanungslehre*. (2 ed. ed.) 1954.
- [33] G. V. Stabler, "The Fundamental Geometry of Cutting Tools," *Proceedings of the Institution of Mechanical Engineers*, vol. 165, (1), pp. 14-26, 1951.
- [34] P. L. B. Oxley, "Rate of Strain Effect in Metal Cutting," *Manufacturing Science*, vol. 85, (4), pp. 335-337, 1963.
- [35] P. L. B. Oxley, "An analysis for orthogonal cutting with restricted tool-chip contact," *International Journal of Mechanical Sciences*, vol. 4, (2), pp. 129-135, 1962.
- [36] An American National Standard, *Twist Drills*. (ASME B94.11M-1993 ed.) 1994.
- [37] P. M. Webb, "Dynamics of the twist drilling process," *Int J Prod Res*, vol. 31, (4), pp. 823-828, 1993.
- [38] W. Chen, "Applying the finite element method to drill design based on drill deformations," *Finite Elements in Analysis and Design*, vol. 26, (1), pp. 57-81, 1997.
- [39] K. Narasimha *et al*, "An investigation into the influence of helix angle on the torque-thrust coupling effect in twist drills," *The International Journal of Advanced Manufacturing Technology*, vol. 2, (4), pp. 91-105, 1987.
- [40] S. V. M. Selvam and C. Sujatha, "Twist drill deformation and optimum drill geometry," *Computers & Structures*, vol. 57, (5), pp. 903-914, 1995.
- [41] T. R. Chandrupatla and W. D. Webster Jr, "Effect of drill geometry on the deformation of a twist drill," in Anonymous 1985, .
- [42] G. Lorenz, "Helix Angle and Drill Performance." *Annals of the CIRP*, vol. 28, (1), pp. 83-86, 1979.

- [43] W. D. Tsai and S. M. Wu, "A Mathematical Model for Drill Point Design and Grinding," *Journal of Engineering for Industry*, vol. 101, (3), pp. 333-340, 1979.
- [44] J. Hsieh and P. D. Lin, "Mathematical model of multiflute drill point," *International Journal of Machine Tools and Manufacture*, vol. 42, (10), pp. 1181-1193, 2002.
- [45] J. Hsieh and P. D. Lin, "Drill point geometry of multi-flute drills," *The International Journal of Advanced Manufacturing Technology*, vol. 26, (5), pp. 466-476, 2005.
- [46] J. Hsieh, "Mathematical model for helical drill point," *Int. J. Mach. Tools Manuf.*, vol. 45, (7-8), pp. 967-977, 2005.
- [47] K. Sambhav, P. Tandon and S. G. Dhande, "Geometric modeling and validation of twist drills with a generic point profile," *Applied Mathematical Modelling*, vol. 36, (6), pp. 2384-2403, 2012.
- [48] S. Kaldor and E. Lenz, "Drill point geometry and optimization," *Journal of Engineering for Industry*, vol. 104, (1), pp. 84-90, 1982.
- [49] T. Radhakrishnan, R. K. Kawlra and S. M. Wu, "A mathematical model of the grinding wheel profile required for a specific twist drill flute," *International Journal of Machine Tool Design and Research*, vol. 22, (4), pp. 239-251, 1982.
- [50] K. F. Ehmann and M. F. DeVries, "Grinding Wheel Profile Definition for the Manufacture of Drill Flutes," *CIRP Annals*, vol. 39, (1), pp. 153-156, 1990.
- [51] K. Ren and J. Ni, "Analyses of Drill Flute and Cutting Angles," *The International Journal of Advanced Manufacturing Technology*, vol. 15, (8), pp. 546-553, 1999.
- [52] W. Zhang *et al*, "A practical method of modelling and simulation for drill fluting," *International Journal of Machine Tools and Manufacture*, vol. 46, (6), pp. 667-672, 2006.
- [53] W. D. Tsai and S. M. Wu, "Computer analysis of drill point geometry," *International Journal of Machine Tool Design and Research*, vol. 19, (2), pp. 95-108, 1979.
- [54] A. Paul, S. G. Kapoor and R. E. DeVor, "Chisel edge and cutting lip shape optimization for improved twist drill point design," *International Journal of Machine Tools and Manufacture*, vol. 45, (4), pp. 421-431, 2005.
- [55] J. Wang and Q. Zhang, "A study of high-performance plane rake faced twist drills.: Part I: Geometrical analysis and experimental investigation," *International Journal of Machine Tools and Manufacture*, vol. 48, (11), pp. 1276-1285, 2008.
- [56] A. R. Watson, "Geometry of drill elements," *International Journal of Machine Tool Design and Research*, vol. 25, (3), pp. 209-227, 1985.

- [57] A. S. Salama and A. H. ElSawy, "The dynamic geometry of a twist drill point," *J. Mater. Process. Technol.*, vol. 56, (1-4), pp. 45-53, 1996.
- [58] C. J. J. Oxford, "On the Drilling of Metals 1—Basic Mechanics of the Process," *Trans.ASME*, vol. 77, (2), pp. 103-114, 1955.
- [59] S. EMA, "Effects of twist drill point geometry on torque and thrust," in 2012, pp. 165-174.
- [60] M. C. Shaw and C. J. J. Oxford, "On the Drilling of Metals 2—The Torque and Thrust in Drilling," *Trans.ASME*, vol. 79, (1), pp. 139-148, 1957.
- [61] Ernst H. H H., "The spiral point drill - A new concept in drill point geometry," *Transactions of the ASME*, vol. 80, pp. 1059-1072, 1958.
- [62] A. Kumar Pal, A. Bhattacharyy and G. Chandra Sen, "Investigation of the Torque in drilling ductile materials," *International Journal of Machine Tool Design and Research*, vol. 4, (4), pp. 205-221, 1965.
- [63] O. W. Boston and C. J. Oxford Sr, "Torque, Thrust and Power in Drilling," *Journal SAE*, vol. 28, (3), pp. 378-383, 1931.
- [64] S. Bera and A. Bhattacharyya, "On the determination of torque and thrust during drilling of ductile materials," pp. 879-892, 1968.
- [65] V. Chandrasekharan, S. G. Kapoor and R. E. DeVor, "A Mechanistic Approach to Predicting the Cutting Forces in Drilling: With Application to Fiber-Reinforced Composite Materials," *Journal of Engineering for Industry*, vol. 117, (4), pp. 559-570, 1995.
- [66] V. Chandrasekharan, S. G. Kapoor and R. E. DeVor, "A mechanistic model to predict the cutting force system for arbitrary drill point geometry," *J. Manuf. Sci. Eng. Trans. ASME*, vol. 120, (3), pp. 563-570, 1998.
- [67] M. Elhachimi, S. Torbaty and P. Joyot, "Mechanical modelling of high speed drilling. 1: predicting torque and thrust," *International Journal of Machine Tools and Manufacture*, vol. 39, (4), pp. 553-568, 1999.
- [68] M. Elhachimi, S. Torbaty and P. Joyot, "Mechanical modelling of high speed drilling. 2: predicted and experimental results," *International Journal of Machine Tools and Manufacture*, vol. 39, (4), pp. 569-581, 1999.
- [69] D. A. Stephenson and J. S. Agapiou, "Calculation of main cutting edge forces and torque for drills with arbitrary point geometries," *International Journal of Machine Tools and Manufacture*, vol. 32, (4), pp. 521-538, 1992.

- [70] M. C. Shaw, *Metal Cutting Principles*. (2nd ed.) 2005.
- [71] R. A. Williams, "A study of the basic mechanics of the chisel edge of a twist drill," *Int J Prod Res*, vol. 8, (4), pp. 325-343, 1970.
- [72] R. A. Williams, "A study of the drilling process," *J. Manuf. Sci. Eng. Trans. ASME*, vol. 96, (4), pp. 1207-1215, 1974.
- [73] E. J. A. Armarego and C. Y. Cheng, "Drilling with flat rake face and conventional twist drills—II. Experimental investigation," *International Journal of Machine Tool Design and Research*, vol. 12, (1), pp. 37-54, 1972.
- [74] E. J. A. Armarego and C. Y. Cheng, "Drilling with flat rake face and conventional twist drills—I. Theoretical investigation," *International Journal of Machine Tool Design and Research*, vol. 12, (1), pp. 17-35, 1972.
- [75] E. J. A. Armarego and J. D. Wright, "Predictive Models for Drilling Thrust and Torque — a comparison of three Flank Configurations," *CIRP Ann. Manuf. Technol.*, vol. 33, (1), pp. 5-10, 1984.
- [76] A. R. Watson, "Drilling model for cutting lip and chisel edge and comparison of experimental and predicted results. I — initial cutting lip model," *International Journal of Machine Tool Design and Research*, vol. 25, (4), pp. 347-365, 1985.
- [77] A. R. Watson, "Drilling model for cutting lip and chisel edge and comparison of experimental and predicted results. II — revised cutting lip model," *International Journal of Machine Tool Design and Research*, vol. 25, (4), pp. 367-376, 1985.
- [78] A. R. Watson, "Drilling model for cutting lip and chisel edge and comparison of experimental and predicted results. III — drilling model for chisel edge," *International Journal of Machine Tool Design and Research*, vol. 25, (4), pp. 377-392, 1985.
- [79] A. R. Watson, "Drilling model for cutting lip and chisel edge and comparison of experimental and predicted results. IV — drilling tests to determine chisel edge contribution to torque and thrust," *International Journal of Machine Tool Design and Research*, vol. 25, (4), pp. 393-404, 1985.
- [80] S. Fujii, M. F. DeVries and S. M. Wu, "An Analysis of Drill Geometry for Optimum Drill Design by Computer. Part I—Drill Geometry Analysis," *Journal of Engineering for Industry*, vol. 92, (3), pp. 647-656, 1970.
- [81] S. Fujii, M. F. DeVries and S. M. Wu, "An Analysis of Drill Geometry for Optimum Drill Design by Computer. Part II—Computer-Aided Design," *Journal of Engineering for Industry*, vol. 92, (3), pp. 657-666, 1970.

- [82] A. Bhattacharyya, A. B. Chattopadhyay and R. Roy, "Chisel-Edge Modification of Small HSS and Carbide Drills for Improved Machinability," *CIRP Annals*, vol. 30, (1), pp. 21-25, 1981.
- [83] G. Spur and J. R. Masuha, "Drilling with Twist Drills of Different Cross Section Profiles," *CIRP Annals*, vol. 30, (1), pp. 31-35, 1981.
- [84] R. H. Thornley, A. B. I. El Wahab and J. D. Maiden, "Some aspects of twist drill design," *International Journal of Machine Tools and Manufacture*, vol. 27, (3), pp. 383-397, 1987.
- [85] B. Y. Lee, H. S. Liu and Y. S. Tarn, "Modeling and optimization of drilling process," *Journal of Materials Processing Technology*, vol. 74, (1), pp. 149-157, 1998.
- [86] A. Vijayaraghavan and D. A. Dornfeld, "Automated Drill Modeling for Drilling Process Simulation," *Journal of Computing and Information Science in Engineering*, vol. 7, (3), pp. 276-282, 2007.
- [87] A. N. Siddiquee *et al*, "Optimization of Deep Drilling Process Parameters of AISI 321 Steel Using Taguchi Method," *Procedia Materials Science*, vol. 6, pp. 1217-1225, 2014.
- [88] A. D. Lukyanov, T. S. Onoyko and T. A. Najafabadi, "Optimization of Processing Conditions when Drilling Deep Holes: Twist Drills," *Procedia Engineering*, vol. 206, pp. 427-431, 2017.
- [89] D. M. Haan *et al*, "An experimental study of cutting fluid effects in drilling," *J. Mater. Process. Technol.*, vol. 71, (2), pp. 305-313, 1997.
- [90] R. Heinemann *et al*, "Effect of MQL on the tool life of small twist drills in deep-hole drilling," *Int. J. Mach. Tools Manuf.*, vol. 46, (1), pp. 1-6, 2006.
- [91] E. Bagci and B. Ozcelik, "Effects of different cooling conditions on twist drill temperature," *The International Journal of Advanced Manufacturing Technology*, vol. 34, (9), pp. 867-877, 2007.
- [92] D. Sun *et al*, "Hole-making processes and their impacts on the microstructure and fatigue response of aircraft alloys," *The International Journal of Advanced Manufacturing Technology*, vol. 94, (5), pp. 1719-1726, 2018.
- [93] N. A. M. M. Nazmul Ahsan, M. G. Kibria and M. R. Ahmed, *An Experimental Study on the Effect of Minimum Quantity Lubrication on Drilling AISI 1040 Steel*. 201528.
- [94] R. M'Saoubi *et al*, "High performance cutting of advanced aerospace alloys and composite materials," *CIRP Annals*, vol. 64, (2), pp. 557-580, 2015.

- [95] L. K. Gillespie, "Economic tradeoffs in deburring," Bendix Corp., Kansas City, Missouri, United States, Tech. Rep. BDX-613-1620, Sept. 1976.
- [96] K. Nakayama and M. Arai, "Burr Formation in Metal Cutting," *CIRP Ann. Manuf. Technol.*, vol. 36, (1), pp. 33-36, 1987.
- [97] S. -. Ko and D. A. Dornfeld, "A study on burr formation mechanism," *J. Eng. Mater. Technol. Trans. ASME*, vol. 113, (1), pp. 75-87, 1991.
- [98] G. -. Chern and D. A. Dornfeld, "Burr/breakout model development and experimental verification," *J. Eng. Mater. Technol. Trans. ASME*, vol. 118, (2), pp. 201-206, 1996.
- [99] G. Chern, "Study on mechanisms of burr formation and edge breakout near the exit of orthogonal cutting," *Journal of Materials Processing Technology*, vol. 176, (1), pp. 152-157, 2006.
- [100] S. S. Pande and H. P. Relekar, "Investigations on reducing burr formation in drilling," *International Journal of Machine Tool Design and Research*, vol. 26, (3), pp. 339-348, 1986.
- [101] K. Lee and D. A. Dornfeld, "Micro-burr formation and minimization through process control," *Precis Eng*, vol. 29, (2), pp. 246-252, 2005.
- [102] L. K. Lauderbaugh, "Analysis of the effects of process parameters on exit burrs in drilling using a combined simulation and experimental approach," *J. Mater. Process. Technol.*, vol. 209, (4), pp. 1909-1919, 2009.
- [103] S. Ko and J. Lee, "Analysis of burr formation in drilling with a new-concept drill," *Journal of Materials Processing Technology*, vol. 113, (1), pp. 392-398, 2001.
- [104] S. L. Ko, J. E. Chang and S. Kaipakjian, "Development of Drill Geometry for Burr Minimization In Drilling," *CIRP Annals*, vol. 52, (1), pp. 45-48, 2003.
- [105] S. -. Ko, J. -. Chang and G. -. Yang, "Burr minimizing scheme in drilling," *J. Mater. Process. Technol.*, vol. 140, (1-3 SPEC.), pp. 237-242, 2003.
- [106] V. N. Gaitonde *et al*, "Genetic algorithm-based burr size minimization in drilling of AISI 316L stainless steel," *Journal of Materials Processing Technology*, vol. 197, (1), pp. 225-236, 2008.
- [107] E. Kilickap, "Modeling and optimization of burr height in drilling of Al-7075 using Taguchi method and response surface methodology," *Int J Adv Manuf Technol*, vol. 49, (9-12), pp. 911-923, 2010.

- [108] M. Ogawa and K. Nakayama, "Effects of Chip Splitting Nicks in Drilling," *CIRP Ann. Manuf. Technol.*, vol. 34, (1), pp. 101-104, 1985.
- [109] L. K. Lauderbaugh Saunders and C. A. Mauch, "An exit burr model for drilling of metals," *J. Manuf. Sci. Eng. Trans. ASME*, vol. 123, (4), pp. 562-566, 2001.
- [110] L. K. L. Saunders, "A finite element model of exit burrs for drilling of metals," *Finite Elements in Analysis and Design*, vol. 40, (2), pp. 139-158, 2003.
- [111] Y. B. Guo and D. A. Dornfeld, "Finite Element Modeling of Burr Formation Process in Drilling 304 Stainless Steel," *Journal of Manufacturing Science and Engineering*, vol. 122, (4), pp. 612-619, 2000.
- [112] S. Segonds *et al*, "A simple analytical model for burr type prediction in drilling of ductile materials," *Journal of Materials Processing Technology*, vol. 213, (6), pp. 971-977, 2013.
- [113] Y. Bu *et al*, "An analytical model for exit burrs in drilling of aluminum materials," *The International Journal of Advanced Manufacturing Technology*, vol. 85, (9), pp. 2783-2796, 2016.
- [114] H. Shikata *et al*, "An Experimental Investigation of Sheet Metal Drilling," *CIRP Ann. Manuf. Technol.*, vol. 29, (1), pp. 85-88, 1980.
- [115] A. Abdul Rahman, A. Mamat and A. Wagiman, *Effect of Machining Parameters on Hole Quality of Micro Drilling for Brass*. 20093.
- [116] M. ELAJRAMI, H. MILOUKI and F. B. BOUKHOULDA, "Effect of Drilling Parameters on Hole Quality," *International Journal of Mining, Metallurgy & Mechanical Engineering (IJMMME)*, vol. 1, (4), pp. 254-257, 2013.
- [117] Y. Hisman Celik, *Investigating the Effects of Cutting Parameters on the Hole Quality in Drilling the Ti-6Al-4V Alloy*. 201448.
- [118] U. Heisel and T. Pfeifroth, "Influence of Point Angle on Drill Hole Quality and Machining Forces When Drilling CFRP," *Procedia CIRP*, vol. 1, pp. 471-476, 2012.
- [119] S. Kundu, S. Das and P. P. Saha, "Optimization of Drilling Parameters to Minimize Burr by Providing Back-up Support on Aluminium Alloy," *Procedia Engineering*, vol. 97, pp. 230-240, 2014.
- [120] J. Kim, S. Min and D. A. Dornfeld, "Optimization and control of drilling burr formation of AISI 304L and AISI 4118 based on drilling burr control charts," *International Journal of Machine Tools and Manufacture*, vol. 41, (7), pp. 923-936, 2001.

- [121] J. Kim and D. A. Dornfeld, "Cost estimation of drilling operations by a Drilling Burr Control Chart and Bayesian statistics," *Journal of Manufacturing Systems*, vol. 20, (2), pp. 89-97, 2001.
- [122] D. Dornfeld and S. Min, "A review of burr formation in machining," in *Burrs - Analysis*, 2010, .
- [123] L. K. Gillespie, "Deburring: An annotated bibliography. volume V," Bendix Corp., Kansas City, Missouri, United States, Tech. Rep. BDX-613-2112, Jan. 1978.
- [124] K. Subramanian and N. H. Cook, "Sensing of drill wear and prediction of drill life," *Journal of Engineering for Industry*, vol. 99, (2), pp. 295-301, 1977.
- [125] J. Tlustý and G. C. Andrews, "A Critical Review of Sensors for Unmanned Machining," *CIRP Annals*, vol. 32, (2), pp. 563-572, 1983.
- [126] M. Nouri *et al*, "Real-time tool wear monitoring in milling using a cutting condition independent method," *International Journal of Machine Tools and Manufacture*, vol. 89, pp. 1-13, 2015.
- [127] N. H. Cook, "Tool wear sensors," *Wear*, vol. 62, (1), pp. 49-57, 1980.
- [128] D. E. Dimla, "Sensor signals for tool-wear monitoring in metal cutting operations—a review of methods," *International Journal of Machine Tools and Manufacture*, vol. 40, (8), pp. 1073-1098, 2000.
- [129] N. Ambhore *et al*, "Tool condition monitoring system: A review," *Materials Today: Proceedings*, vol. 2, (4-5), pp. 3419-3428, 2015.
- [130] Y. Altintas, "In-process detection of tool breakages using time series monitoring of cutting forces," *Int. J. Mach. Tools Manuf.*, vol. 28, (2), pp. 157-172, 1988.
- [131] J. Lee *et al*, "Real-time tool breakage monitoring for NC milling process," *CIRP Annals*, vol. 44, (1), pp. 59-62, 1995.
- [132] T. Kim and J. Kim, "Adaptive cutting force control for a machining center by using indirect cutting force measurements," *Int. J. Mach. Tools Manuf.*, vol. 36, (8), pp. 925-937, 1996.
- [133] M. A. Mannan, S. Broms and B. Lindström, "Monitoring and Adaptive Control of Cutting Process by Means of Motor Power and Current Measurements," *CIRP Annals*, vol. 38, (1), pp. 347-350, 1989.
- [134] D. Cuppini, G. D'errico and G. Rutelli, "Tool wear monitoring based on cutting power measurement," *Wear*, vol. 139, (2), pp. 303-311, 1990.

- [135] H. S. Liu, B. Y. Lee and Y. S. Tarn, "Monitoring of drill fracture from the current measurement of a three-phase induction motor," *International Journal of Machine Tools and Manufacture*, vol. 36, (6), pp. 729-738, 1996.
- [136] X. Li and S. K. Tso, "Drill wear monitoring based on current signals," *Wear*, vol. 231, (2), pp. 172-178, 1999.
- [137] A. Simoneau and J. Meehan, "Investigating the use of peak power measurement in endmilling to identify process features," in *Proceedings of the Canadian Society of Mechanical Engineering International Congress*, 2014, pp. 1-6.
- [138] T. Gutowski, J. Dahmus and A. Thiriez, "Electrical energy requirements for manufacturing processes," in *13th CIRP International Conference on Life Cycle Engineering*, 2006, .
- [139] N. Diaz, E. Redelsheime and D. Dornfeld, "Energy consumption characterization and reduction strategies for milling machine tool use," in *Proceedings of the 18th CIRP International Conference on Life Cycle Engineering*, 2011, pp. 263-267.
- [140] M. Mori *et al*, "A study on energy efficiency improvement for machine tools," *CIRP Annals*, vol. 60, (1), pp. 145-148, 2011.
- [141] S. Kara and W. Li, "Unit process energy consumption models for material removal processes," *CIRP Annals*, vol. 60, (1), pp. 37-40, 2011.
- [142] P. T. Mativenga and M. F. Rajemi, "Calculation of optimum cutting parameters based on minimum energy footprint," *CIRP Annals*, vol. 60, (1), pp. 149-152, 2011.
- [143] Y. Guo *et al*, "Optimization of Energy Consumption and Surface Quality in Finish Turning," *Procedia CIRP*, vol. 1, pp. 512-517, 2012.
- [144] Z. Deng *et al*, "Optimization of process parameters for minimum energy consumption based on cutting specific energy consumption," *Journal of Cleaner Production*, vol. 166, pp. 1407-1414, 2017.
- [145] N. Weinert, S. Chiotellis and G. Seliger, "Methodology for planning and operating energy-efficient production systems," *CIRP Annals*, vol. 60, (1), pp. 41-44, 2011.
- [146] A. A. G. Bruzzone *et al*, "Energy-aware scheduling for improving manufacturing process sustainability: A mathematical model for flexible flow shops," *CIRP Annals*, vol. 61, (1), pp. 459-462, 2012.
- [147] S. T. Newman *et al*, "Energy efficient process planning for CNC machining," *CIRP Journal of Manufacturing Science and Technology*, vol. 5, (2), pp. 127-136, 2012.

- [148] J. Kaminski, R. Crafoord and N. Mårtensson, "Position Accuracy of Drilled Holes," *CIRP Annals*, vol. 40, (1), pp. 503-506, 1991.
- [149] J. Kaminski and R. Crafoord, "Positional Accuracy of Holes When Drilling in Inclined Workpiece Surfaces Part 1: Experimental Results," *Proc. Inst. Mech. Eng. Pt. B: J. Eng. Manuf.*, vol. 208, (2), pp. 129-139, 1994.
- [150] J. Kaminski and R. Crafoord, "Positional Accuracy of Holes When Drilling in Inclined Workpiece Surfaces Part 2: Mathematical Force Model," *Proc. Inst. Mech. Eng. Pt. B: J. Eng. Manuf.*, vol. 208, (2), pp. 141-152, 1994.
- [151] Y. Gong, C. Lin and K. F. Ehmann, "Dynamics of Initial Penetration in Drilling: Part 1—Mechanistic Model for Dynamic Forces," *Journal of Manufacturing Science and Engineering*, vol. 127, (2), pp. 280-288, 2005.
- [152] Y. Gong, C. Lin and K. F. Ehmann, "Dynamics of Initial Penetration in Drilling: Part 2—Motion Models for Drill Skidding and Wandering with Experimental Verification," *Journal of Manufacturing Science and Engineering*, vol. 127, (2), pp. 289-297, 2005.
- [153] R. J. Furness, C. L. Wu and A. G. Ulsoy, "Statistical Analysis of the Effects of Feed, Speed, and Wear on Hole Quality in Drilling," *Journal of Manufacturing Science and Engineering*, vol. 118, (3), pp. 367-375, 1996.
- [154] S. Y. Park *et al*, "Effect of drilling parameters on hole quality and delamination of hybrid GLARE laminate," *Composite Structures*, vol. 185, pp. 684-698, 2018.
- [155] L. K. Gillespie, "Burrs produced by drilling," Bendix Corp., Kansas City, Missouri, United States, Tech. Rep. BDX-613-1248, Aug. 1976.
- [156] F. Ke, J. Ni and D. A. Stephenson, "Chip thickening in deep-hole drilling," *Int. J. Mach. Tools Manuf.*, vol. 46, (12-13), pp. 1500-1507, 2006.
- [157] M. Bono and J. Ni, "The effects of thermal distortions on the diameter and cylindricity of dry drilled holes," *Int. J. Mach. Tools Manuf.*, vol. 41, (15), pp. 2261-2270, 2001.
- [158] ASTM International, "*Standard Specification for Aluminum-Alloy 6061-T6 Standard Structural Profiles*," 2010.
- [159] Y. Sun, N. Tsuji and H. Fujii, "Microstructure and Mechanical Properties of Dissimilar Friction Stir Welding between Ultrafine Grained 1050 and 6061-T6 Aluminum Alloys," *Metals*, vol. 6, (10), 2016.
- [160] D. O. Iruikwu and A. Simoneau, "Peck depth optimization in deep-hole drilling operations," in *Proceedings of the 27<sup>th</sup> CANCAM*, Sherbrooke, Quebec, Canada, 2019, .

[161] Standard Test Methods for Vickers Hardness and Knoop Hardness of Metallic Materials, ASTM International. *ASTM E92-17*, 2017.

[162] F. Ke, J. Ni and D. A. Stephenson, "Continuous chip formation in drilling," *Int. J. Mach. Tools Manuf.*, vol. 45, (15), pp. 1652-1658, 2005.

[163] M. Sato *et al.*, "Variation of temperature at the bottom surface of a hole during drilling and its effect on tool wear," *International Journal of Machine Tools and Manufacture*, vol. 68, pp. 40-47, 2013.

[164] Trent, E. M., Wright, Paul Kenneth., *Metal Cutting*. (4th ed.) 2000.

## Appendix A. Drilling Energy Consumption

The energy expended in the drilling of a through hole has been estimated from the experimental data obtained. This is shown in Table 7.1. The specific energy consumption (SEC) is the energy consumed in cutting the workpiece material, while the feed energy consumed (FEC) is the energy resulting from the thrust action as the tool feeds into the workpiece material during the chip formation process

Table 7.1: Energy consumed in drilling through-hole using type A twist drill on 8.9 mm thick Al 6061-T6 alloy.

Feed (mm/rev)	Spindle speed			
	2037 (rpm)		2547 (rpm)	
	SCE (Joules)	FEC (Joules)	SCE (Joules)	FEC (Joules)
0.05	1475.20	3.92	1555.30	4.72
0.10	1154.61	7.44	1186.02	7.80
0.15	924.76	9.11	933.48	9.59
0.20	874.62	11.29	853.96	10.90

The energy-difference approach used here gives the energy expended by thrust/feed action and the cutting of chips via shearing, estimated between an arbitrary drilled depth referenced at a steady state drilling operation and an incremental depth travelled by the twist drill prior to breakout of the twist drill through the exit surface. The incremental depth selection must occur after the arbitrary depth traveled by the twist drill. With reference to the results of the feed energy-difference shown in Figure 6.3 and Figure 6.4, and the cutting energy difference shown in Figure 6.13 and Figure 6.14. By comparing the energy expended by the thrust and cutting forces, it is observed that the energy used up by the feed/thrust forces are very small in relation to that of the cutting forces. This is due to the

very low axial speed at which the cutting tool travels as it feeds into the workpiece material, whereas, the cutting speed at the cutting edges are very high in comparison to the feed. Also, for each plot of the energy-difference for both the feed and cutting power, the results show that the lowest feed-energy was expended at the lowest feed and increased with increasing feed. Whereas, the cutting energy showed a contrary result with its highest energy expended when cutting at the lowest feed and vice versa. This agrees with the results of the energy consumption in drilling a through-hole reported in Table 7.1. The differences occur due to the dominance of the feed power/thrust over feed-rate in the feed energy estimation, whereas the feed-rate and/or spindle speed hold prominence in the cutting energy. When the cutting time is reduced due to increasing feed-rate, the feed energy still increases, whereas, reducing cutting time due to increasing feed-rate reduces the cutting energy expended and vice versa. Therefore, as feed-rate increases the rate at which drilling time reduces is much less than the magnitude by which the feed power increases, but much greater than the magnitude by which the cutting power is increased.

## Appendix B. Okuma Machine Type ES-V4020 Power Requirements

Item	Standard Spec.		Option Spec.		Formula**
	Rated Power (KW) *	Req'd Power (KVA) *	Rated Power (KW) *	Req'd Power (KVA) *	
Spindle VAC Motor					
(cont./30min.)	5.5/7.5	7.1			1
Axis Feed Motor:					
X-Axis Servo	3.0	1.95			3
Y-Axis Servo	3.0	1.95			3
Z-Axis Servo	4.2	2.73			3
MG-Axis Servo (ATC)	1.0	0.65			4
A-Axis Servo			1.0	0.32	4
NC and Auxiliary Equipment:					
NC/EC Control Power	1.25	1.50			11
Coolant Motor			0.98	1.18	10
Thru Spindle Coolant Motor			3.0	3.6	10
Chip Wash			1.6	1.92	7
Chip Conveyor Motor			0.10	0.12	10
<b>TOTALS</b>		15.88		6.82	

Voltage (V)	Main Circuit Breaker Current Rating (A)	User Facility's Branch Breaker or Fuse Rating (A)	User Supply Cable Conductor (AWG/mm <sup>2</sup> )
220V+/-10%	80	80	(6/14)

\* Values are rounded to two (2) decimal places.

\*\* Refer to Appendix C for power requirement formulas and calculations.

## Appendix C. Common Machining Center Power Calculations

Power requirements for NC lathes are calculated using the formula indicated below.

Basic Formula:

$$\text{Require power (KVA)} = K \times \text{Cont. rated power (KW)}$$

$$\text{where } K = \frac{\text{Loss factor (L)} \times \text{Load factor (R)}}{\text{Power factor (Cos Q)} \times \text{Efficiency (n)}}$$

Formula No.	Item	Coefficient (K)	Coefficient factors		
			Loss factor (L)	Load factor (R)	PF X Eff. (cosQ) x (n)
1	Main Spindle VAC Motor	1.29	1.1	1	0.85
2	Main Spindle DC Motor	1.38	1.1	1	0.8
3	NC Servo Axes (X, Y, Z)	0.65	1.1	0.5	0.85
4	Additional NC Servo Axes A, B, C Axes or APC, ATC	0.32	1.1	0.25	0.85
5	Hydraulic Motor	1.2	1	1	0.83
6	Coolant Motor	1.2	1	1	0.83
7	Chip Clean Motor	1.2	1	1	0.83
8	Spindle Head Cooling Unit	1.2	1	1	0.83
9	NC robot Loader	0.32	1.1	0.25	0.85
10	Chip Conveyor or other auxiliary motors	1.2	1	1	0.83
11	NC/EC Control Power IGF, MOP	1.2	1	1	0.83

## Curriculum Vitae

Candidate's full name: Daniel Obiora Iruikwu

Universities attended (with dates and degrees obtained):

HAMK University of Applied Sciences, Finland, 2010, BEng in Mechanical Engineering and Production Technology.

Aalto University, Finland, 2013, MSc in Electronics and Electrical Engineering.

Publications:

Conference Presentations:

- 1) Iruikwu, D. O., Isomaa, J. M., Korkolainen, P., Kiviluoma, P., Kuosmanen, P., Calonius, O. (2012), Dynamic loading system for air bearing testing, Proceedings of the 8th International Conference of DAAAM Baltic Industrial Engineering, Tallinn, Estonia. 1, 309-314.
- 2) Daniel Iruikwu, Anouar Belahcen, Deepak Singh, Antero Arkkio. (2013), 2D FE Analysis of Mechanical Stresses in a Synchronous Reluctance Machine, 9th International Symposium on Electric and Magnetic Fields Bruges, Belgium.
- 3) D. O. Iruikwu and A. Simoneau. (2019), Peck depth optimization in deep-hole drilling operations, in Proceedings of the 27Th CANCAM, Sherbrooke, Quebec, Canada.